Development of recovery and suppression techniques for potential-induced degradation of photovoltaic modules based on p-type c-Si solar cells

（p 型多結晶シリコン太陽電池モジュールにおける

電圧誘起劣化の回復および抑制方法の開発）

Environmental and Renewable Energy System Division,
Graduate School of Engineering,

Gifu University, Japan.

GO SIAN HUAI

March 2023

Development of recovery and suppression techniques for potential-induced degradation of photovoltaic modules based on p-type c-Si solar cells

（p 型多結晶シリコン太陽電池モジュールにおける電圧誘起劣化の回復および抑制方法の開発）

GO SIAN HUAI

Thesis adviser: Associate Professor Fumitaka OHASHI

A thesis submitted for the degree of Doctor of Philosophy from the Gifu University

Environmental and Renewable Energy System Division,
Graduate School of Engineering, Gifu University.

March 2023

For my beloved family.
This doctoral dissertation is dedicated to the memorial of my dad who passed away on March 18th, 2018.

Contents

Abstract

Carbon neutral is a key word which is an important target for many countries to be achieved to prevent further global warming by next a few decades. To realize the target, reductions of exhausts of greenhouse effect gases during the generation of electricity by using renewable energies is one of key topics. Among the renewable energies, photovoltaic (PV) technologies are known to have advantages such as low-cost maintenances with long-term lifetime. However, further reduction of power generation costs of PV systems is an important issue to enhance their installation as a main power source. PV modules based on single crystalline silicon (c-Si), or multi-crystalline (Mc-Si) solar cells are widely used because of their low cost and high energy conversion efficiencies. However, degradation of PV modules with various modes has been reported, such as corrosion of cell electrodes, discoloration, and delamination of encapsulants, breakage of cover glass, and cracking of solar cells in PV modules.

As one of the degradation modes, shunt-type potential-induced degradation (PID) occurs with PV systems operated at high system voltage and occasionally reduces energy conversion efficiency quickly and drastically compared with other degradation modes. The shunt-type PIDs have been observed in mega-solar system consisting of p-type crystalline Si based PV modules with Al frame. In high temperature and humidity environments, the operating voltage gives rise to the migration of metal ions such as Na^+ from the soda-lime cover glass toward the solar cells in PV modules. The metal ions migrate further into solar cells. The above process is considered to form shunt passes in p-n junctions and to result in PID. Hence, the development of a recovery method as well suppression method are key issues to extend their lifetime and, therefore, minimize power generation costs. In this study, we developed a simple PID recovery method by the application of a reverse DC bias and a technique to delay the PID occurrence by coating a glass layer (GL) on a cover glass of PV modules.

As a general recovery method, the application of a voltage bias opposite the bias wherein PID occurred is well known. Reportedly, this method reduces Na concentrations around the solar cells and restores the conversion efficiency of PV modules. This recovery method is

performed at high voltage (~ – 1000 V) and high temperature (~85 °C) for several hours. The recovery process is generally conducted in the laboratory because it requires a high-voltage source with a large equipment for temperature control while the PV modules are removed from the PV system. Therefore, a new recovery method which can be conducted easily in short time is required. In this study, we developed a simple recovery method by an application of a reverse bias voltage (RV) of -20 and -30 V between p-n junctions of PID affected PV modules at room temperature. The recovery occurred within a few minutes. Such a low voltage application in a short time without the need for temperature control is expected to be a low-cost recovery method. Additionally, during the recovery process, nonuniform temperature increase of the PV modules appeared after the recovery. We considered the RV are possibly induced the slight shifts of the Na ions in the p-n junctions. Such shifts of Na ions reduced the leakage current of the p-n junction and photovoltaic characteristics are recovered. However, many Na ions Na remained around the p-n junction which possibly affected nonperfect recoveries of PID.

Many ways to suppress the occurrence of PID have been proposed such as the use of Na-free front cover glass and Na barrier at a surface of cover glass. Moreover, high-electrical resistance encapsulants such as ethyl-vinyl acetate (EVA) encapsulants with high cross-linking conditions, ionomer or thin polyethylene films are also known to delay PID. However, the most of anti-PID techniques are not applicable to practical PV systems because of their high costs, and the techniques must be applied during the manufacture process of PV modules. Furthermore, PV technologies are still now developed not only on the conversion efficiency but also on the structure and shape adoptable to various locations such as at building walls and car roofs. Therefore, the alternative low-cost and simple technique for anti-PID applicable to various structures and shapes is now highly required for acceleration of the spread of the solar PV system. In this study, anti-PID technique was developed by formations of glass layer (GL) on the surface of cover glass using liquid glass. Conventional p-type multi-crystalline Si PV module prepared with the GLs at the bottom side of cover glass showed up to 4 times slower occurrence of PID compared with that of the PV module without GL. Additionally, less anti-PID effects were observed even if the GL was formed at top side

of cover glass. We considered that the GL acts not only as the barrier to prevent Na ion moving from the cover glass to the solar cell but also as the high resistivity material which lower the voltage distributed to the cover glass. We considered that this technique is one of the powerful tools to suppress the occurrence of PID with low cost in the various PV modules.

Chapter 1
Introduction

Carbon neutral became a key issue for the world as the global warming came to be recognized as a critical problem for our daily life. Developments of the technologies for renewable energies have been considered to be crucial to reduce the emission of a gas, carbon dioxide, which is known as a main cause of the greenhouse effect. Among the renewable energies, technologies for the conversion of solar power into electricity, photovoltaic (PV) technologies, arose great attentions of researchers, because the techniques have possibilities to reduce the levels of power generation costs same with or lower than those of fossil fuels. Additionally, PV systems can be installed wherever the sunlight is irradiated without the necessity of massive facilities such as electric power grid, and of difficult maintenances. Therefore, not only the developed countries but also the emerging countries started to install the power generation systems. However, as the installations spread in the world and the systems has been enlarged into megawatt, degradation phenomena originated from the system structures and components became apparent. Such degradations induce shortenings of the system lifetime and therefore the increases of power generation costs. Therefore, many researchers started to investigate the mechanism of degradation phenomena and to develop their recoveries and suppression techniques. This dissertation aims to develop a recovery and suppression techniques of potential-induced degradation (PID) which is known as one of degradation phenomena occurring on PV modules, a component of PV system. In the introductory part 1.1 provides some historical background of solar cells and related information on it. Section 1.2 explained PV system briefly and section 1.3 summarize the

potential-induced degradation of PV modules. Chapter 1 end us with section 1.4 which explains the purpose of this study.

1.1 Solar cells

1.1.1 Photovoltaic phenomena

A photovoltaic (PV) cell is a solid-state device that converts the energy of sunlight into electricity by the photovoltaic effect. The physical effect of photovoltaic was first observed by Becquerel [1] in 1839, when he produced a current by exposing silver electrodes to radiation in an electrolyte. The effect was described in more detail by Adams and Day [2] in 1877. The first solid state materials that showed a significant light-dependent voltage between two contacts were selenium in 1876 and later cuprous oxide [3-6], which indicated already that semiconductors would eventually be the most promising class of materials for photovoltaic energy conversion. Technological development began with the development of a diffuse silicon p-n junction in 1954 [7], a forerunner of the present silicon solar cell which converted light into electricity with reasonable efficiency.

The working principle of a PV cell is bases on the photovoltaic effect which converted light energy into electrical energy as illustrated in Fig.1.1. A PV cell is a p-n junction diode which are formed by joining n-type and p-type extrinsic semiconductor materials. N-type and p-type extrinsic semiconductor materials are formed by adding different atoms to intrinsic semiconductor materials and known as adding impurities. In the case of a silicon (Si), by

adding a phosphorus (P) atom and a boron (B) atom as an impurity result in a p-type semiconductor and an n-type semiconductor, respectively. Si atoms are tetravalent atoms, but phosphorus belongs to Group III elements and therefore has five valence electrons. On the other hand, boron (B) has three valence electrons because it is a group III element. Therefore, n-type semiconductor was formed by adding a phosphorous which has an excess of electrons. On the other hand, by adding boron which has an excess of hole to intrinsic semiconductor, p-type semiconductor was formed as shown in Fig.1.2.

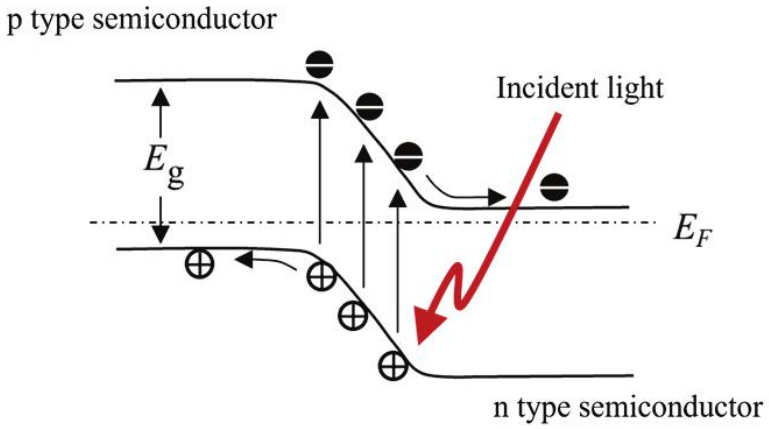

Fig. 1.1 Photovoltaic effect of a p-n junction.

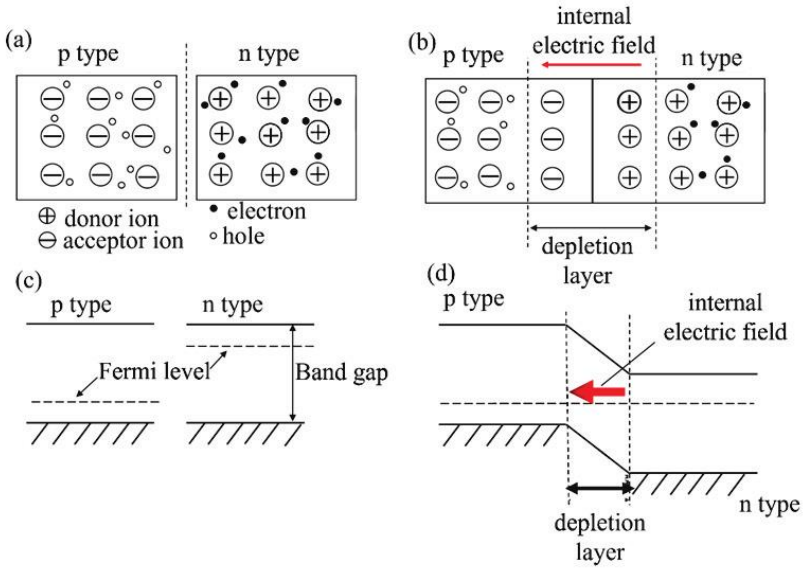

Fig.1.2 Schematic view of the inside of the semiconductor before and after the p-n junction (a) before p-n junction formation, (b) after p-n junction formation, (c) before energy band diagram formation, (d) after energy band diagram formation.

1.1.2 PV cell parameters

The main parameters that are used to characterize the performance of solar cells are the peak power, P_{max}, the short-circuit current density, J_{SC}, the open-circuit voltage, V_{OC}, and the fill factor, FF. These parameters are determined from the illuminated *J*-*V* characteristic as illustrated in Fig.1.3. The conversion efficiency η can be determined from these parameters.

(a) Short-circuit current density, *J*sc

The short-circuit current *I*sc is the current that flows through the external circuit when the electrodes of the solar cells are short circuited. The short-circuit current of a solar cell depends on the photon flux density incident on the solar cell, which is determined by the spectrum of the incident light. For a standard solar cell measurement, the spectrum is standardized to the AM 1.5 spectrum. *I*sc is measured in ampere (A) or milli-ampere (mA). The current density is denoted by *J* and the short circuit current density is denoted by *J*sc. The short current density is obtained by dividing the short circuit current by the areas of the solar cells. The maximum current that the solar cell can deliver strongly depends on the optical properties of the solar cell, such as absorption in the absorber layer and reflection.

(b) Open-circuit voltage (V_{OC})

The open-circuit voltage is the voltage at which no current flows through the external circuit. It is the maximum voltage that a solar cell can deliver. It is measured in volt (V) or milli-volt (mV). V_{OC} is mainly dictated by various recombination processes that determine the bulk lifetime of minority charge carriers in crystalline silicon (c-Si) wafer.

(c) Fill factor (FF)

Fill factor gives a measure of the maximum power that can be extracted from a solar cell. The fill factor is the ratio between the maximum power generated by a solar cell, P_{max}, and the product of Voc with Jsc. This parameter is mainly limited by parasitic series and shunt resistances in the device.

$$FF = \frac{P_{\max}}{V_{\mathrm{OC}} \times J_{\mathrm{SC}}} \qquad 1.1$$

(d) Conversion efficiency (η)

The conversion efficiency is calculated as the ratio between P_{max} and the incident power. As mentioned above, solar cells are measured under the standard test condition (STC), where the incident light is described by the AM1.5 spectrum and has an irradiance of I_{in}= 1000 W/m^2 at the temperature of 25°C. Mathematically, it is written as-

$$\eta = \frac{P_{\max}}{P_{\mathrm{in}}} \times 100 \ \ (\%) \qquad 1.2$$

(e) Degradation rate ($\%\eta_{\mathrm{D}}$) and recovery rate ($\%\eta_{\mathrm{R}}$)

The reduction in conversion efficiency of a tested PV module after PID test is defined as the degradation rate. Then, the recovery rate in conversion efficiency after recovery tests using RV and HV were defined as follows.

$$\%\eta_{\mathrm{D}} = \frac{\eta(after\ PID\ test)}{\eta(before\ PID\ test)} \times 100(\%) \tag{1.3}$$

and

$$\%\eta_{\mathrm{R}} = \frac{\eta(after\ recovery\ test)}{\eta(before\ PID\ test)} \times 100(\%) \tag{1.4}$$

(f) Current at maximum power (I_{MP})

It is the current that results in maximum power. I_{MP} is also called the rated current of the cell.

(g) Voltage at maximum power (V_{MP})

The voltage that results in maximum power output is called voltage at maximum power. V_{MP} is also called rated voltage of the cell.

(h) Maximum power output *(*P_{max}, P_{MP})

It is the maximum power that can be delivered from the cell under specific environmental conditions. The point at *I-V* curve at which the maximum power is also called maximum power point (P_{MP}).

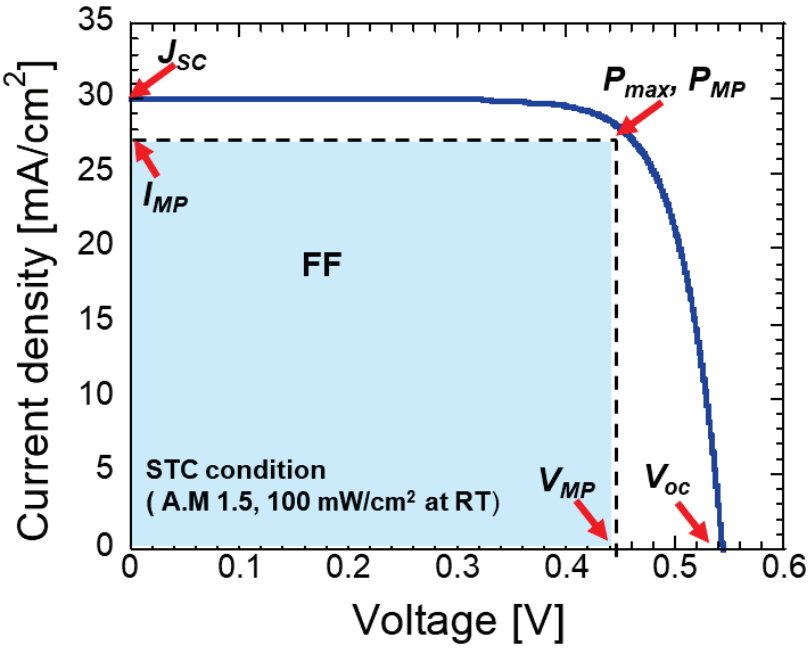

Fig.1.3 Photo *J-V* characteristics of a one cell PV module under 1 sun illumination.

1.1.3 Equivalent circuit of a PV cell

To understand the electronic behavior of a solar cell, it is useful to create a model which is electrically equivalent and is based on discrete electrical components whose behavior is well known. An ideal solar cell may be modelled by a current source in parallel with a diode, in practice no solar cell is ideal, so a shunt resistance and a series resistance component are added to the model. The resulting equivalent circuit of a solar cell is shown in Fig.1.4. Fig.1.5 is the schematic representation of a solar cell for use in circuit diagrams.

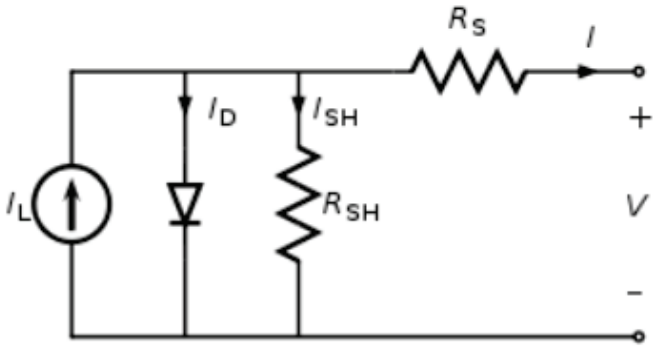

Fig.1.4 The equivalent circuit of a solar cell.

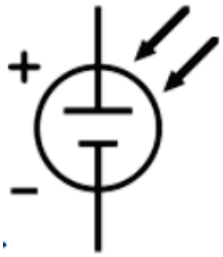

Fig.1.5 The schematic symbol of a solar cell.

From the equivalent, circuit it is evident that the current produced by the solar cell is equal to that produced by the current source, minus that which flows through the diode, minus that which flows through the shunt resistor is,

$$I = I_L - I_D - I_{SH} \tag{1.5}$$

Where, I = output current (Amperes)

I_L = photogenerated current (Amperes)

I_D = diode current (Amperes)

I_{SH} = shunt current (Amperes).

The current through these elements is governed by the voltage across them:

$$V_j = V + IR_S \tag{1.6}$$

Where, V_j = voltage across both diode and resistor R_{SH} (Volts)

V = voltage across the output terminals (Volts)

I = output current (Amperes)

R_S = series resistance (Ω).

By the Shockley diode equation, the current diverted through the diode is:

$$I_D = I_0 \left\{ exp\left(\frac{qV_j}{nk_BT}\right) - 1 \right\} \tag{1.7}$$

Where, I_0 = reverse saturation current (Amperes)

n = diode ideality factor (1 for an ideal diode)

q = elementary charge

k_B = Boltzmann's constant

T = absolute temperature

By Ohm's law, the current diverted through the shunt resistor is:

$$I_{SH} = \frac{V_j}{R_{SH}} \tag{1.8}$$

Substituting (1.8) into (1.5) produces the characteristic equation of a solar cell, which relates solar cell parameters to the output current and voltage is,

$$I = I_{\mathrm{L}} - I_0\left\{exp\left[\frac{q(V+IRs)}{nk_{\mathrm{B}}T}\right] - 1\right\} - \frac{V+IR_{\mathrm{S}}}{R_{\mathrm{SH}}} \quad (1.9)$$

When the cell is operated at open circuit, $I = 0$ and the voltage across the output terminals is defined as the open-circuit voltage, V_{OC},

$$V_{\mathrm{OC}} = \frac{k_{\mathrm{B}}T}{q} ln\left\{1 + \frac{I_{\mathrm{L}}}{I_0}\right\} \quad (1.10)$$

Similarly, when the cell is operated at short circuit $= 0$ and the current I through the terminals is defined as the short-circuit current, I_{SC} is,

$$I_{\mathrm{SC}} = I_{\mathrm{L}} \quad (1.11)$$

1.1.4 Types of PV cells

PV cells can be made of only one single layer of light-absorption materials (single-junction) or use multiple physical configuration (multi-junction) to take advantage of various absorption and charge separation mechanisms. PV cells can be classified into first, second and third generation PV cells as summarized in Fig.1.6. In addition, reported timeline of research solar cell energy conversion efficiencies since 1976 also shown in Fig.1.7[8].

The first generations PV cells also called conventional, traditional, or wafer-based PV cells are made of crystalline silicon. It is the oldest and the most popular technology due to high power efficiencies. The silicon wafer-based technology is further categorized into two subgroups named as [9-13],

(i) Single/ mono-crystalline silicon solar cells

(ii) Poly/multi-crystalline silicon solar cells.

Most of thin film PV cells and a-Si are second generation solar cells and were considered more economical as compared to the first-generation silicon wafer solar cells. Silicon-wafer cells have light absorption layers up to 350 mm thick, while thin-film solar cells have a very thin light absorption layers, generally of the order of 1 μm thickness [14]. Thin film solar cells are classified as,

(i) a-Si

(ii) CdTe

(ii) CIGS (copper-indium gallium di-selenide).

Third generation PV cells are the new promising technologies but are not commercially investigated in detail. Most of the developed third generation PV cell types are [9],

(i) Nanocrystal based solar cells

(ii) Polymer based solar cells

(iii) Dye sensitized solar cells

(iv) Concentrated solar cells

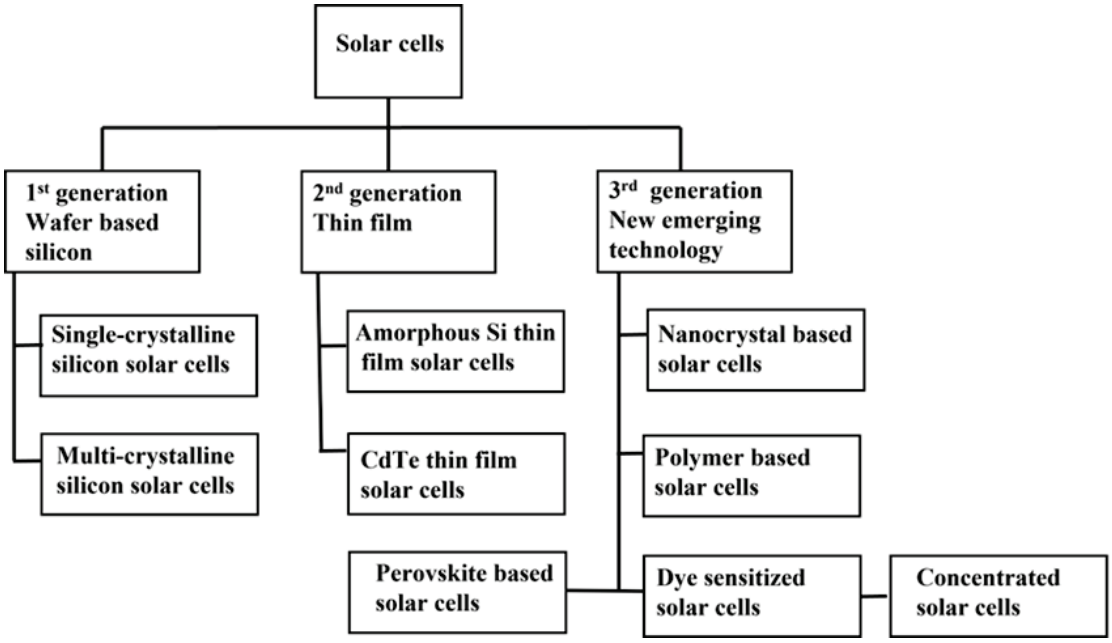

Fig.1.6 Various types of solar cell technologies and current trends of development.

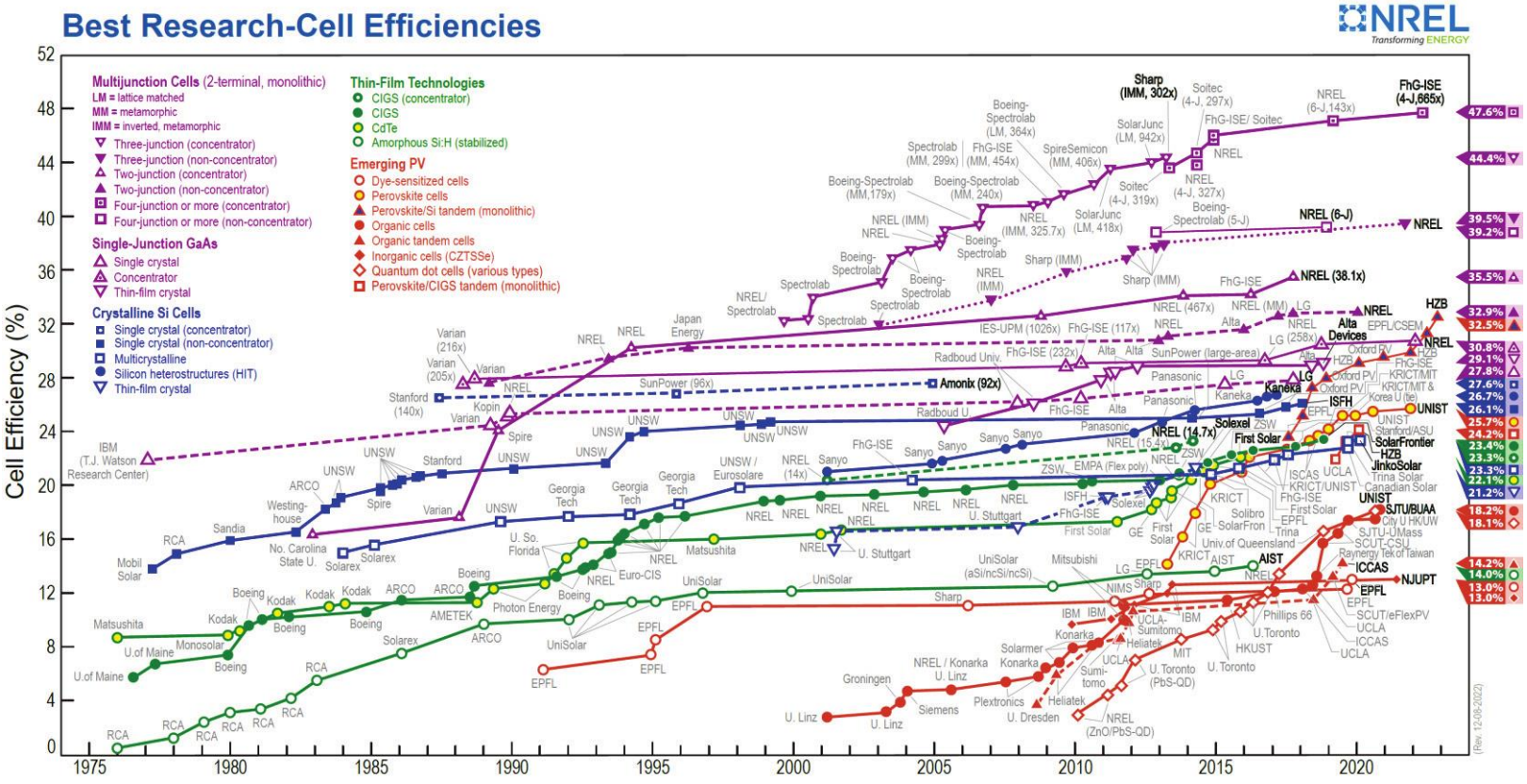

Fig.1.7 Transition of the conversion efficiency of solar cell [8].

1.1.5 Crystalline silicon PV cells

The crystalline silicon PV cell is one of many silicon-based semiconductor devices. Crystalline silicon PV cells are the most popular solar cells on the market and provide the highest energy conversion efficiencies of all commercial solar cells and modules. The structure of typical commercial crystalline-silicon PV cells is shown in Fig.1.8. Standard cells are produced using one of two different boron-doped p-type silicon substrates: mono-crystalline and poly-crystalline. The cell sizes are typically 125 mm (5 inches) or 156 mm (6 inches) square. Mono-crystalline solar cells are produced from pseudo-square silicon wafer substrates cut from column ingots grown typically by the Czochralski (CZ) process. Poly-crystalline (multi-crystalline) cells, on the other hand, are made from square silicon substrates cut from poly-crystalline ingots grown in quartz crucibles. The efficiencies of typical commercial crystalline silicon solar cells with standard cell structures are in the range of 16–18% for mono-crystalline substrates and 15–17% for poly-crystalline substrates. The current technologies used for the production and application of crystalline silicon PV cells are broadly discussed in [15].

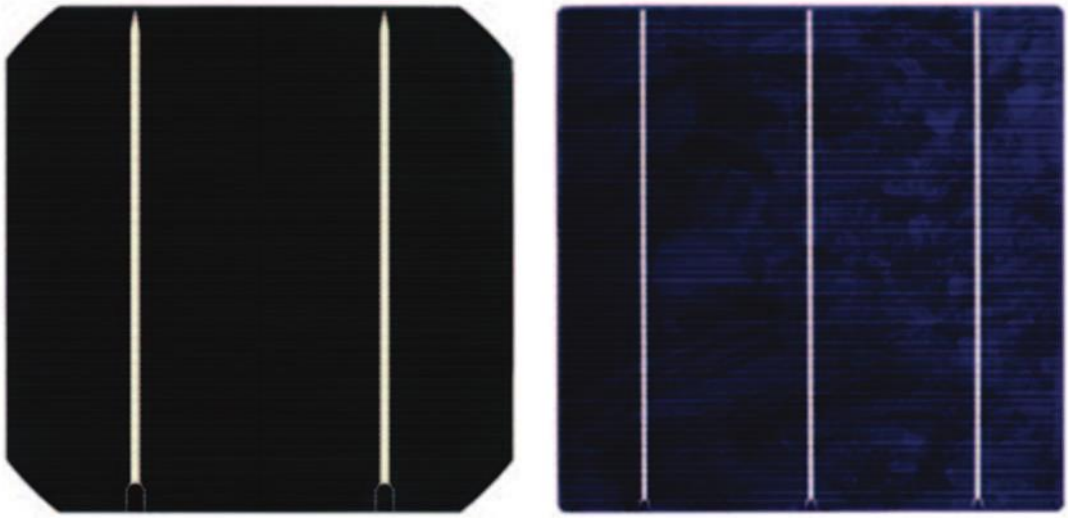

Fig.1.8 Typical mono-crystalline silicon solar cell (left), and multi-crystalline silicon solar cell (right) [15].

1.2 PV systems

1.2.1 Component and layout of PV system

As discussed in previous section 1.1.1, a solar cell can convert the energy contained in the solar radiation into electrical energy. Due to the limited size of the solar cell, it only delivers a limited amount of power under fixed current-voltage conditions that are not practical for most applications. To use solar electricity for practical devices, several solar cells must be connected to form a PV module, sometimes called as solar panel. A PV module, as illustrated in Fig.1.9 (b) consists of PV/solar cells as shown in Fig.1.9 (a) that are electrically connected in series and parallel connections. For large-scale generation of solar

electricity, PV modules are connected into a solar array. An example of such an array is shown in Fig.1.9 (c). A PV array is a series connected PV modules. A PV system is PV arrays with power conditioner. This array consists of strings, where string means PV modules connected in series. Thousands or even millions of PV modules are arranged into a vast solar farm which provides electricity to large urban populations. Such kind of solar panels arrangement is called mega solar system as shown in Fig.1.10.

PV systems can be classified in three main types; stand-alone, hybrid and gird connected PV system as shown in Fig.1.11. Stand–alone PV systems required battery energy storage for DC mode or with inverter for AC mode but others without battery bank and linked directly to a load [18,19]. hybrid PV system is composed of PV solar panels with other source of energy like wind farm, fuel cell or water turbines [18, 20-22]. Grid connected PV system is the best option that using PV panels directly with grid to supply any reduction in electrical energy from solar panel array with or without battery storage [18, 23, 24]. Detailed explanations are summarized in [15].

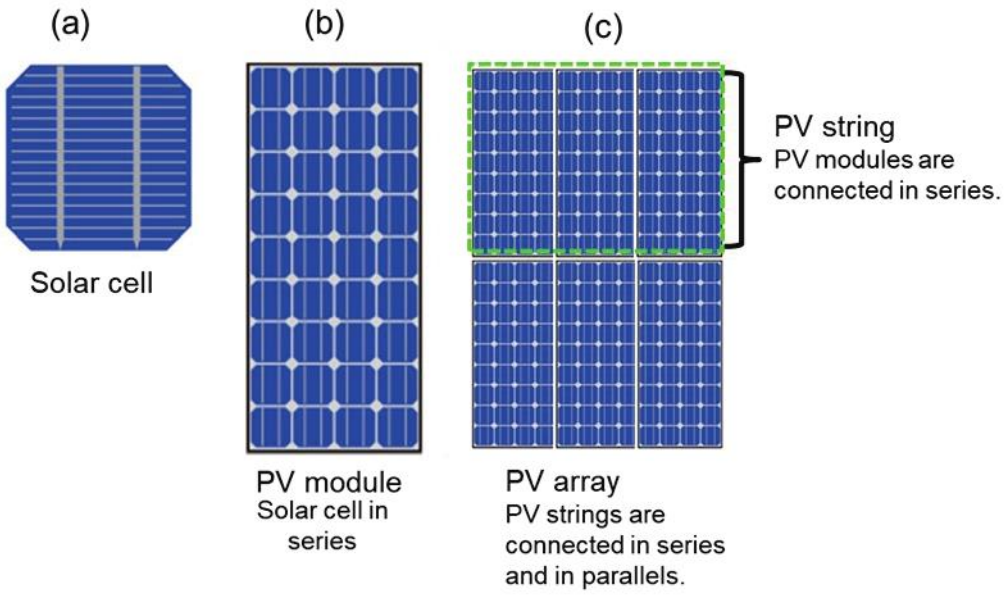

Fig.1.9 Illustration of (a) solar cell, (b) PV module, (c) PV arrays [15].

Fig.1.10 An example of mega power solar plants which is in Yokkaichi, Japan [16].

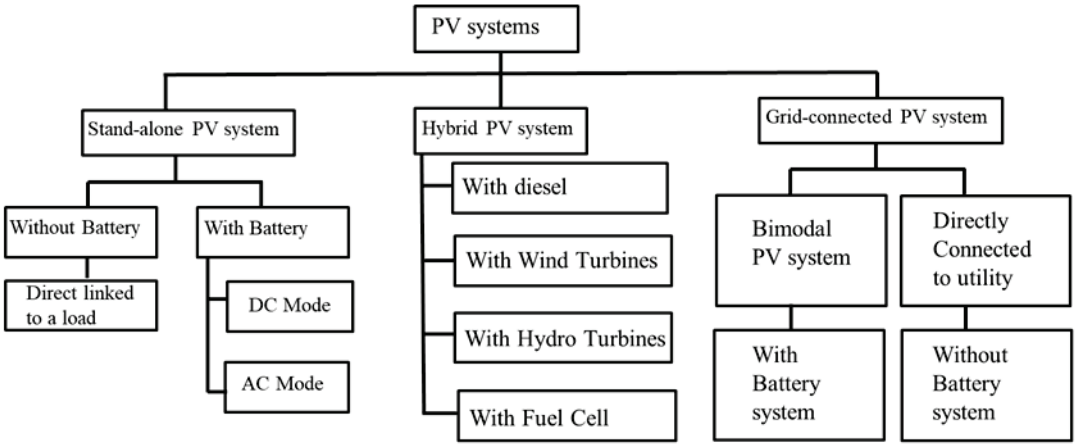

Fig.1.11 Classification of PV system [17].

1.2.2 Structure of PV module

In this section, the typical components of a usual crystalline silicon PV module are briefly explained. The layer stack may consist of different materials dependent on the manufacturer. The typical components are soda-lime glass, two layers of encapsulants, a solar cell, a back sheet layer, a frame usually made from aluminum and a junction box which is usually placed at the back of PV module. Fig.1.12 shows the components of a typical c-Si PV module. One of the most important steps during module production is laminating where EVA is used as encapsulant. The choice of the layers that light traverses before entering the solar cell is also very important from an optical point of view. If these layers have an

appropriate refractive index, they deliver the sun light to solar cells as much as possible, and thus increases the current produced by the solar cell.

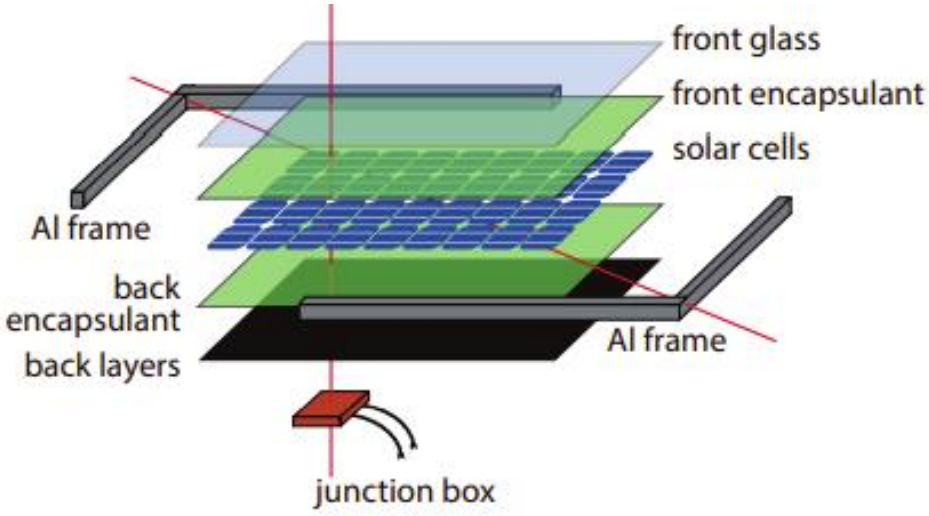

Fig.1.12 The components of a typical c-Si PV module [16].

In this study, one cell PV module which is consisted with one solar cell was fabricated to conduct the experiments in the laboratory. All the components and fabrication process were the same with those of a commercialized PV module as explained in previously. Please note that an Al frame and junction box was not prepared in this study. Detailed explanation for the fabrication process of one cell PV module is presented in section 2.1.

1.2.3 Power generation cost of PV systems

As already explained in section 1.1, PV is the technology that generates direct current (DC) electrical power measured in watts (W) or kilowatts (kW) from semiconductor materials when they are illuminated by photons. As long as sunlight shining on the solar cell

or PV modules, it will generate electrical power. A PV system consists of PV modules and other electrical and hardware components such as inverter, electrical cabling, module mounts, and controls, which are mounted on rooftops or in fields. The cost of PV system initially measured by $/Watt which lacks many aspects (e.g., financial policies, system lifetime and solar equipment performance) [25]. LCOE, also called Levelized Cost of Electricity is a more accurate energy cost calculation; well-known, accepted and widely used technique and it has been adapted by many researchers and agencies [26,27].

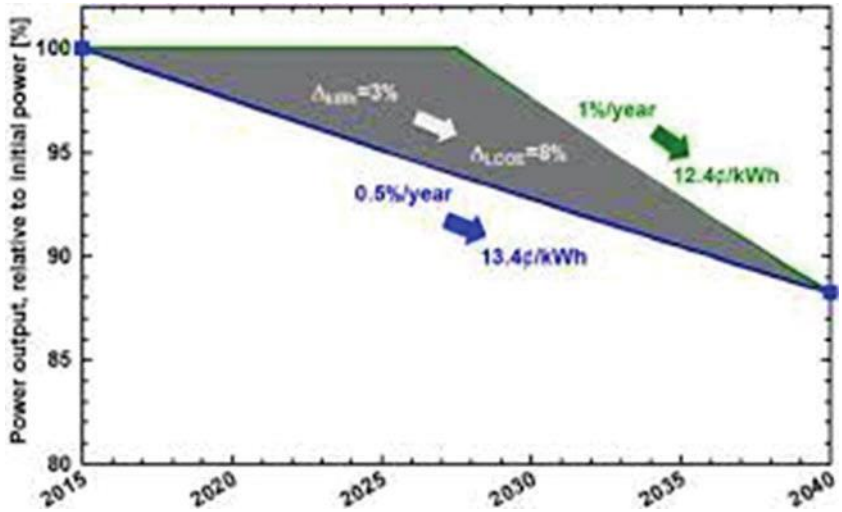

Fig.1.13 Example of how non-linear degradation rate can affect levelized cost of energy (LCOE) [28].

The cost of solar PV modules can also be reduced by efficiency improvements, such as the reduction of materials costs, increased efficiency in converting sunlight into electricity and development in recovery and prevention for the occurrence of degradation in PV system.

1.2.4 Various degradation modes of PV modules

PV modules based on crystalline Si are the most reliable component of a photovoltaic system, and according to the manufactures, the PV modules have a lifetime from 25 to 30 years. However, some modules degrade or fail along their services time under outdoor exposure. Identification of degradation failure modes on PV modules is important to evaluate its performance along time and lifetime. The main factors which cause the degradation are temperature, humidity, irradiation, and mechanical shocks. The degradation causes can be divided into following three levels [29].

(i) Packaging degradation: This degradation mode occurs when there is a damage on the packaging material or when it degrades along normal operation. This category includes the glass breakage, dielectric breakdown, bypass diode failure, encapsulant discoloration, and backsheet cracking or delamination [30].

(ii) Interconnect degradation: The interconnect degradation is the result of the segregation of metals, such as SbPb, in the soldering alloy causing structural changes on it.

(iii) Devices level degradation: The semiconductor device has shown performance stability in operation. However, it can degrade during operation due to environmental conditions such as UV light exposure, temperature, moisture, thermal cycling, high voltage etc. [31]. Currently, the potential-induced degradation (PID) has systematically been topic of discussion by photovoltaic researchers and will discuss from the various point of view in the next section.

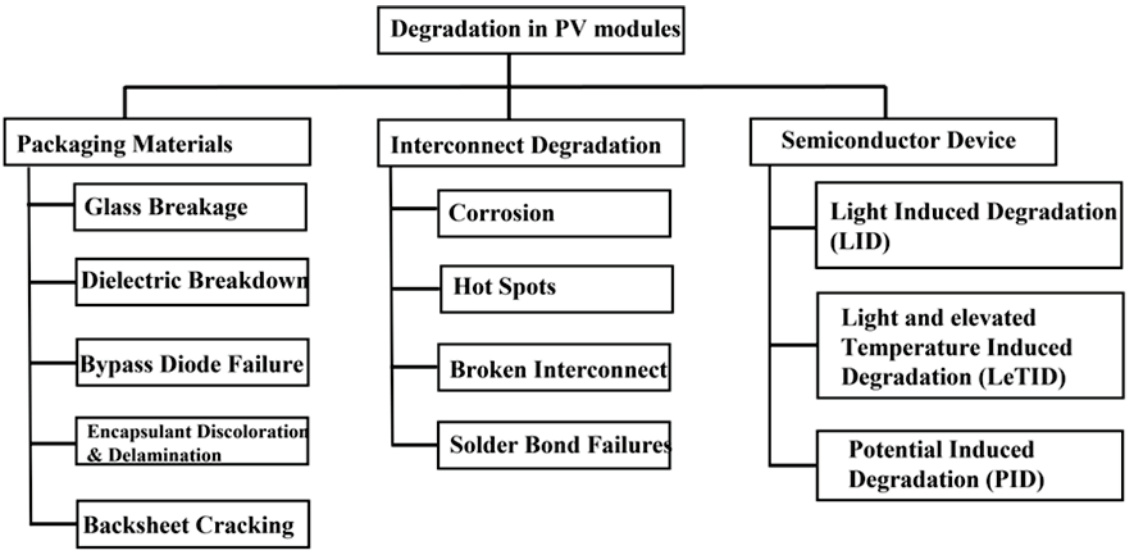

Fig.1.14 Various possible photovoltaic module degradation modes belonging to packaging, interconnect, and device levels [29].

1.3 Potential-induced degradation (PID) of PV modules

1.3.1 PID of PV modules based on p-type crystalline Si

The term "potential-induced degradation" (PID) was first introduced in English language by S. Pingel and coworkers in 2010 [32]. It was introduced as a degradation mode resulting from voltage potential between the cells in the photovoltaic module and ground. Research in this PID field was pioneered by the Jet Propulsion Laboratory for both crystalline and amorphous silicon photovoltaic modules [32]. Currently, the term PID is used widely in the PV industry for the degradation effect of standard p-type multi-crystalline silicon solar cells [32]. As one of the degradation modes, potential-induced degradation (PID) occurs with

PV systems operated at high system voltage and occasionally reduces energy conversion efficiency quickly and drastically compared with other degradation modes. Fig.1.15 shows a schematic diagram of the PID occurrence in the PID system. It has been proposed that Na ions arising from the front cover glass of the PV modules drift through the encapsulant by the electric field due to the electric potential difference between the cell and the grounded Al frame, and also diffuse inside of the cells. Such Na ions migration is a possible origin of PID for p-type crystalline Si PV modules. The source of the sodium could be either from soda-lime glass that is commonly used as a PV module glass [33-38], or the contaminants entered during the cell fabrication process [39]. Therefore, the stacking faults in the cell are decorated by Na impurities. It is known that this Na migration results in the significant shunting of the cell and degrades its efficiency, and shunting is the most common feature of PID in standard p-type crystalline Si PV modules.

Several PID mechanisms have been suggested, and the most probable PID mechanisms is the shunting-type mechanism which was intensively studied by Naumann and coworkers [40-45]. Fig.1.16 presents a schematic drawing of a cross section of a PV module that is undergoing PID. Due to the assistance of an electric field between the grounded frames and the cells, Na^+ in the cover glass or in contaminants in other components of PV module migrates toward cells and reaches the SiN_x passivation layers and reaches the SiN_x/Si interface. Consequently, some of the Na accumulating in the SiN_x/Si interface is localized to dislocations and is segregated laterally on {111} planes as Na-decorated stacking faults. The Na-decorated stacking faults produce multiple defect levels within the c-Si bandgap. If the local defect concentration in the stacking faults is considerably high, then the orbitals of

neighboring defect levels ("Process 1" in Fig.1.16). Consequently, the Na-decorated stacking faults penetrating the p-n junction might behave as 2D electrically conductive layers, which leads to short-circuiting of the p-n junction. At low defect concentrations, one can observe recombination via defect levels of different energies located at the same place in the depletion region ("process 2" in Fig.1.16). More detailed concerning with PID phenomena in conventional p-type c-Si PV modules are available in a comprehensive review presented by Luo *et al* [32].

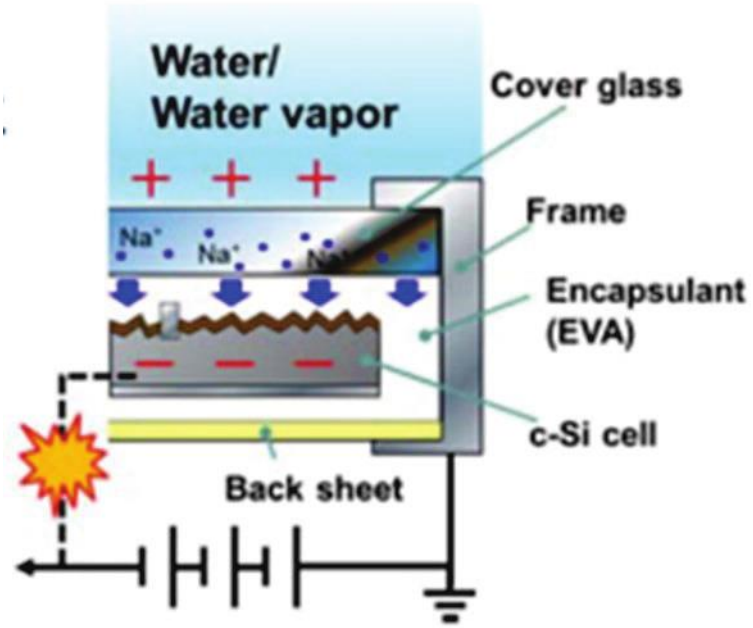

Fig.1.15 Proposed PID mechanism by migration of Na ion from front cover glass to PV cell.

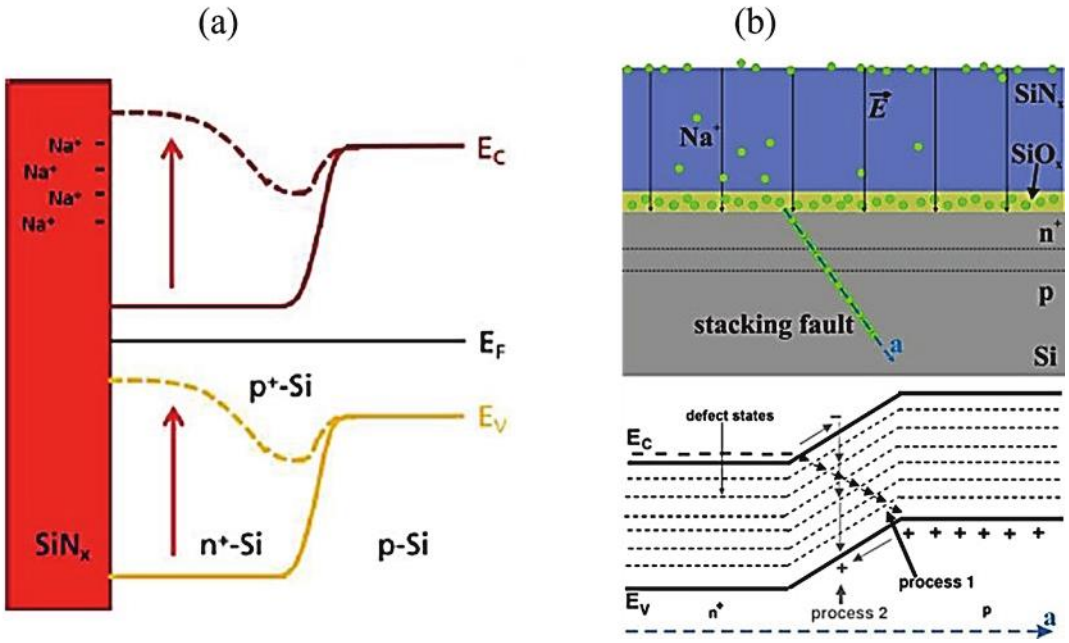

Fig.1.16 (a) Cross Section of Solar Cell and (b) Band Diagram of the Proposed PID Mechanism Using the Stacking Fault [41,42].

1.3.2 Recovery from PID of PV modules based on p-type crystalline Si

Recovery phenomena are also a remarkably feature of PID of PV modules-based p-type crystalline Si compared with other degradation modes. As a general PID recovery method, the application of a voltage bias opposite the bias where PID occurred is well known [39, 46-49] Reportedly, this method reduces Na concentrations and restores the conversion efficiency of PV modules. This recovery method is performed at high voltage (HV), ∼1000 V, and high temperature, ∼85 °C, for several hours [39]. The recovery process is generally conducted in the laboratory because it requires a high-voltage source with large equipment for temperature control and the PV modules are removed from the PV system. Therefore, it is difficult to apply the method to commercialized PV modules.

It was also reported that PID can be recovered by storage at a high temperature even without a positive high bias application [50]. After thermal recovery by heating to 250 °C for 2.5 h to PID-affected PV cells, the out-diffusion of Na was observed [51]. It was also observed that PD recovery accelerates with an increase in module temperature [47,52-56]. Moreover, Oh *et al*., carried out the recovery test of without high voltage at room temperature, and they found that residual Na remains in the stacking fault and causes the incomplete recovery [48-49].

Another recovery method reported by Jonai *et al*. [57] included the application of a reverse bias voltage (RV) of − 20 and − 30 V between p-n junctions of PID-affected PV modules without temperature control. The recovery occurred in a few minutes. A low-voltage application in a short time, without the need for temperature controls, is expected to be a low-

cost recovery method. However, details regarding the PID recovery phenomena of this method have not yet been reported. In this study, a detailed analysis of the recovery process by the application of reverse bias voltage (RV) to the p-n junction of PID-affected PV modules.

1.3.3 Suppression for PID of PV modules based on p-type crystalline Si

To prevent PID and improve the long-term stabilities of PV modules, new techniques for the suppression of PID is crucial. Several ways to suppress the occurrence of shunting-type PID have been reported as follows. The use of Na-free front cover glass can suppress the PID diminishing migrations of Na ions [58,59]. A thin TiO_2 film deposited on the cell side surface of cover glass performed as a Na barrier to suppress the drifting of alkali ions [60]. An ALD-grown Al_2O_3 layer of 30 nm also acts as an ion diffusion barrier, and it could effectively suppress PID [61]. In addition, high-electrical resistance ethyl-vinyl acetate (EVA) encapsulants [62-63] and high cross-linking conditions can delay PID [64].

To suppress Na migration, inserting ionomer [65] or thin polyethylene films between the EVA and the cover glass or cells were also reported [66,67]. Glass materials is well known to have a strong effect on PID. Borosilicate glass [68], quartz glass [69-71], and chemically strengthened glass [72] are also able to prevent PID. However, the most of anti-PID techniques are not applicable in practical PV systems because of their high costs. In practice, the Si-rich SiN_x film used as an anti-reflection (AR) coating on the Si solar cell also functions to suppress PID [73-79]. However, the optimum composition of SiN_x for suppression of PID is different from that for AR coating. More Si rich is required for anti-

PID. Such the modification of SiN_x film results in increase of refractive index and light absorption which possibly reduce the conversion efficiency of solar cells.[80] Solar PV technologies are still now developed not only on the conversion efficiency but also on the structure and shape adoptable to various locations such as at building walls and car roofs. Therefore, the alternative low-cost and simple technique for anti-PID applicable to various structures and shapes is now highly required for acceleration of the spread of the solar PV system.

In this research, a new technique to delay the PID occurrence was developed by coating a glass layer (GL) on a cover glass of PV module. By forming a glass layer with high volume resistance at the surface of cover glass is considered to suppress PID. The glass layer is almost the same material with the coating for car bodies, and easily formed by using a chemical solution containing poly-siloxane. Schematic image of the suppression technique studied in this work is shown in Fig.1.17.

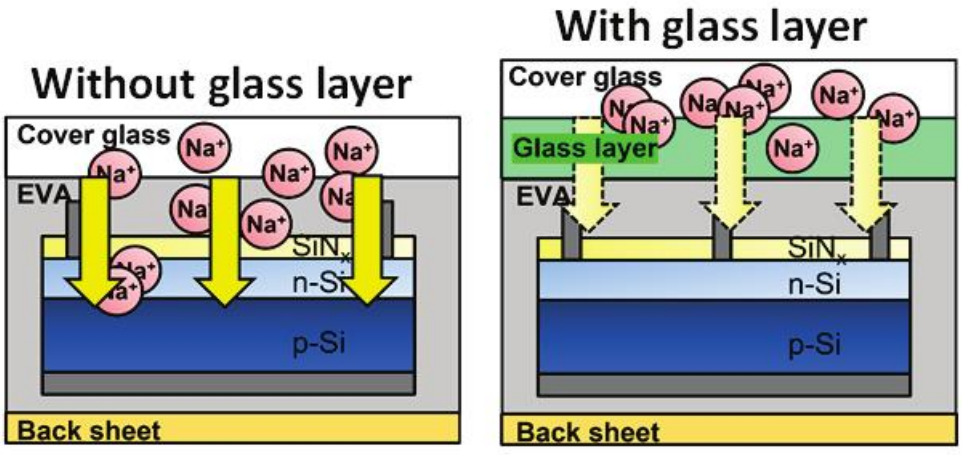

Fig.1.17 A new suppression method by forming a glass layer with high volume resistance.

1.3.4 PID occurring on other PV modules

Understanding the behaviors and mechanisms of PID occurred in PV cells also crucial from the viewpoint of the application of PV cells in large-scale PV systems. An earlier comprehensive review presents more detailed information related to PID [32]. Although significant progress has been made towards understanding the PID in PV modules, there are still many questions that remain unanswered. PID effects are influenced by many factors such as the properties of the solar cell's antireflective (AR) coating encapsulation materials, module construction (*e.g.,* frame or frameless) and system topologies. Even for the same type of modules, different extents of power degradation may be induced, depending on the environmental stress (temperature, humidity, condensation, *etc.*), grounding conditions of the glass surface (wet or dry), and exposure to light.

The root causes of PID are different for different types of module technologies. Different PID modes may also occur when the same type of PV modules is stressed under different conditions. Hence, PID mechanisms for both c-Si based, and thin-film PV modules are briefly summarized in this section,

(i) c-Si based technologies: PID-shunting (PID-s) is the most common type of PID in conventional p-type c-Si PV modules. Decrease in shunt resistance of PV modules owing to influence of Na+ ion on p-n junction seems to be main reasons leading to PID in p-type based c-Si PV modules. Depending on the PV cell structures, n-type c-Si PV modules can be affected by polarization type PID, Na-penetration-type PID and corrosion-type PID. Discussion of

PID in several kinds of n-type c-Si PV modules are extensively presented by Yamaguchi *et al*. [81].

(ii) Thin film technologies: Amorphous silicon (a-Si), copper indium gallium selenide (CIGS) and cadmium telluride (CdTe) thin-film modules have all been reported in the literature to be suffering from PID, when the solar cells are negatively biased [82-85]. In thin-film modules is principally attributed to Na ion migration The root cause of PID of thin-film Si PV modules is thought to be the delamination between a transparent conductive oxide film and a glass substrate. Detailed analysis of PID on thin film technologies were seriously discussed in [32].

1.4 Purpose of this study

Over the last decade, PV systems, which directly convert solar energy to electricity, have attracted considerable attention as one of the promising clean and renewable energy resources. Recently, potential-indued degradation (PID) in Si-based PV modules has been observed and reported especially in large PV systems, where huge numbers of PV modules are serially interconnected. To reduce the power generation cost by increasing the lifetime of PV system, to prevent PID on PV modules and recover on PID-affected PV modules is crucial with, a series of systematic investigations. Furthermore, the extension of the PV modules results in the reduction of PV module wastes which will be disposed in large amount in near future due to the end of field in tariff. Hence, in this study, two main research was conducted to extend the lifetime of PV modules. The first one is optimization of recovery

techniques by the application of reverse bias voltage (RV) to p-n junction of PID-affected one cell PV module. Detailed discussion concerning with this recovery method was presented in Chapter 3 of this thesis. The second research one is about the development of suppression method for one cell PV modules as explained in section 1.3.3. Step by step experimental approach and results were described in Chapter 4 of this thesis. Experimental methodologies such as once cell PV module fabrication, evaluation methods and development of recovery and suppression method were clearly explained in Chapter 2. General conclusions and future scope were summarized in the last chapter, Chapter 5.

Chapter 2
Experimental methods

In this study, one cell PV modules with and without glass layer (GL) were fabricated. The PV modules without GL is denoted by a standard PV module in this thesis. Followings are the explanations of the PV module components and how to prepare the PV modules and GL. Then the characterization methods of the PV modules and the components are explained later.

2.1 PV module preparation

2.1.1 Fabrication of once cell PV module

One cell PV modules were prepared by using a vacuum laminator. Fig.2.1 shows the components of conventional PV module. Vacuum lamination is the process that bonds each component of PV modules such as cover glass, EVA, solar cell, and back sheet layers under high temperature. The major components used to prepare PV module are explained as follows.

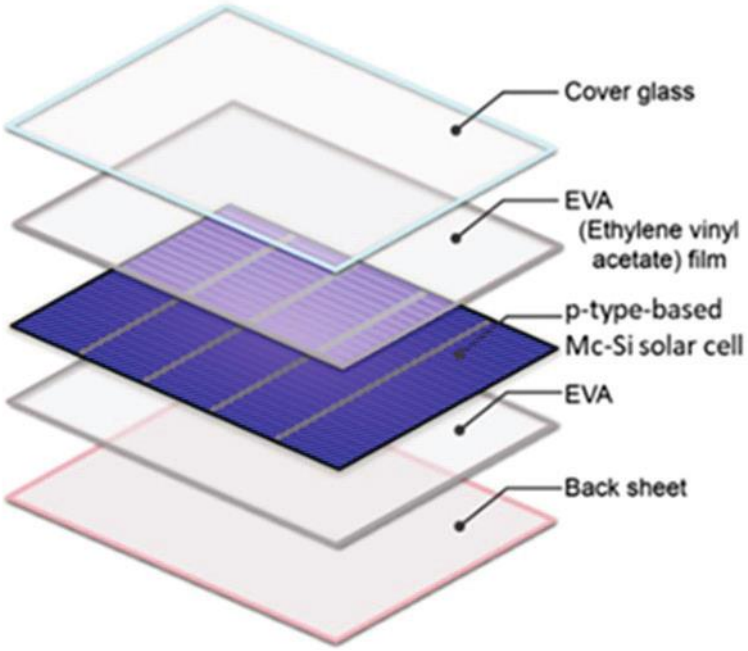

Fig.2.1 Schematic diagram of a one cell PV module and its components [86].

(a) Cover glass

Soda-lime glass with a thickness of 3.3 mm is used as a cover glass of PV module to protect solar cells from chemical and physical degradation caused by wind, rain, snow, hail, dust, sand and so on. The bottom side of cover glass has a rough surface to avoid a formation of bubbles between the cover glass and EVA during the lamination process. It is also important that glass should include low iron content because irons lead to absorption of light in the glass [16]. The cover glass needs to offer low reflection, high transmission, and high strength for safety reason. In this study, cover glasses with the sizes of 18 × 18 mm^2 or 180 × 180 mm^2 from AGC were used depending on the experiments. Specific and detailed explanation of cover glass used in this study was summarized in [87].

(b) Encapsulant

EVA is the abbreviation for the ethylene vinyl acetate which is a thermoplastic polymer that possess good radiation transmission and low degradability to sunlight. EVA sheet is a milky-white colored rubbery substance and a key material to bond between cover glass, a solar cell and back sheet layer. EVA sheet prevents air and moisture from reaching solar cells and degrading it. EVA sheets are transparent and flexible, have excellent durability and water resistances. In this study, EVA sheet with the size of 180 × 180 mm^2 with a thickness of about 0.45 mm were used.

(c) p-type multi-crystalline Si solar cell

In this study, one cell PV module was fabricated using a multi-crystalline Si solar cell of one cell size (156 × 156 mm^2). Multi-crystalline also known as polycrystalline silicon or

poly-Si is a high purity, polycrystalline form of silicon used as a raw material by the photovoltaic and electronic industry. In solar cells, there are metallic contacts called busbars which conduct the direct current generated by the solar photovoltaic cells. These busbars are constructed from copper, coated with silver. The silver coating is necessary to enhance current conductivity (front side) as well as to lower oxidation (rear side). Perpendicular to the busbars are the metallic and thinner gird fingers also called fingers electrode which collect the generated current for delivery to the bus bars. The distance between the finger electrode is 1.4 mm.

(d) Back sheet

Back sheet is on the outermost layer of the PV module. The back sheet is designed to protect the inner components of the module, specifically the photovoltaic cell and electrical components from external stresses as well as an electrical insulator. The color of back sheet is white, and it reflects light passing through the gap between the solar cell in PV module and light transmitted through the solar cells and causes sunlight to enter the solar cells again.

(e) Laminator

A laminator is a device that heats PV module components in a vacuum and seals it by pressure. To laminate a PV module, two layers of EVA are used in the following sequence: glass/ EVA/ solar cell/ EVA/ back sheet. During lamination process, the 5-layers are placed in the lamination machine and heated to maximum temperature about 135 °C or a period of approximately 15 minutes. The vacuum laminator used in this study

was shown in Fig.2.2. Figs.2.3 and 2.4 show a photo image of a one cell PV module and cross-sectional structure of the PV modules used in this study.

Fig.2.2 Vacuum Laminator (left chamber, right: operation panel).

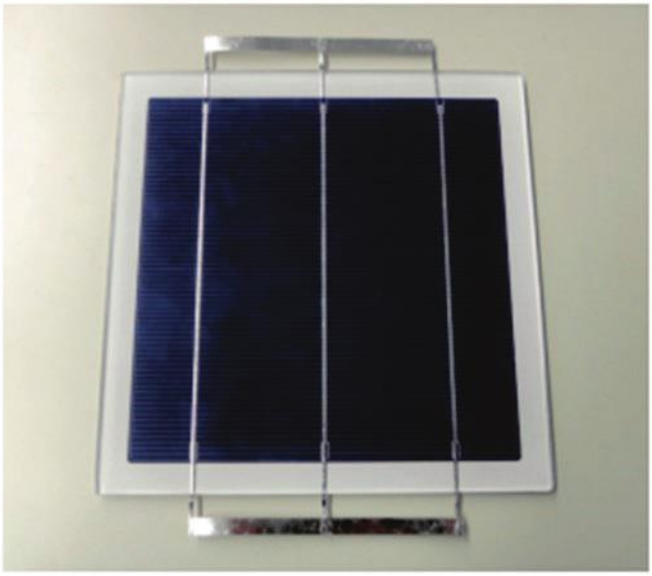

Fig.2.3 Photographic image of one cell PV module after lamination.

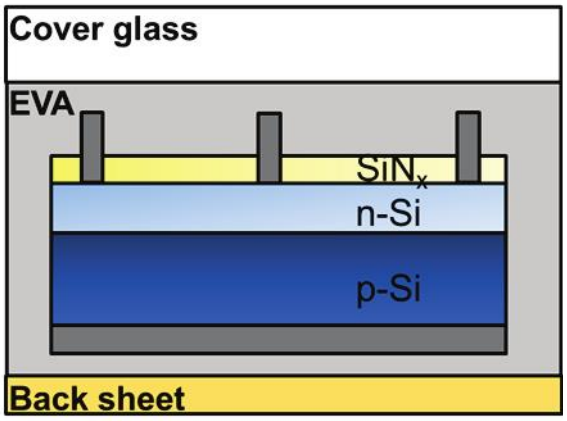

Fig.2.4 Cross-sectional image of one cell PV module after lamination.

2.1.2 Fabrication of one cell PV module with glass layer (GL)

In this study, glass layer (GL) was formed in PV modules as anti-PID technique as shown in Figs. 2.5. Cover glass coated with GL on the top side (light incidence side) and the bottom side (EVA side) were prepared to investigate the effect of GL for the suppression of PID. The starting material of GL is a chemical solution based on poly-siloxane and isopropanol called as liquid glass (Naruse Seijo). The solution of 100 μL was dropped by a pipette on a cover glass or a substrate and spread by using a tissue (Kim Wipe). Then, the liquid glass is solidified into a GL by keeping in air at room temperature (RT) for 24 h. The cover glasses with GL were used to prepare one cell PV module by a vacuum lamination method as explained in section 2.1.1. Photo image of chemical solution and drying process of liquid glass at RT was shown in Fig. 2.6.

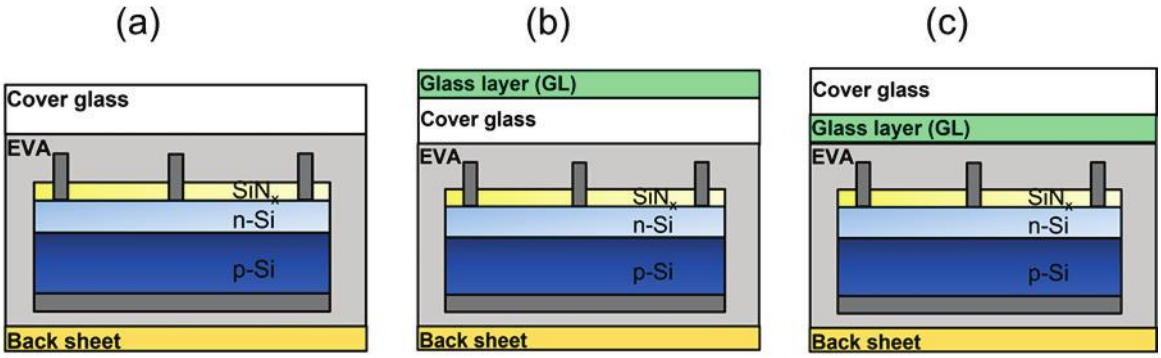

Fig.2.5 Cross-sectional images of one cell PV module: (a) without glass layer, (b) with glass layer at the top side of cover glass and (c) with glass layer at the bottom side of cover glass.

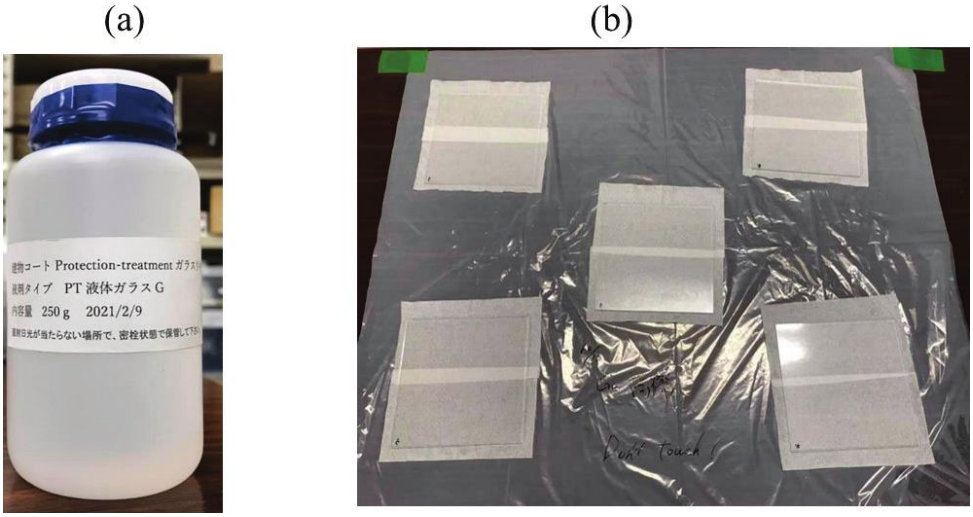

Fig.2.6. (a)Photographic image of liquid glass solution and (b)Solidification of liquid glass solution into glass layer on the top and bottom side of cover glass by keeping at RT.

2.2 PID tests and PID recovery tests

2.2.1 PID tests by Al plate method

PID acceleration tests were conducted on PV modules using the Al-plate method [39,46,57]. High stress voltages of −1000 V were applied between the electrically shorted interconnector ribbons, terminates, of the PV modules and the grounded Al plate placed on the light incidence side of the cover glass. A conducting rubber film was used for uniform electrical contact between the cover glass and the Al plate. During PID acceleration tests, the PV modules were placed in an electric furnace and the module temperature was kept at 85 °C by using apparatuses as shown in Fig.2.7. The degradation rate of each PV module was controlled by changing the duration of the HV application time of PID tests. Polytetrafluoroethylene (PTEF) was attached to prevent the inclusion of water vapor into the PV modules during the PID acceleration tests.

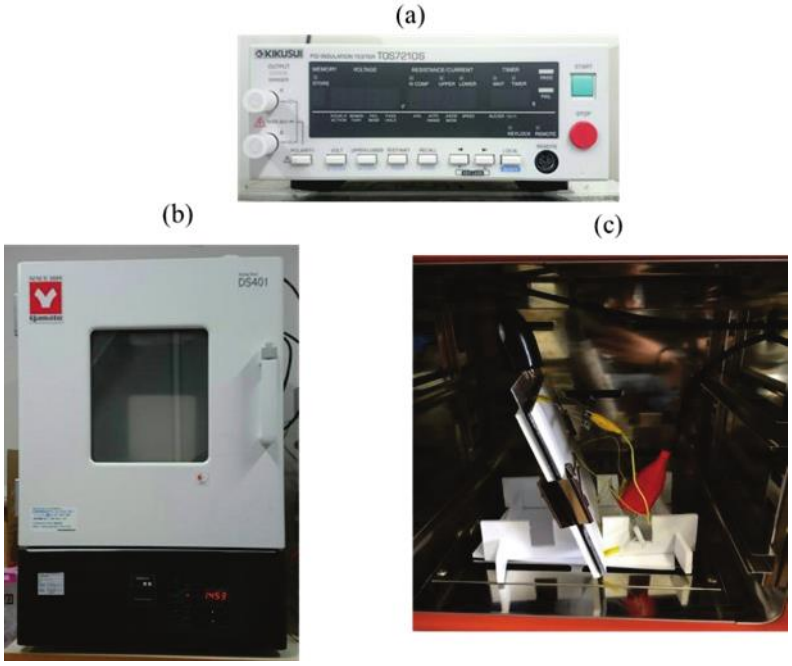

Fig.2.7 Photographic images of PID acceleration test by Al-plate method. (a) PID insulation test, (b) constant temperature dryer, (c) one cell PV module inside of constant temperature dryer for PID test.

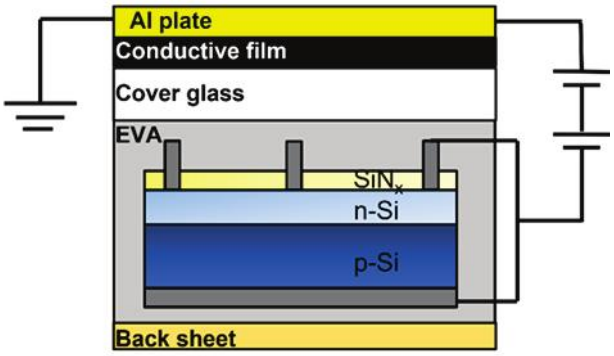

Fig.2.8 Schematic diagram of PID test by Al-plate method.

2.2.2 PID recovery test by the application of high voltage (HV)

In the case of the recovery test using HV which is conventional recovery method, a positive voltage of +1000 V was applied between electrically shorted electrodes of PV modules and grounded Al plate on the light incidence side of the cover glass [39,46]. Recovery using HV was conducted at 85 ℃, whereas the relative humidity was kept below 2%. High voltage application time might be taken from a few hours to several hours [39,46]. Note that the sign of voltage applied for the PID recovery test were opposite to that for PID test. Schematic setup of the PID recovery test is shown in Fig. 2.9.

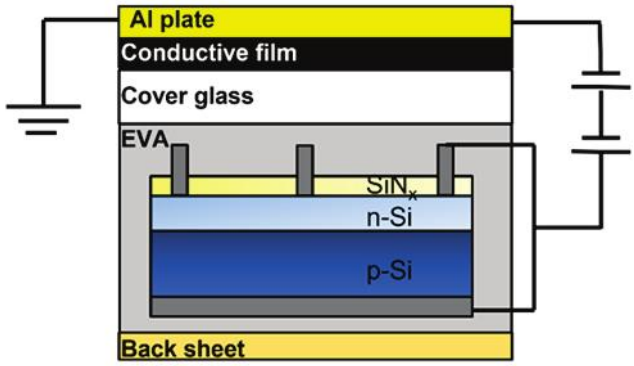

Fig.2.9 Schematic diagram of PID recovery test by using HV method.

2.2.3 PID recovery test by the application of reverse bias voltage (RV)

In the case of the recovery process using reverse bias voltage (RV), DC voltages were applied to the p-n junction of a solar cell in reverse direction. Reverse bias, V_R, were applied in the range from -6 to -19 V between the electrodes of the PV modules at room temperature environment. RV application time, t_R was varied from 10 to 600 min. The p-layer and n-layer

electrodes of a solar cell were directly connected with positive and negative terminals of DC stabilized power supply as shown in Fig.2.10. For the application of RV, a DC stabilized power supply (TEXIO PSW – 360 L80) was used, connected to a PC, and controlled with function of excel software. The value of voltage and current were set to appropriate values and intermittently applied as recovery process. Note that characterization of the PV modules was conducted after each RV application after the PV modules were cooled down to room temperature.

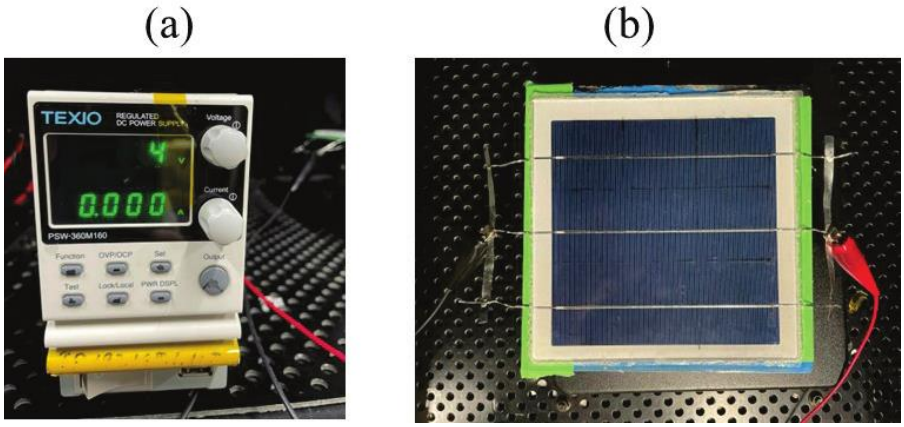

Fig.2.10 Photographic images of PID recovery by HV method. (a) A DC stabilized power supply and (b) one cell PV module under reverse bias application at RT.

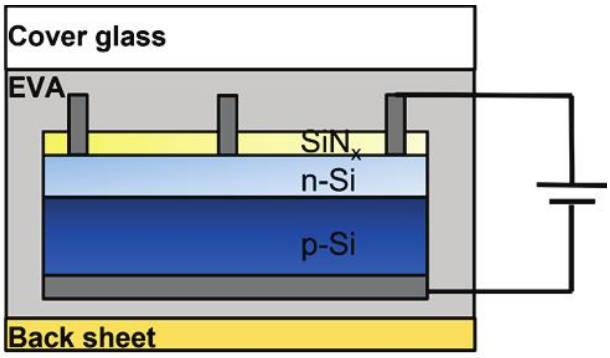

Fig.2.11 Schematic diagram of PID recovery test by using RV method.

2.3 Resistance measurements

2.3.1 RT resistance measurement system

To investigate the influence of glass layer formations on the cover glass, the resistances were measured as a leakage current for cover glasses with and without glass layer at RT. The setup of resistance measurements at RT is schematically shown in Fig.2.12. During the measurement, conductive rubber sheets (ρ_v = 1.2×10 2 Ω cm) with the thickness of 1 mm were inserted at the top and bottom side of cover glass because of the non-flat surface structure of the cover glass. A voltage of -100 V was applied from the bottom side of cover glasses for 3 h while the electrodes pressed the cover glass together with the rubber sheets by 3 kg weight to obtain better contacts between the electrodes of the resistivity chamber and cover glass for the homogeneous voltage applications. A high resistance measurement system (ADC Corp., 5450) was used with a resistivity chamber (ADC, 12702B) in a Faraday cage as shown in Fig.2.13.

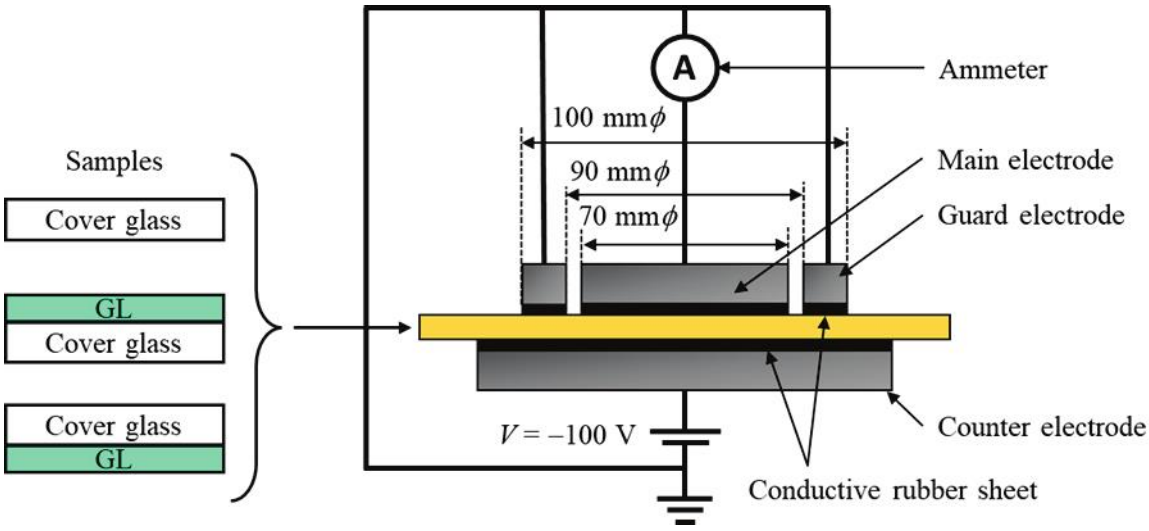

Fig.2.12 Schematic diagram of RT resistance measurement system.

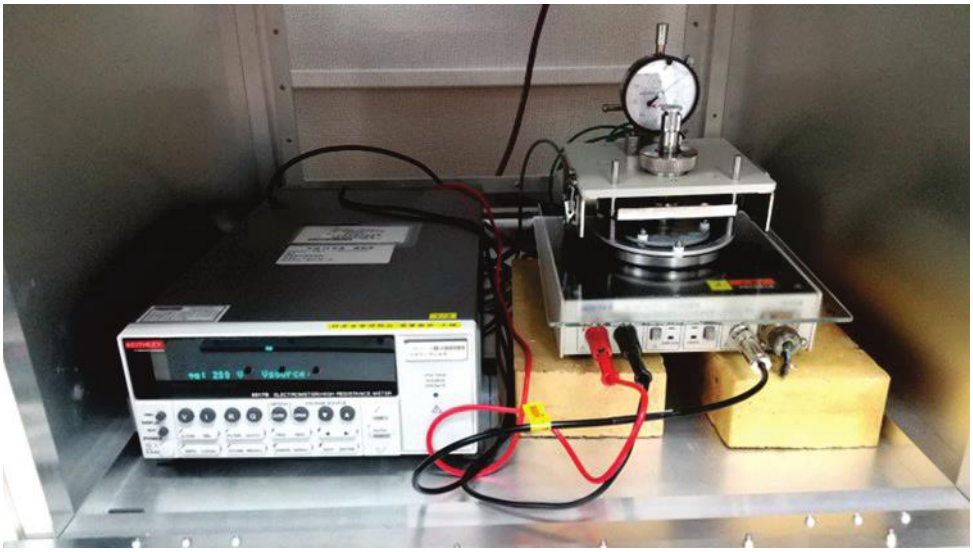

Fig.2.13 Photographic image of RT resistance measurement system with a resistivity chamber inside a Faraday cage.

2.3.2 Resistance measurement with PID test system

To investigate the effects of the GL insertions in PV modules as the anti-PID technique, the resistance between the Al plate and the electrode of solar cell was measured by using a function of the insulation resistance measurement system with a data logger during the PID tests. Schematic diagram of resistance measurement during PID test system was shown in Fig.2.14.

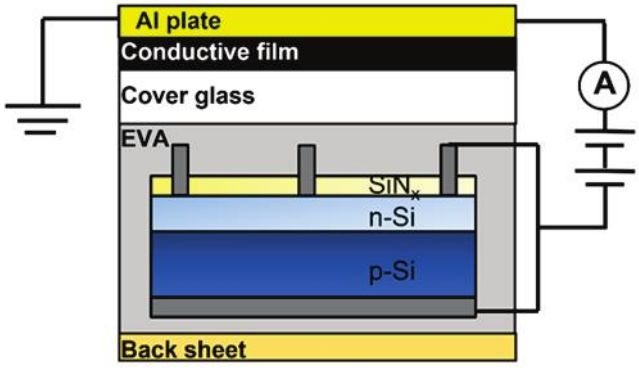

Fig.2.14 Schematic diagram of resistance measurement with PID test system.

2.4 Characterization methods

2.4.1 Photo *J-V* measurement

Photo *J-V* characterization was carried out with the use of a solar simulator (YSS-50A, Yamashita Denso Co., Ltd.). A solar simulator is a device that irradiate the artificial sunlight by using xenon as a light source. The current and voltage of the solar cell during light irradiation were measured under computer control using an automatic measurement program constructed by programming software LabVIEW. DC voltage current source (R6243) manufactured by ADVANTEST was used as a voltage source. All measurements were carried out at standard test conditions (STC). This means, that the total irradiance on the solar cell is equal to 1000 W/m^2. Further, the spectrum should resemble the AM 1.5 spectrum. Additionally, the temperature of the solar cell should be kept constant at 25 °C. Photo *J-V* characterization measurement system set up was shown in Fig.2.15. Each parameter of solar cell under light irradiation such as J_{SC}, V_{OC}, FF, η is already explained in section 1.1.2.

Fig.2.15 Photographic image of a solar simulator used in this study.

2.4.2 Dark *J-V* measurement (Leakage current measurement)

Leakage current was measured to estimate the leakage resistance, R_L, from the slope of the dark *J–V* measurements in the range from − 0.5 to 0 V. Note that, in this study, we investigate the recovery phenomena of PV modules by applying voltages to the p-n junction. Therefore, shunt resistance was not employed to characterize the p-n junction because the photo *J–V* measurements of PID-affected PV modules could also possibly induce partial recovery of the PV characteristics.

2.4.3 Electroluminescence imaging (EL imaging)

Electroluminescence (EL) imaging technique is a powerful photographic diagnosis tool to provide spatially resolved information about the electronic material properties of solar cell [89-91]. EL testing brought to the attention of the PV community by Fuyuki and his co-workers in 2005, has become a very popular technique for inspecting PV modules minority carrier lifetimes [92], micro cracks, shunts, and a voltage difference [93]. EL principle is based on the radiative recombination of excited charged carrier when forward bias is applied. The luminescence intensity depends exponentially on the energy separation of the electron and hole Fermi level in the bulk material. Hence, the output of luminescence imaging is the local lifetime distribution or the diffusion length. In this study, EL imaging is used to identify module failures and defects such as cell cracks, disconnected cell areas, broken ribbons and fingers, increased series resistance regions, PID, shunted cells, humidity corrosion, or cell manufacturing defects. In this study, Nikon D70) camera was used for taking the electroluminescence images of PV module and DC power supply source of TEXIO, PSW-

360M160 was used as a voltage and current supplier. A typical set up for EL imaging was shown in Fig.2.16, and the photo and EL images of one cell PV modules is shown in Fig. 2.17.

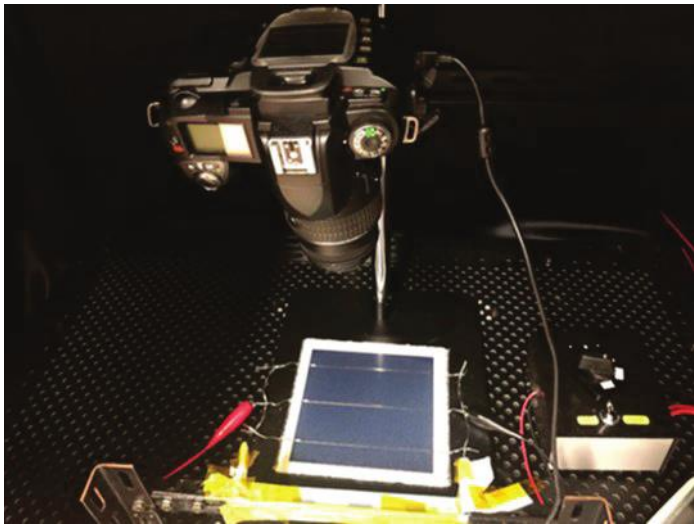

Fig.2.16 Experimental set up of an electroluminescence imaging.

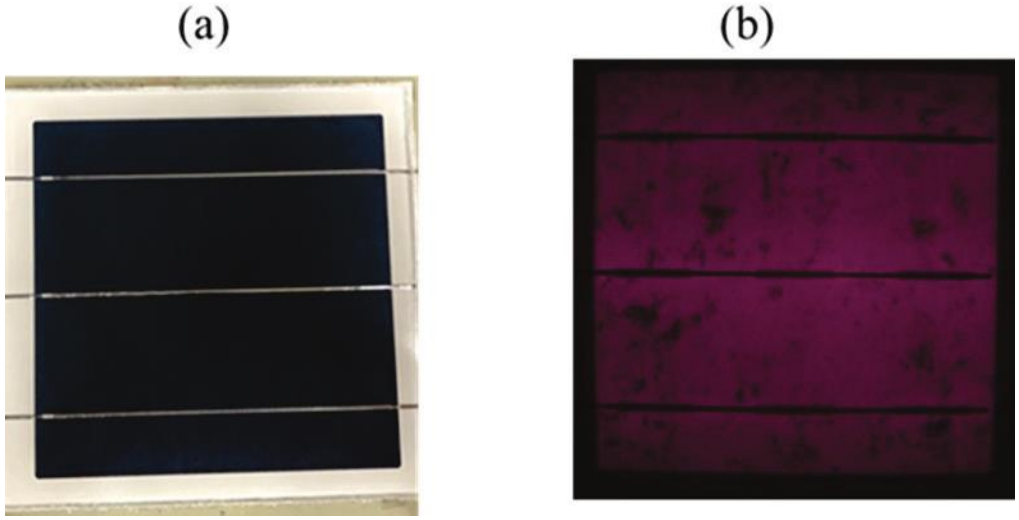

Fig.2.17(a)Optical image and (b) EL image of one cell PV module.

2.4.4 Infrared imaging (IR imaging)

Infrared thermography is an equipment which detects infrared energy emitted from object converts it to temperature and displays image of temperature distribution. It captures as a temperature distribution on a surface, and it can display as a visible information. Temperature can be measured from a distance without contacting an object in real time.

Infrared thermography has been used for detecting shunts in solar cells under reverse bias in the dark since 1990 [94]. According to the black-body radiation law, any object above absolute zero will emit infrared radiation and its characteristics can be used to measure the temperature. Therefore, infrared measuring devices acquire infrared radiation emitted by an object and transform it into an electronic signal [95]. The detected radiation from the objects can be images from IR camera and abnormalities in the temperature of the objects can be observed. In this study, infrared thermography was used as a tool for better understanding of the various degradation mechanisms and their impact on the thermal behavior of PV modules. Surface temperature variation of PV module during the application of reverse DC bias was captured by using an infrared thermography camera (R300-SR-H, Nippon Avionics Co., Ltd.). Fig.2.18 shows the infrared image of the one cell PV module used in this study.

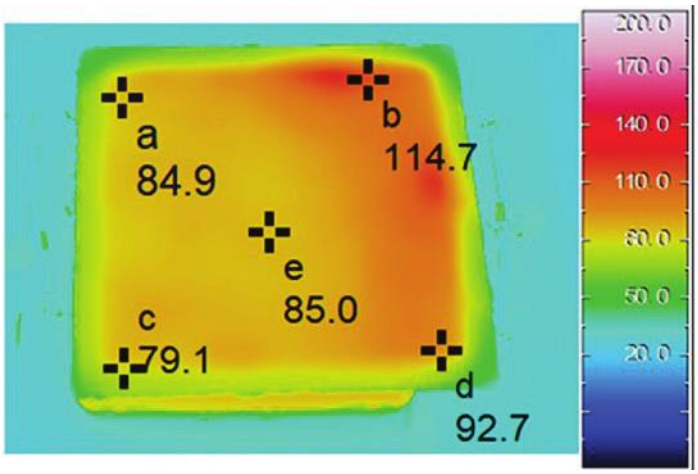

Fig.2.18 Infrared image of one cell PV module.

2.4.5 Scanning electron microscope (SEM)

Scanning electron microscope (SEM) is a type of electron microscope that uses an electron beam to scan the sample. The scanning electron microscope works on the principle of applying kinetic energy to produce signals on the interaction of the electrons. These electrons are secondary electrons, backscattered electrons, and diffracted backscattered electrons which are used to view crystallized elements and photons. Secondary and backscattered electrons are used to produce an image. The secondary electrons are emitted from the specimen play the primary role of detecting the morphology and topography of the specimen while the backscattered electrons show contrast in the composition of the elements of the specimen. A schematic diagram of the interaction between electron beams and the sample is shown in Fig.2.19. In the present research work, Hitachi-4300 device has been used

for the characterization of surface morphology of the GL formed on cover glass. Fig.2.20 shows the schematic diagram of a typical SEM device configuration [96].

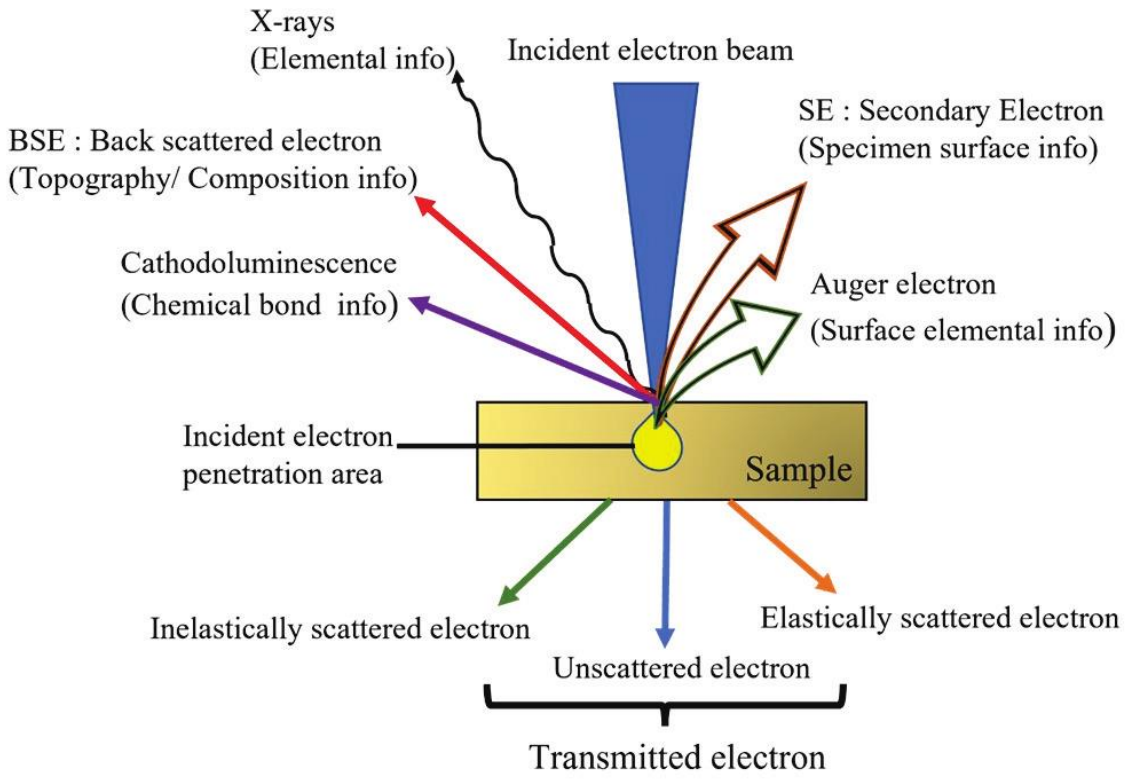

Fig.2.19 Electron sample interaction.

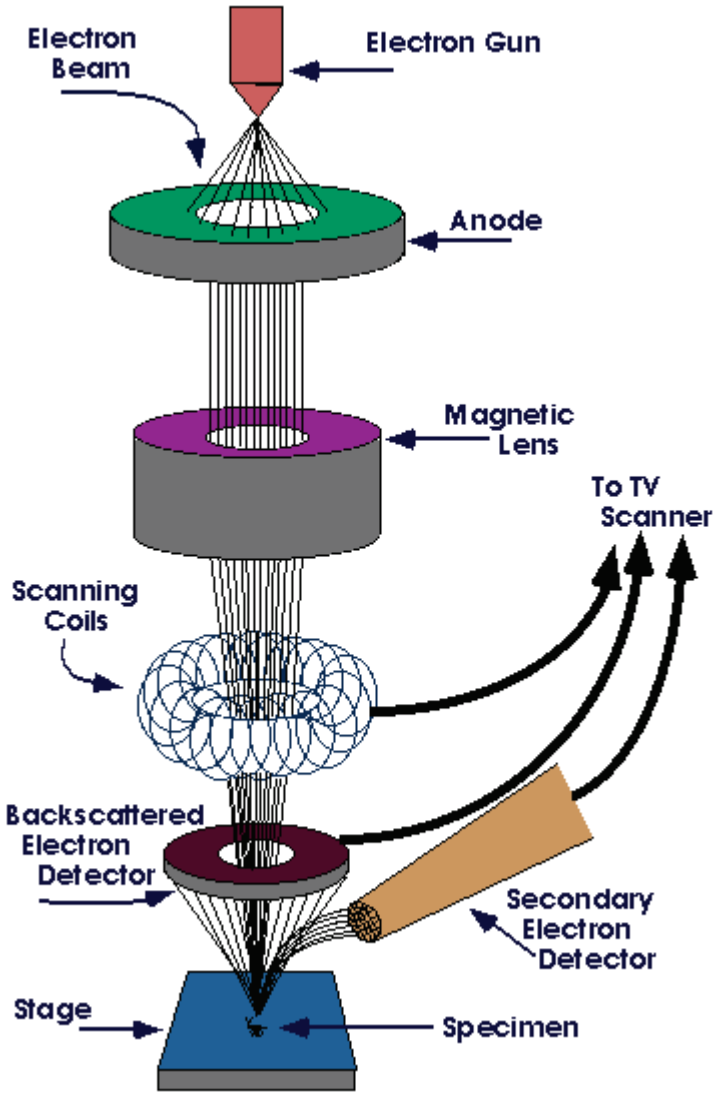

Fig.2.20 Set up of scanning electron microscope (SEM) [96].

2.4.6 X-ray photon spectroscopy (XPS)

X-ray photoelectron spectroscopy (XPS), also referred to as electron spectroscopy for chemical analysis (ESCA) is one of the most widely used surface sensitive analytical techniques in which x-rays bombard the surface of a material and the kinetic energy of the emitted electrons is measured. All materials have surfaces, and it is those surfaces that interact with other materials. Studying and understanding surfaces are important because all factors such as surface wettability, adhesion, corrosion, charge transfer, and catalysis are all determined by surface and surface contamination. All elements except hydrogen and helium can be detected, and XPS has been used to study the surface of almost every material from plastic to textiles to soil to semiconductors. The two major characteristics of XPS that make. it powerful as an analytical method are its surface sensitivity and its ability to reveal chemical state information from the elements in the sample.

XPS is based on the photoelectric effect, first discovered by Heinrich hertz in 1887. In XPS, the sample is irradiated with soft x-rays (energies lower than ~ 6 keV) and the kinetic energy of the emitted electrons is analyzed as shown in Fig.2.21. The emitted photoelectron is the results of complete transfer of the x-ray energy to a core level electron. This is expressed mathematically in Eq 2.1.

$$h\nu = BE + KE + \Phi_{spec} \quad (2.1)$$

$$BE = h\nu - KE - \Phi_{spec} \quad (2.2)$$

It simply states that the energy of the x-ray is equal to the binding energy (BE) of the electron (how tightly it is bound to the atom/orbital to which it is attached.), plus the kinetic

energy (KE) of the electron that is emitted, plus the spectrometer work function, a constant value. To determine the binding energy of an electron, Eq. (2.1) can be rearranged to obtain Eq. (2.2), where the terms on the right are either known ($h\nu$ and Φ_{spec}) or measured in the XPS experiment (KE),

Note that the photoelectron binding energy is measured with respect to the sample Fermi level (not the vacuum level) which is the reason that Φ_{spec} is included. Photoelectron peaks are notated by the element and orbital from which they were ejected. For example, "O 1s" describes electrons emitted from the 1s orbital of an oxygen atom. Any electron with a binding energy less than the x-ray source energy should be emitted from the sample and observed with the XPS technique. The binding energy of an electron is a material property and is independent of the x-ray source used to eject it. When experiments are performed with different x-ray sources, the binding energy of photoelectrons will not change; however, the kinetic energy of the photoelectrons emitted will vary as described by Eq. (2). The detailed description of instruments components is summarized in [97].

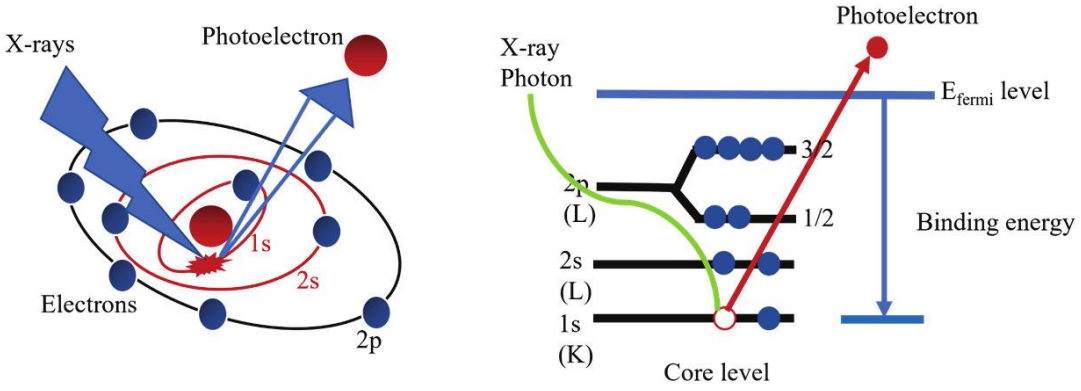

Fig.2.21 Working principle of XPS.

2.4.7 Laser microscopy

Laser microscope uses laser illumination to generate high-resolution, high-contrast 3D imagery of samples by scanning them point by point. Two common types of laser scanning microscopes include confocal laser scanning microscopes and multiphoton laser scanning microscopes. Confocal laser scanning microscope is commonly used for various observations and analyses such as surface roughness, three-dimensional shape and so on. In this study, a 3D Laser scanning microscope (Keyence, VK-X200K) was used to estimate the thickness of transparent glass layer formed on the surface of cover glass.

2.4.8 UV-vis spectroscopy

The principle of UV-vis spectroscopy is based on the absorption of ultraviolet light or visible light by chemical compounds, which results in the production of distinct spectra. Spectroscopy is based on the interaction between light and matter. When the matter absorbs the light, it undergoes excitation and de-excitation, resulting in the production of a spectrum.

UV-Vis spectroscopy is a type of absorption spectroscopy in which a sample is illuminated with electromagnetic rays of various wavelengths in the ultraviolet (UV) and visible (Vis) ranges. Depending on the substance, the UV or visible light rays are partially absorbed by the sample. The remaining light, i.e., the transmitted light, is recorded as a function of wavelength by a suitable detector. The detector then produces the sample's unique UV-vis spectrum (also known as the absorption spectrum). In this study, UV-3100 PC was used to analyze the transmittance of GL. The detailed explanation concerning with UV-vis spectrum were presented in [99].

Chapter 3
Development of recovery method for PID-affected PV module by the application of reverse bias voltage (RV)

Development of a recovery method for PID-affected PV modules is a key issue to extend the lifetime of PV modules and to minimize power generation costs. In this chapter, a detailed analysis of the recovery process by the application of reverse bias voltage (RV) to the p-n junction of PID-affected PV modules was presented. To understand conventional recovery on PID-affected PV module occurred by using high voltage (HV), analysis of recovery phenomena by the application of HV was presented in section 3.1. Influenced by the recovery tests with the application of various reverse bias voltage (RV) and duration were explained in section 3.2. Recovery model by RV method was proposed in section 3.3. Conclusions of this chapter is presented at section 3.4.

3.1 Recovery test by using HV method

To understand the differences in the recovery methods, recovery by using HV method was conducted as a conventional recovery process. Fig.3.1 shows photo *J-V* characteristics before and after the PID test and after recovery test by HV method. Parameters such as J_{sc}, V_{oc}, FF and η which were obtained from photo *J-V* curve, and R_{leak} which was obtained from dark *J-V* characteristics were summarized in table 3.1. PID test was carried out for 30 min by Al-plate method (as explained in Chapter 2). A decrease in η was observed mainly with the decrease in V_{oc} and FF. This suggests that PID was occurred on the PV module by PID test.

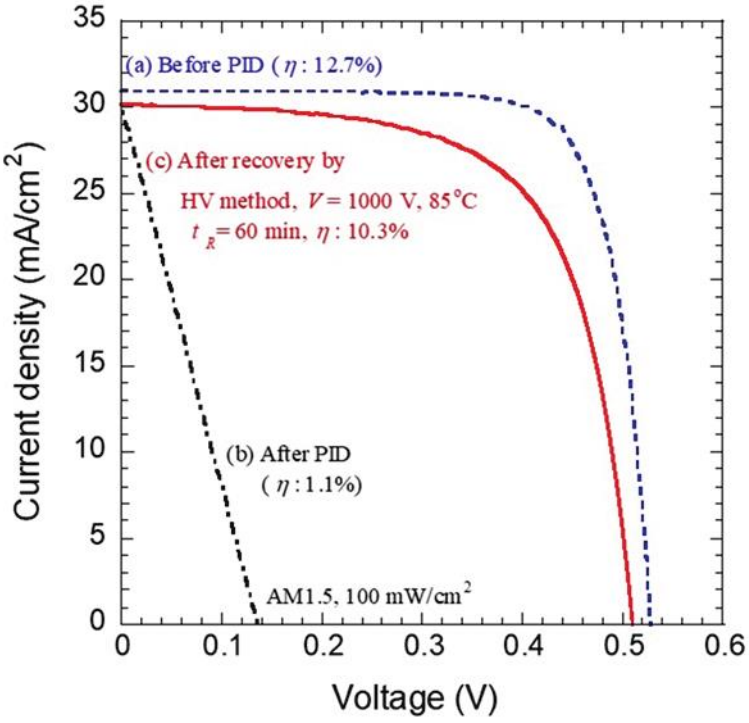

Fig.3.1 Photo *J-V* characteristics for a one cell PV module (a) before and (b) after PID acceleration test and (c) after recovery test by HV application for 60 min.

Table 3.1 Summary of photo *J-V* and dark *J-V* parameters of one cell PV module under applied voltage of + 1000 V at 85 ℃ for 60 min.

Condition	*J*sc(mA/cm^2)	*V*oc (V)	FF	η(%)	%η_D(%)	%η_R(%)	R_{leak}(Ω)
Before PID	30.33	0.56	0.77	12.7	-	-	2000
After 30 min PID	30.15	0.25	0.29	1.1	8.7	-	0.5
After 60 min recovery	30.21	0.55	0.71	10.3	-	81	3.8

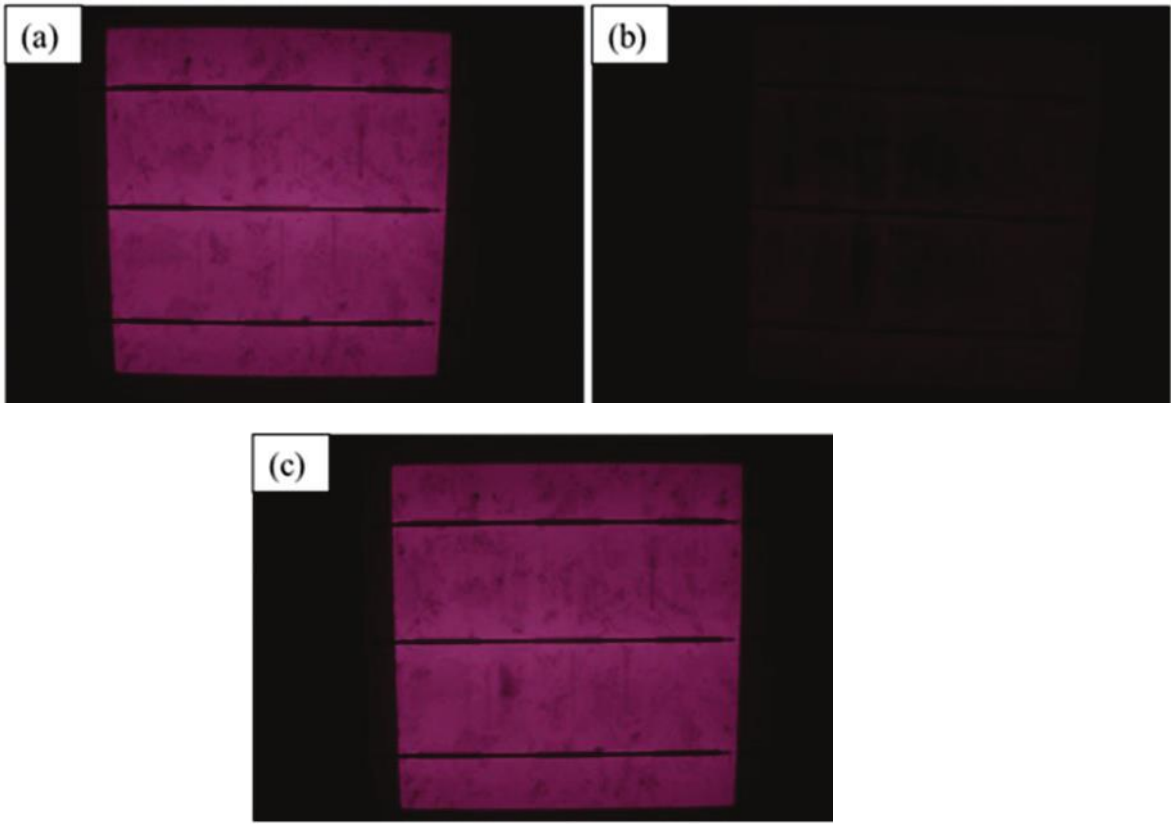

Fig.3.2 EL images before and after the PID test and after recovery test by the application of HV for 60 min.

Fig.3.2 shows the EL images of PV module before and after the PID test and after the recovery by using HV method. Darkening of the EL image appeared after the PID test suggests the weak photovoltaic phenomenon appeared by the degradation of solar cell after the PID test. After the recovery process by HV method, the EL images became brighter and is suggesting the photovoltaic effects of solar cells was recovered by the HV method.

3.2 Evaluation of the effect of recovery by RV method

As already explained in section 1.3.2, Jonai *et al*.,[57] conducted recovery test by the application of a RV in the range of from – 20 V to – 30 V. We focused the phenomena as a low-cost recovery method because of the low-voltage application in a short time without the necessity of temperature controls by the furnace. However, the detailed analysis of recovery phenomena by using the RV is still not reported. In this section, details analysis regarding with recovery by the various RV application are shown. Recovery tests were caried out by the application voltage of – 6 V, – 10 V, – 17 V and – 19 V. RV application time t_R was also varied up to 600 min to understand the time dependence of the recovery phenomena.

3.2.1 Analysis on photo *J-V* parameters by using various RV applications

To analyze the effect of the application of various RV on PID-affected PV module, recovery tests were carried out to four PV modules. The RVs were limited up to V_R = – 19 V to avoid breakdown of the p-n junction of solar cells. The duration of voltage application time t_R was changed from a few minutes to 16 hours to analyze the increases of the module temperature by RV application [57].

Fig.3.3 (a)-(d) show photo *J-V* before, after PID tests and after recovery tests with various RV applications under the illumination of light of AM 1.5. By the application of V_R = – 19 V, recovery with $\%\eta_R$ = 90 % was observed after t_R = 5 min as shown in Fig.3.3 (a). In Fig.3.3(b), an almost complete recovery was also observed after t_R = 10 min by the

application of V_R = – 17 V. In addition, %η_R was slightly increased with t_R and reached %η_R = 92 % with t_R = 360 min. However, %η_R with V_R = – 10 V and – 6 V was 74 % and 70 % even after t_R = 360 min, respectively.

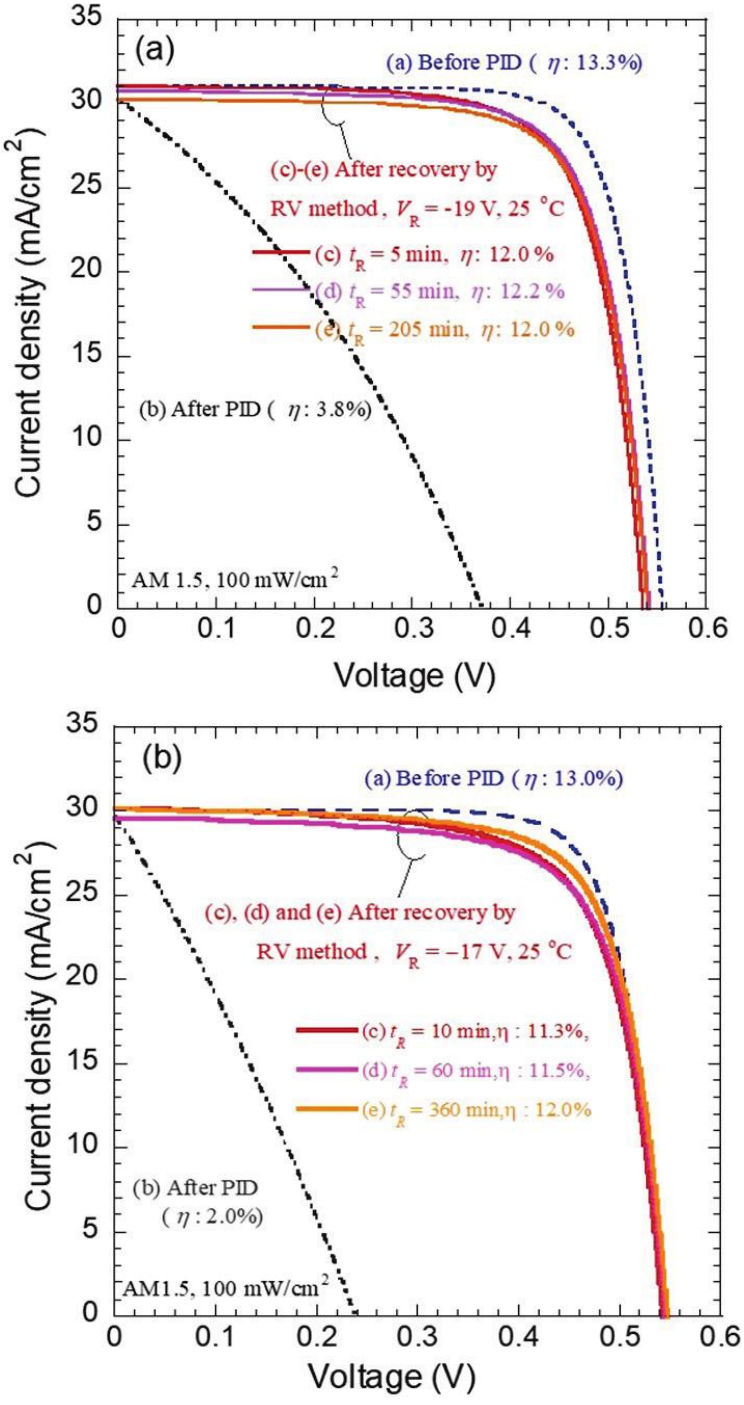

Fig.3.3 Photo *J-V* characteristics before and after PID tests and step by step recovery tests by the application of various RV. (a) Recovery test by V_R = -19 V, (b) recovery test by V_R = -17 V.

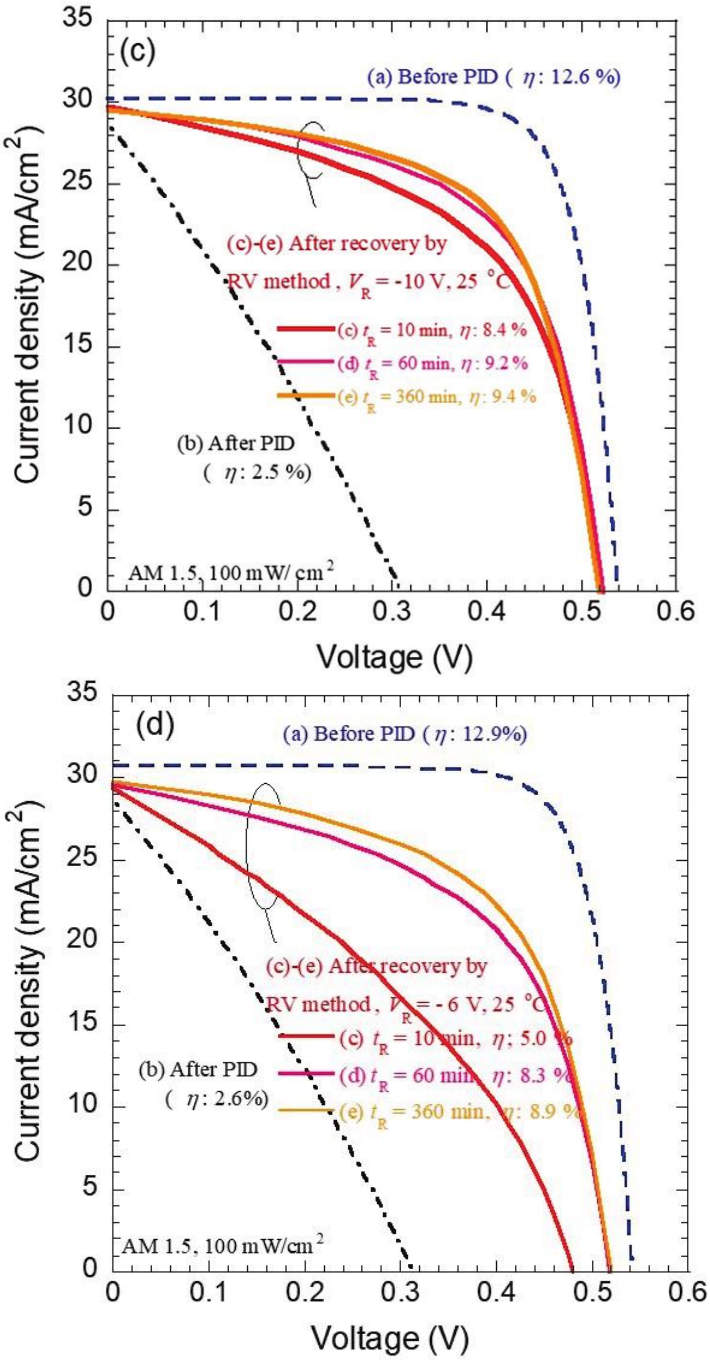

Fig.3.3 Photo *J-V* characteristics before and after PID tests and step by step recovery tests by the application of various RV. (c) recovery test by V_R = -10 V and (d) recovery test by V_R = -6 V.

Table 3.2 Summary of photo *J-V* and dark *J-V* parameters of one cell PV module obtained from the *J-V* curves shown in Fig.3.3.

V_R= -19 V	*J*sc(mA/cm^2)	*V*oc (V)	FF	η(%)	%η_D (%)	%η_R (%)	R_{leak} (Ω)
Before PID	30.9	0.56	0.77	13.3	-	-	799.7
After 90 min PID	30.7	0.37	0.33	3.8	29	-	11.8
After 5 min recovery	30.9	0.54	0.73	12.0	-	90	165.4
After 55 min recovery	30.7	0.54	0.74	12.2	-	92	205.7
After 205 min recovery	30.1	0.54	0.74	12.0	-	90	151.4
V_R= -17 V	*J*sc(mA/cm^2)	*V*oc (V)	FF	η(%)	%η_D (%)	%η_R (%)	R_{leak} (Ω)
Before PID	30.3	0.55	0.78	12.9	-	-	3230
After 90 min PID	29.81	0.24	0.28	2.0	16	-	13.5
After 10 min recovery	30.15	0.54	0.71	11.5	-	89	43.6
After 60 min recovery	30.19	0.54	0.72	11.6	-	90	64.3
After 360 min recovery	30.3	0.54	0.73	12.0	-	93	55.8
V_R= -10 V	*J*sc(mA/cm^2)	*V*oc (V)	FF	η(%)	%η_D (%)	%η_R (%)	R_{leak} (Ω)
Before PID	30.27	0.54	77.26	12.6	-	-	3333.3
After 60 min PID	28.56	0.31	28.77	2.5	20	-	0.9
After 10 min recovery	29.73	0.52	54.76	8.5	-	67	6.2
After 60 min recovery	29.59	0.52	59.83	9.2	-	73	14.1
After 360 min recovery	29.53	0.52	61.4	9.4	-	75	20.3
V_R= -6 V	*J*sc(mA/cm^2)	*V*oc (V)	FF	η(%)	%η_D (%)	%η_R (%)	R_{leak} (Ω)
Before PID	30.71	0.54	77.38	12.9	-	-	3333.3
After80 min PID	28.62	0.32	28.1	2.6	20	-	0.9
After 10 min recovery	29.34	0.48	35.54	5.0	-	39	1.9
After 60 min recovery	29.51	0.52	54.39	8.3	-	65	6.3
After 360 min recovery	29.76	0.52	57.81	8.9	-	69	11

Fig.3.4 shows time dependence of the photovoltaic parameters of PID affected PV modules with application of various V_R. t_R was ranged from 10 to 360 min. It was observed that an increase in J_{SC} appeared after a short RV application time like t_R = 10 min, whereas long RV application times resulted in a slight decrease of J_{SC} in some PV modules as summarized in Table.3.3.

When t_R was extended up to 960 min with V_R = -6 V using different PV modules as shown in Fig.3.5, further decrease in J_{SC} was observed, whereas V_{OC} did not change significantly. This suggests that long hours of RV application cause some damages to the PV module components and optical constants of the materials may have changed such as peeling off of EVA.

Table 3.3 Summary of photo *J-V* and dark *J-V* parameters of one cell PV module under recovery test by the application of V_R = -17 V up to 600 min.

V_R= -17 V	Jsc(mA/cm^2)	Voc (V)	FF	η(%)	%η_D (%)	%η_R (%)	R_{leak} (Ω)
Before PID	30.59	0.55	76.8	12.8	-	-	1227.5
After 80 min PID	28.1	0.35	32.2	3.1	24	-	13.4
After 60 min recovery	29.6	0.53	66.6	10.3	-	81	68.6
After 240 min recovery	28.71	0.53	67.6	10.2	-	80	43.1
After 600 min recovery	28.47	0.53	68	10.1	-	79	35.5

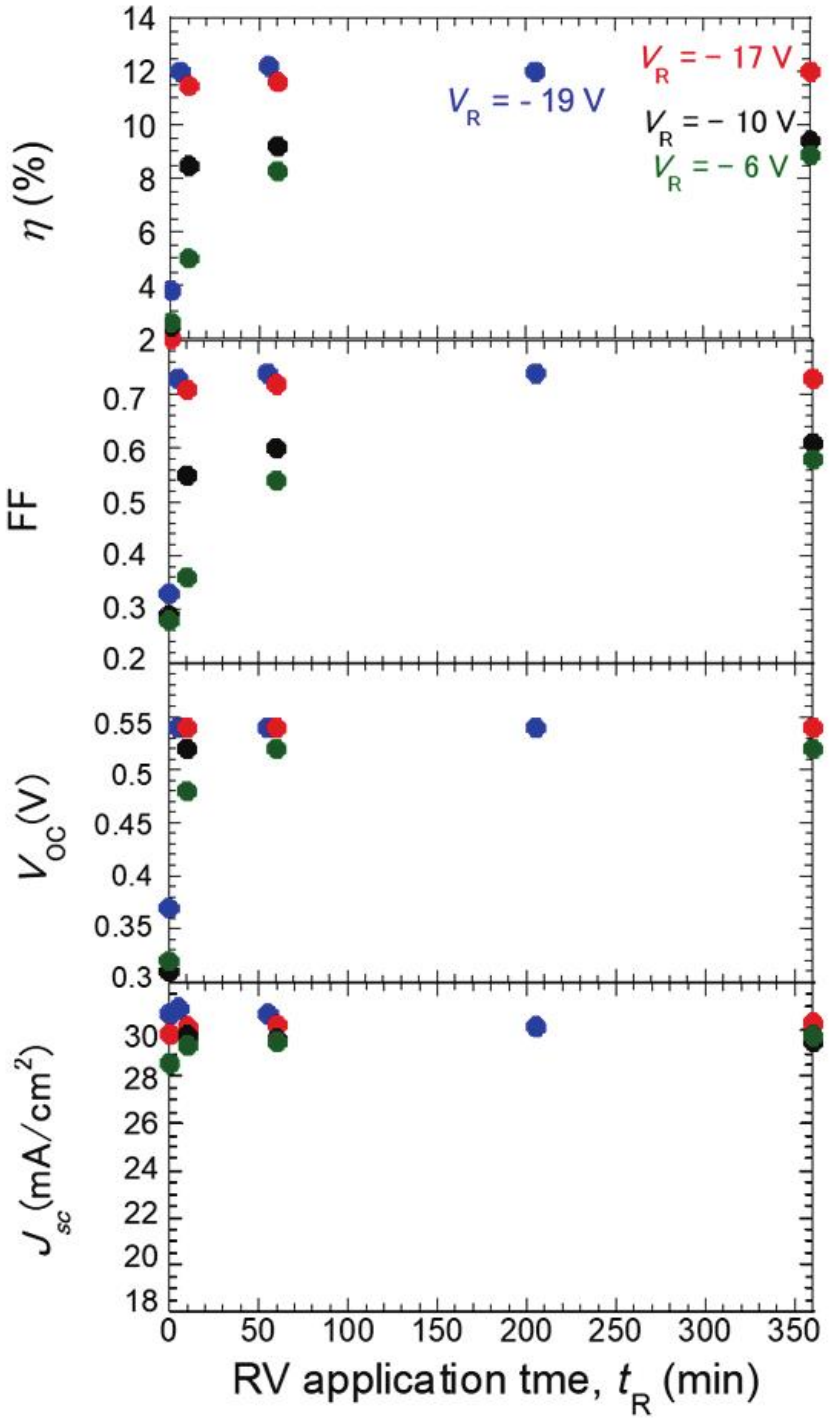

Fig.3.4 The change of photovoltaic characteristics (η, FF, V_{OC}, J_{SC}) of PV modules recovered using various V_R as a function of t_R.

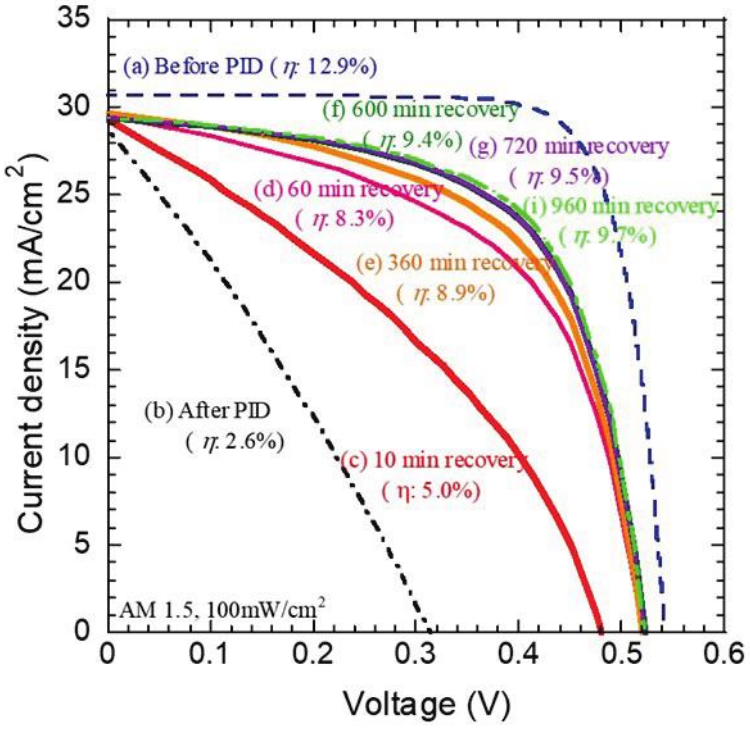

Fig.3.5. Photo *J–V* characteristics for a PV module (a) before and (b) after PID acceleration test and after recovery tests by RV application at $V_R = -6$ V, 4A with t_R=(c) 10 min, (d) 60 min, (e) 360min, (f) 600 min, (g) 720 min and (i) 960 min.

3.2.2 Analysis on dark *J-V* parameters by using RV method

Here, effect of voltage application on leakage current resistance, R_{leak} estimated from dark *J-V* characteristics was discussed. Fig.3.6 show the normalized R_{leak} value as a function of RV application time. The R_{leak} was normalized by the R_{leak} obtained before PID test. The R_{leak} before and after PID acceleration tests were 799.7 Ω and 11.8 Ω , and the R_{leak} after recovery tests using V_R = -19 V with t_R = 5, 55, 250 min were 165.4 Ω, 205.7 Ω, 151.4 Ω, respectively.

Table 3.4 shows the before and after the PID tests and after the application of RV with various voltage and application time. Under the RV application of V_R = -17 V, R_{leak} was recovered gradually until t_R = 60 min. However, when t_R = 360 min. slight decrease in the R_{leak} appeared. In the case of RV application with V_R = –10 V and – 6 V, recoveries of R_{leak} were saturated with values of below 1% of initial values. It is suggested that some of shut paths still exist in the p-n junction even after the recovery.

Table 3.4 Summary of the value of R_{leak} obtained from dark *J-V* characteristic. The unit of R_{leak} is Ω

Condition	V_R = -17 V	V_R = -10 V	V_R = -6 V
Before PID	3230	3333.3	3333.3
After PID	13.5	0.9	0.9
After 10 min recovery	43.6	6.2	1.9
After 60 min recovery	64.3	14.1	6.3
After 360 min recovery	55.8	20.3	11

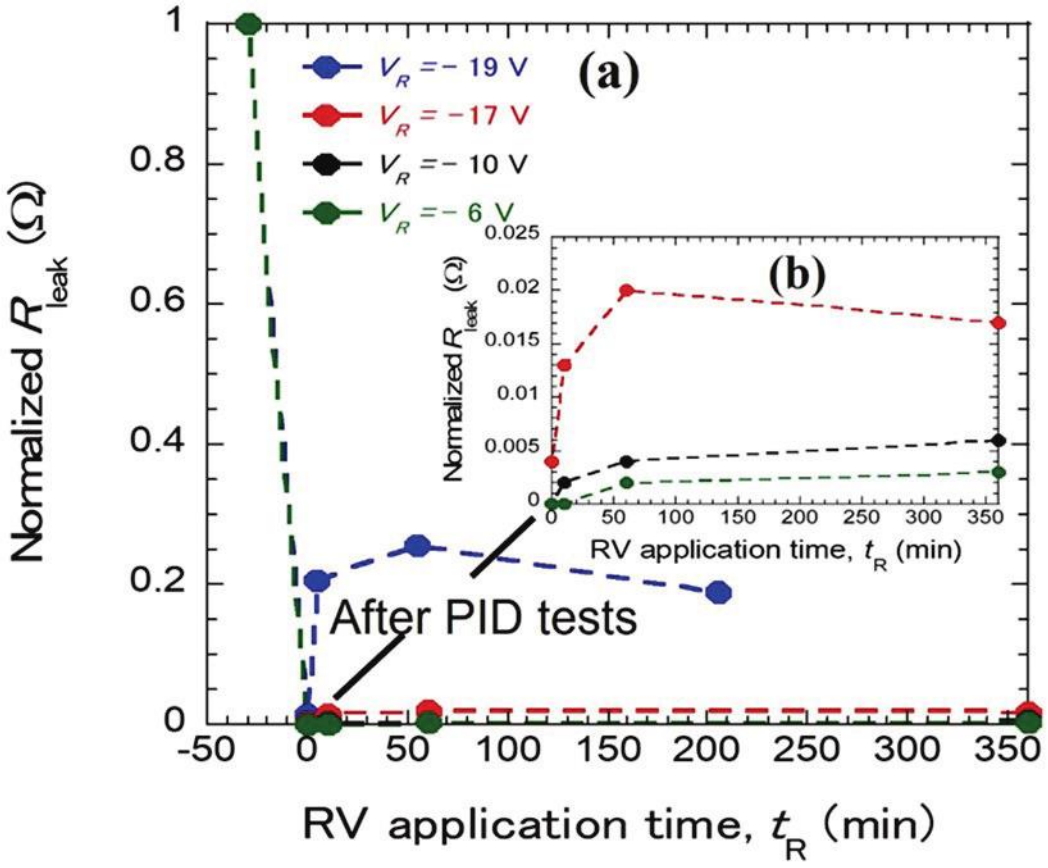

Fig.3.6 Normalized R_{leak} as a function of voltage application time after recovery tests with V_R= − 17 V for t_R = (c) 10, (d) 60, and (e) 360 min. Each initial parameter before the PID test was normalized to one.

3.2.3 EL images before and after recovery using RV method

Characterization of PV modules before and after the PID tests and after the recovery by using RV method was conducted by using EL imaging. Fig.3.7 shows the EL images before and after the PID tests and after the application of $V_R = -17$ V for $t_R = 10$, 60 and 360 min. As shown in Fig.3.7 (a) and (b), darkening of EL-illuminance was observed after the PID test, suggesting the occurrence of PID on the PV module. However, by applying RV, the El intensity is recovered to near that before the PID acceleration test, whereas no significant change in the dark spots was observed, as depicted as white circle in Fig.3.7. Similar darkening and brightening of EL images were observed after the PID test and recovery using HV method.

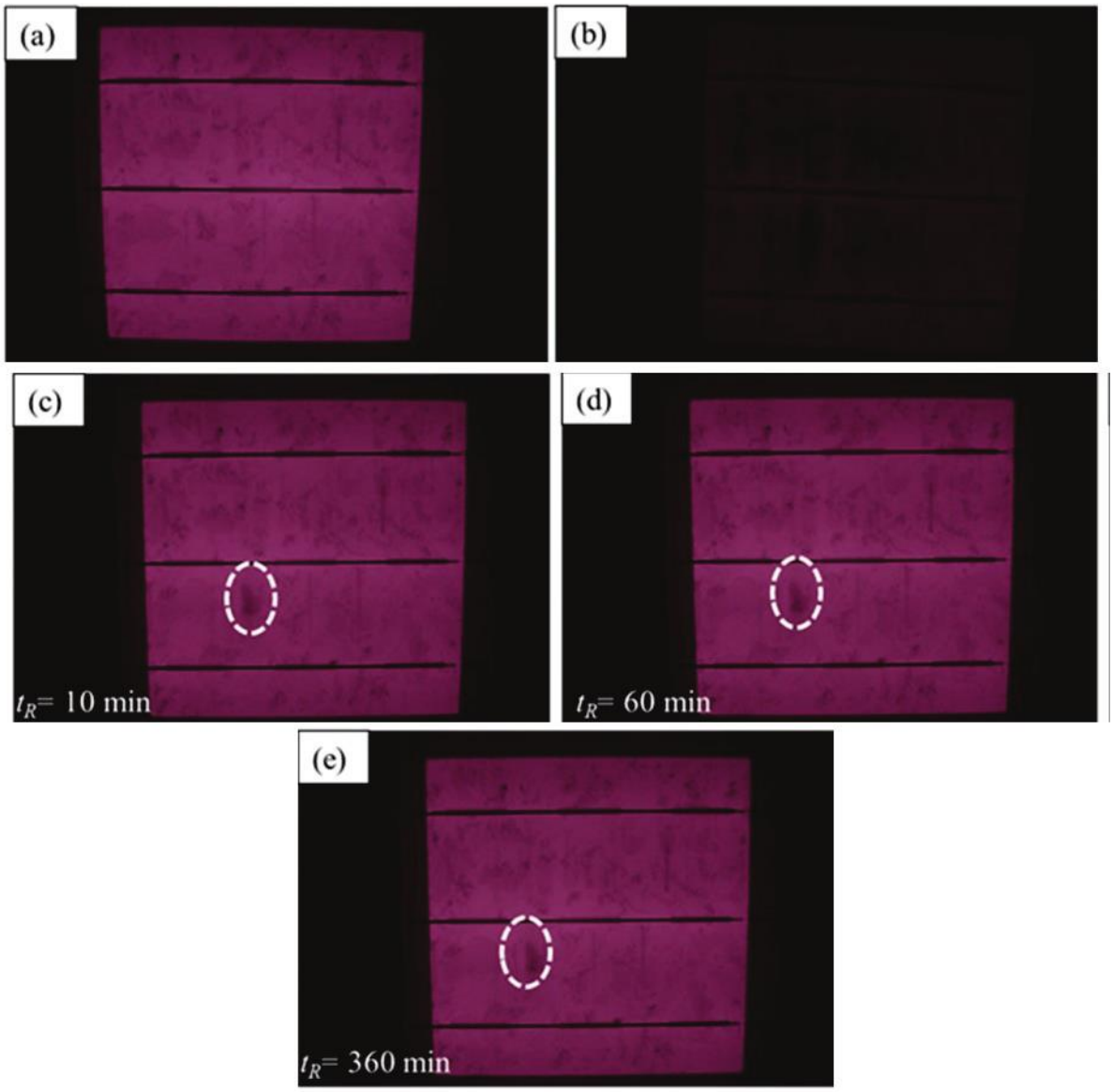

Fig.3.7 EL images of PV modules (a) before and (b) after PID acceleration tests, and after recovery tests with $V_R = -17$ V for t_R = (c) 10, (d) 60, and (e) 360 min.

3.2.4 Effect of surface temperature distribution during RV application

The surface temperature of PV modules during the recovery process using RV was analyzed using IR imaging. Fig.3.8 shows the IR images obtained by the application of V_R = -6, -10 and -17 V for t_R = 60 min. During recovery test by the application of various RV, non-uniform surface temperature distribution was observed as shown in Fig.3.8. Fig.3.9 shows the time dependence of the maximum surface temperatures of PV modules observed by the application of V_R = -6, -10 and -17 V for t_R = 10, 60 and 100 min. The maximum temperature was increased with the V_R and the temperature during recovery test reached almost 115 ℃ after 60 min recovery when the application of V_R = -17V as shown in Fig.3.9. It is also worthy to note that the higher temperature distributions area did not corresponding to the positions of the bass bar but to the edges of the solar cell. All the temperature trends showed that surface temperature was decreased after 60 min voltage application time.

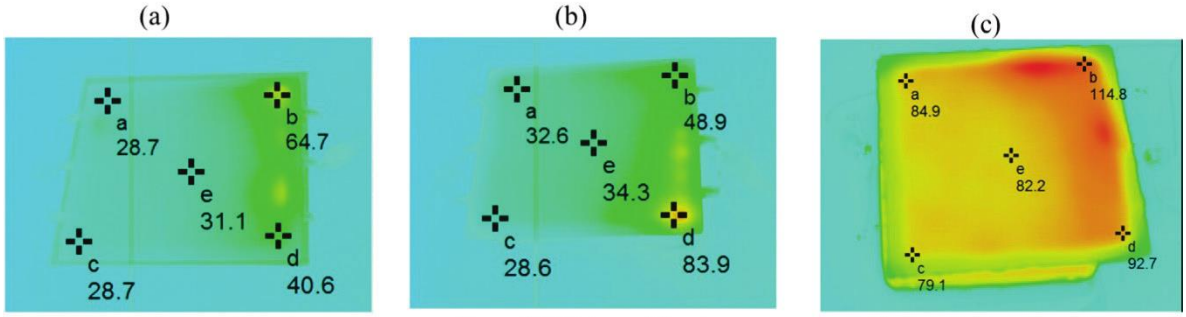

V_R = -6V, t_R = -60 min V_R = -10 V, t_R = -60 min V_R = -17 V, t_R = -60 min

Fig.3.8 Module surface temperature distribution during recovery test by various RV.

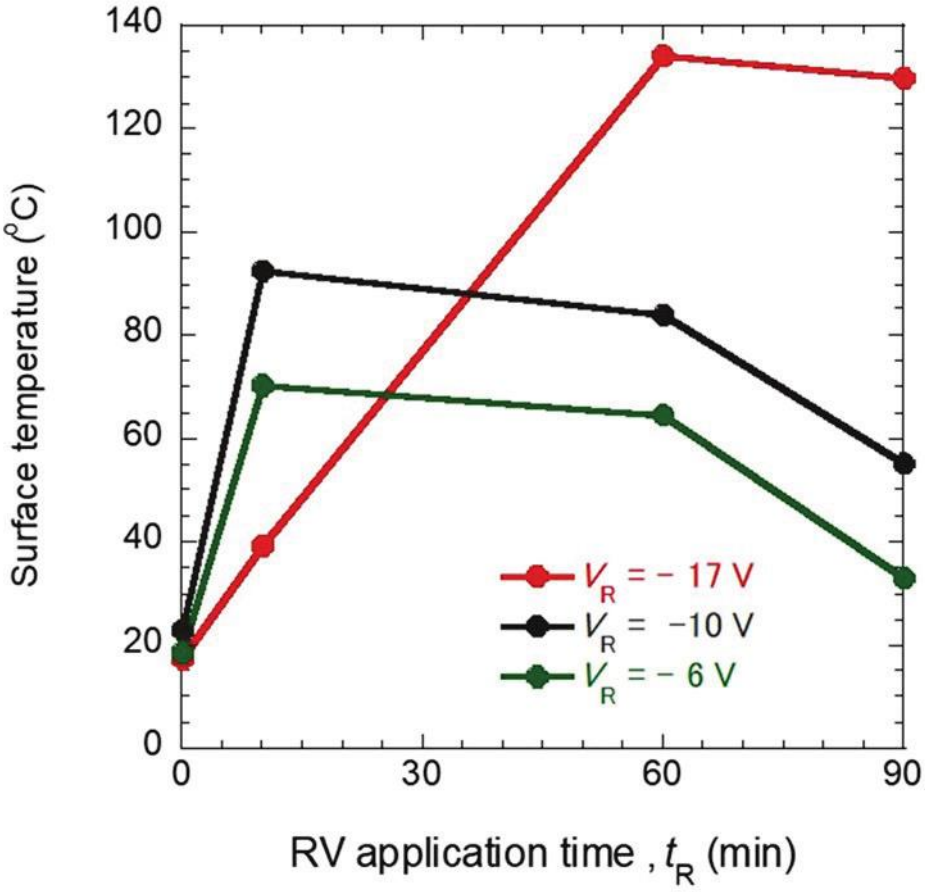

Fig.3.9 Module surface temperature distribution of PV modules during recovery tests by the application of various RV.

To analyze further the influence of RV application, the surface temperature of the PV modules was measured during RV application with and without PID tests with various V_R. Fig.3.10 shows IR images of the one cell PV module with and without PID test with the application of various V_R. Note that the points in the figure denoted by from “a” to “d” correspond to the measured points where near the edge of PV modules and the points denoted by “e” correspond to the center of PV modules. Additionally, in Fig.3.10 (b), the point denoted by a black circle corresponds to the position where the highest temperature was

observed in the PV module. In the case of one cell PV module without PID test, V_R = -17 V was applied for 60 min and no significant temperature increase was observed at all points. However, in the case of RV application on the PV modules after the PID test, distributions of surface temperature appeared as shown in Fig.3.10 (b) – (d). The surface temperature was increased with V_R.

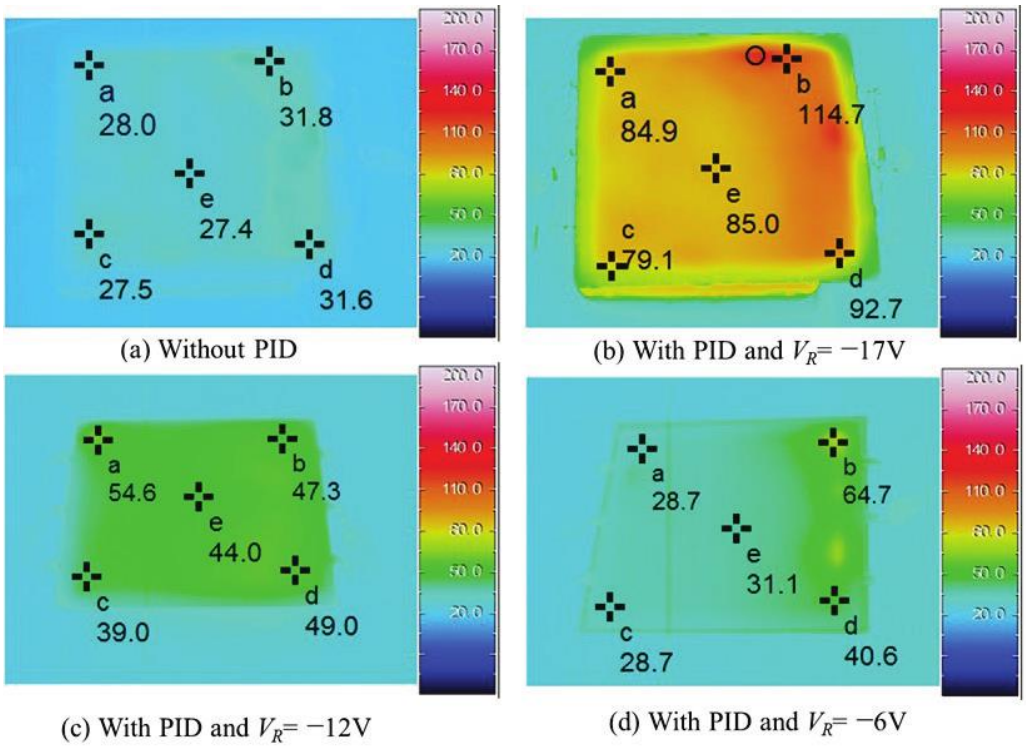

Fig.3.10 Module surface temperature distribution of PV modules with the application of RV (a) before PID acceleration test with t_R = 60 min and after PID acceleration tests with PID recovery tests at (b) V_R = −17 V, t_R = 30 min; (c) V_R = − 12 V, t_R = 30 min; and (d) V_R = − 6 V, t_R = 30 min. The black circle in Fig. 3.10 (b) is the point where the temperature reached around 130 °C.

To analyze the temperature changes depending on t_R, an additional surface temperature measurement was conducted to PID affected PV module by using V_R = -17V. Fig.3.11 shows time dependent changes of the surface temperature of PV modules obtained by thermography data at various points. In the figure, note that the points denoted from “a” to “c” correspond to near the edges of the PV module and the points denoted by from “d” to “g” correspond to the points where a few centimeters closer to the center of the PV modules than the points near the edges. An increase of surface temperature at all measured points was observed from the start of RV application, and the temperature were saturated after ~ 1500 s (25 min). Therefore, RV application to PV module is considered to induce Joule heating at the solar cells, and several tens of minutes were required to reach a stable temperature for entire PV module. Compared with the saturation time of η shown in Fig.3.4, the recovery of PV modules occurs much faster than temperature saturation at the surface of the PV modules.

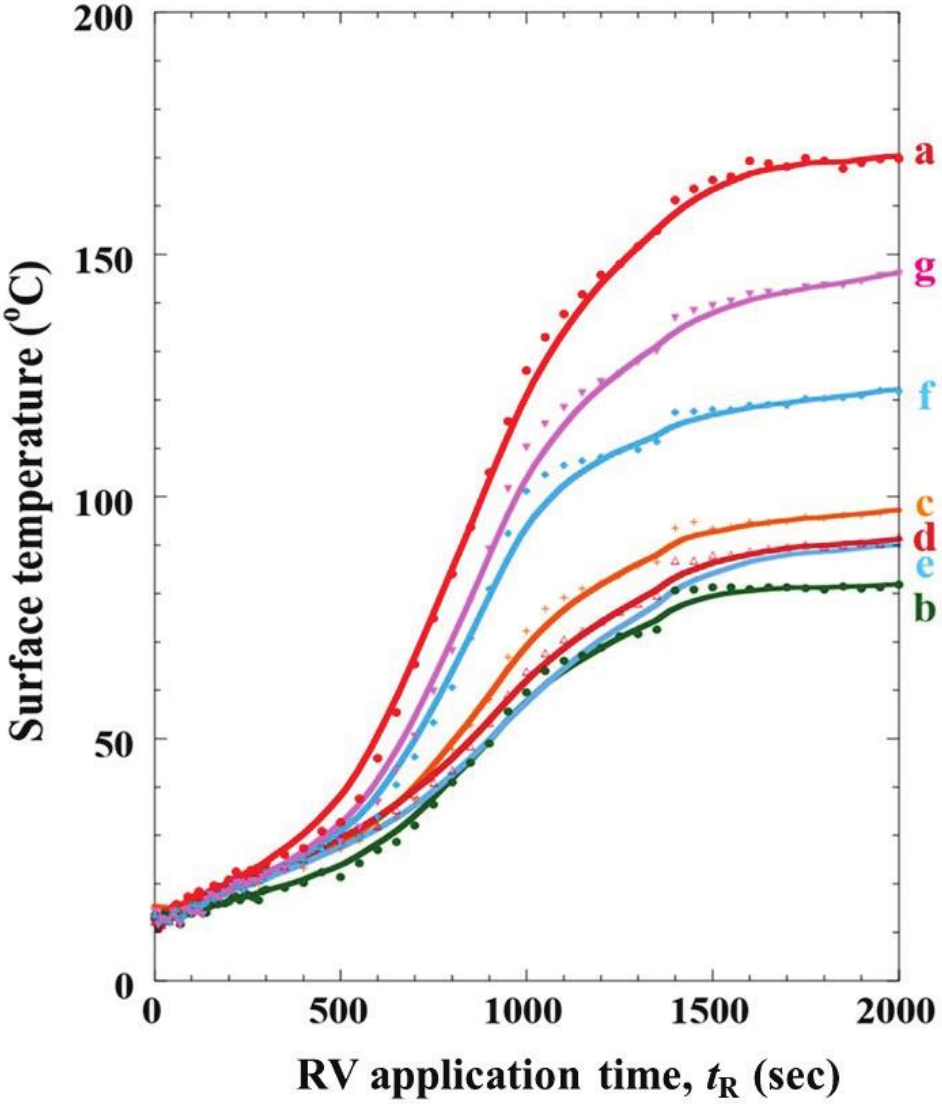

Fig.3.11 Time-dependent changes of surface temperature measured at various points on PV modules with $V_R = -17$ V.

3.3 Recovery models by HV and RV applications

In this section, the PID recovery models of PV modules by the applications of HV and RV are discussed. Fig.3.12 shows recovery models by HV and RV applications. When the HV was applied to terminals of PID affected PV modules, the Na ions around the solar cells are migrate towards the cover glass as shown in Fig.3.12 (a). The reductions in the Na ions in solar cells results in the reductions of shunt-path and the conversion efficiency is recovered. On the other hand, as shown in Fig.3.12 (b), when a reverse bias was applied to the p-n junction after the PID test, a current possibly flowed though shunt-path in the p-n junction as a leakage current, and induced Joule heating. As a consequence, application of RV to p-n junction induced Na ions migrations toward the p-type Si slightly. In addition, an increase in temperature possibly caused in longer migrations of Na ions and resulted in the decrease of shunt-path. This recovery model suggests that many Na ions remain in the p-n junctions, even after the recovery, and the residual Na possibly affected nonperfect recoveries of PID. Finally, PID recovery can be accelerated since Na ions within p-n junction may drift to the p-type base region, leading to a reduction in deep impurity level in the depletion layer in p-n junction. In the case of recovery by HV application, Na back diffusion occurred not only from the surface of solar cells but also from the inside of solar cells. It is suggested that reductions of Na ions in solar cells by the application of HV resulted in the reduction of shunt paths.

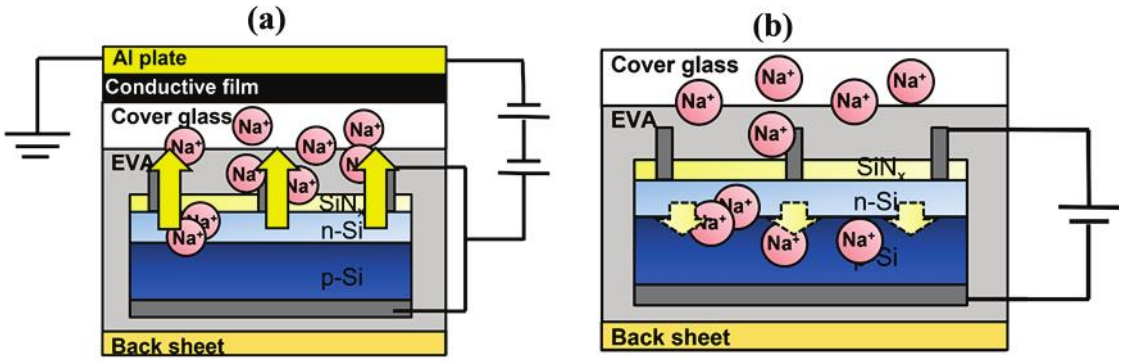

Fig.3.12 Schematic diagram of a cross section of recovery models of p-type c-Si PV module. (a) Na ions back diffusion process under HV application and (b) Drifting of Na ions to the p-type region under RV application.

3.4 Conclusions

The followings can be concluded from this study.

1. Recovery of PID affected PV modules were conducted with various V_R and t_R.
2. Higher V_R resulted in the higher and faster recovery. In the cause of V_R = -17 V, the recovery was saturated in 10 min application.
3. Non uniform temperature increase during RV application was observed.
4. Long hours of RV application of V_R = -17 V resulted in the maximum temperature about more than 130 °C with the slight decrease in the J_{sc}. The RV applications for long hours possibly cause some damage to the PV module components.
5. RV application of V_R = -17 V with short time, about 10 min, is the best recovery conditions in this research to obtain better recovery and to avoid the damage to solar cells and other module components.

Chapter 4
Development of suppression method for PV module by the application of glass layer (GL)

To achieve the long-term operations of PV modules for the low power generation cost, anti-PID techniques have been increasingly required. In this chapter, development of a new technique to delay the PID occurrence by using a glass layer (GL) on a cover glass of PV module was presented. In the section 4.1, the physical properties of GL were investigated from the viewpoint of atomic composition, surface morphology, thickness estimation, resistance measurement and transmittance spectra. In the section 4.2, PID suppression effect on PV modules were mainly discussed by photo *J-V* measurement results. Discussions of PID suppression effects by the formation of GL in PV modules were presented in section 4.3. This chapter was ended with conclusion section 4.4.

4.1 Physical properties of GL

4.1.1 Atomic compositions of GL and cover glass

Analyses for atomic composition of GL and cover glass were performed by using XPS measurements. Fig.4.1 shows XPS spectra of GL measured at the surface and inside of GL. According to the wide scan spectra as shown in Fig.4.1(a), no peaks originated from metallic elements appeared while the peaks originated from the elements of silicon, oxygen and carbon appeared. Note that the peaks appeared at 242 eV in the spectrum of inside of GL

is originated from argon which was used for the etching of GL during the XPS measurements. Additionally, the narrow scan spectra for Na 1s shown in Fig.4.1(b) shows no peak around at 1072 eV. Furthermore, no significant difference in the spectra were obtained at the surface and the inside of GL. The detection limit of XPS is known as below 0.1%. Therefore, we concluded that the GLs prepared from liquid glass include the metal elements with atomic compositions of below 0.1%. Table 4.1 shows atomic ratio of GL measured at the surface and the inside. The atomic ratio was obtained from the narrow scan measurement of Si 2p, O 1s, and C 1s. The element of carbon was included about a few tens of % with elements of silicon and oxygen which is possibly originated from the residual element of the organic solvent in the liquid glass.

Table 4.1 Atomic composition of glass layer

Position	C 1s	O 1s	Si 2p
Surface of GL	38.8	38.8	24.0
Inside of GL	36.5	36.0	28.3

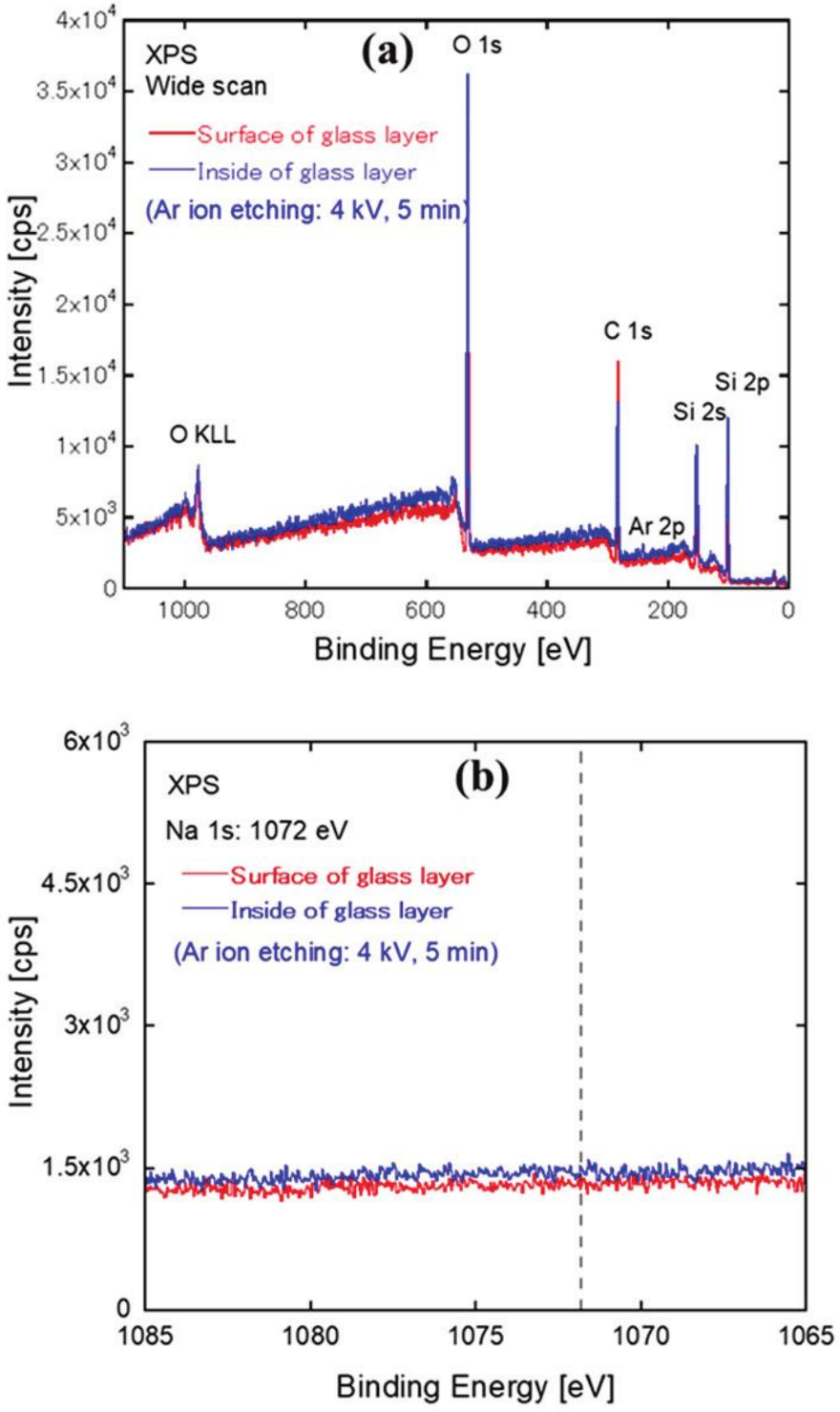

Fig.4.1 (a) Wide scan spectra and (b) Na 1s narrow scan spectra of the surface and inside of GL.

Analysis of atomic compositions of a bare cover glass before and after the PID tests was also performed with a depth profile by XPS to compare the composition of Na in cover glass with GL and to understand the Na ion migrations by the PID tests. Fig.4.2 shows the wide scan spectra of cover glass before and after PID test. Peaks originated from Na, Si, O, C Mg and Ca were observed. Note that the peaks originated from Ar were observed by the Ar ion etching for the depth profile. The observed elements by the XPS showed good agreements with the atomic compositions of cover glass shown by the company, AGC [87]. Fig.4.3 shows the atomic ratio of Na, Si, O and C with etching time. Before the PID test, the atomic ratio of Na was about 5 to 6 %. It is also suggested that Na from Na_2O existed in the cover glass even before PID tests. After the PID acceleration test, atomic ratio of Na was increased at near the surface of the cover glass where the -1000 V was applied by the PID test. It is suggested that the large amount Na ions are existed in the cover glass and the Na ions migrate by the applications of high voltage.

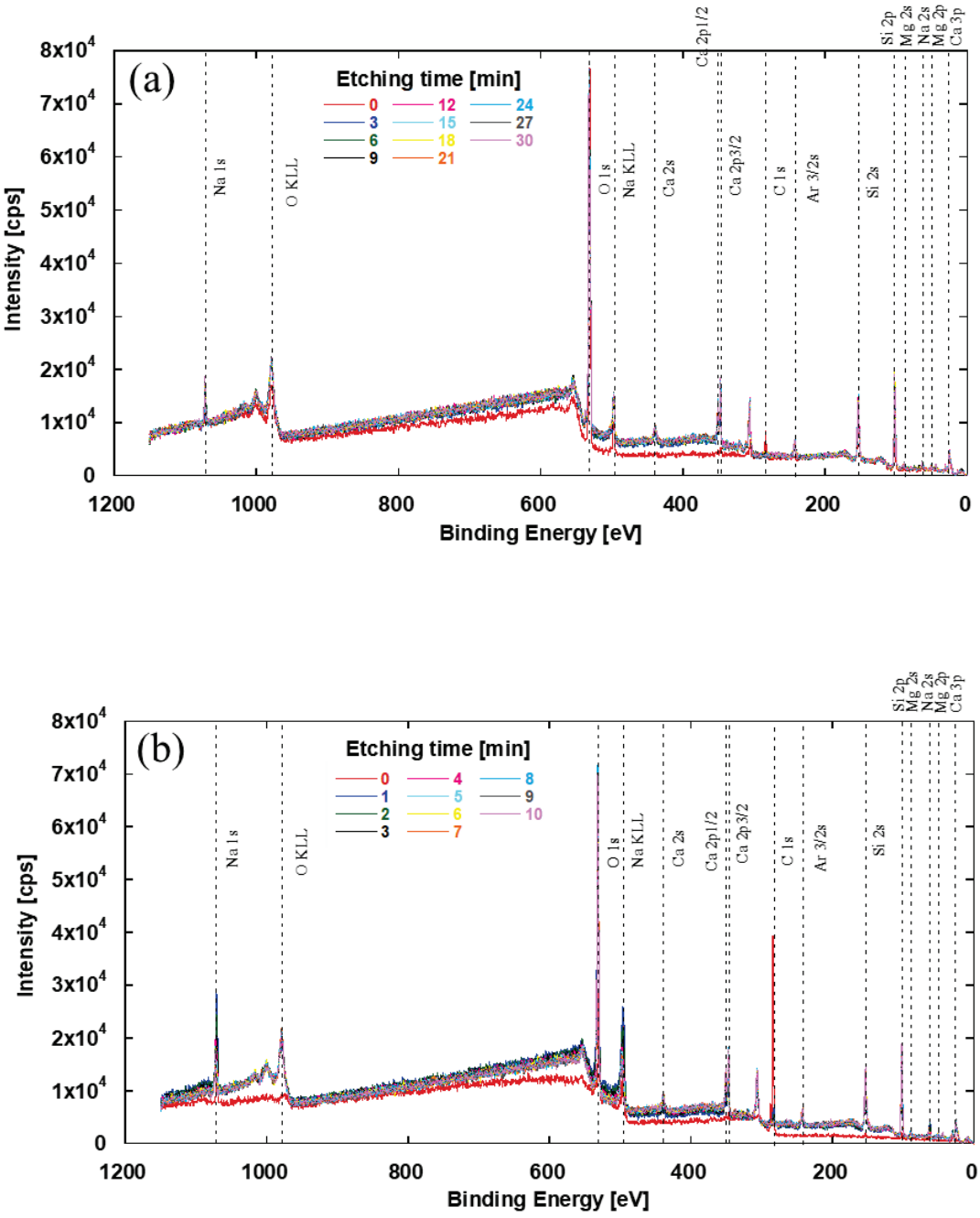

Fig.4.2 Wide scan XPS spectra of cover glass (a)before PID test and (b) after PID test conditions.

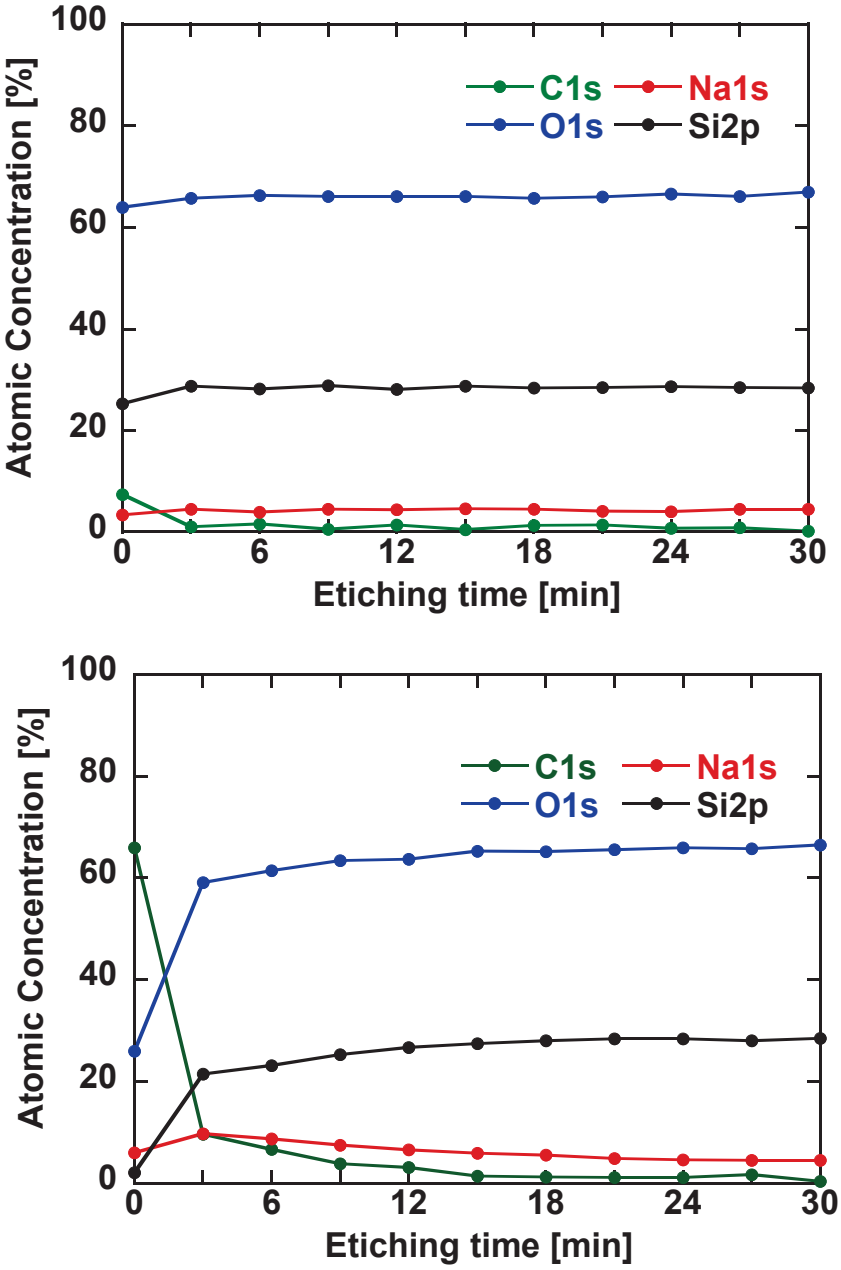

Fig.4.3 Depth profile of atomic ratio of cover glass (a) before PID test and (b) after PID test conditions.

4.1.2 Surface morphology of cover glass with and without GL

Surface morphologies of cover glass with and without GL were analyzed by using SEM. Fig.4.4 shows SEM images of cover glass measured at the light incident side (top side) and the side where EVA is contacting (bottom side) with and without GLs. The cover glass of top and bottom side without GL shows a clear difference in the surface morphology as shown in Fig.4.4 (a). The top side was relatively flat while the bottom side showed a grid structure that is visible with naked eyes. It is known that the grid is constructed in order to avoid forming of air bubbles in the PV modules on vacuum lamination. Note that the height of the grid structure was about 0.3 mm which is about the one tenth of the thickness of cover glass.

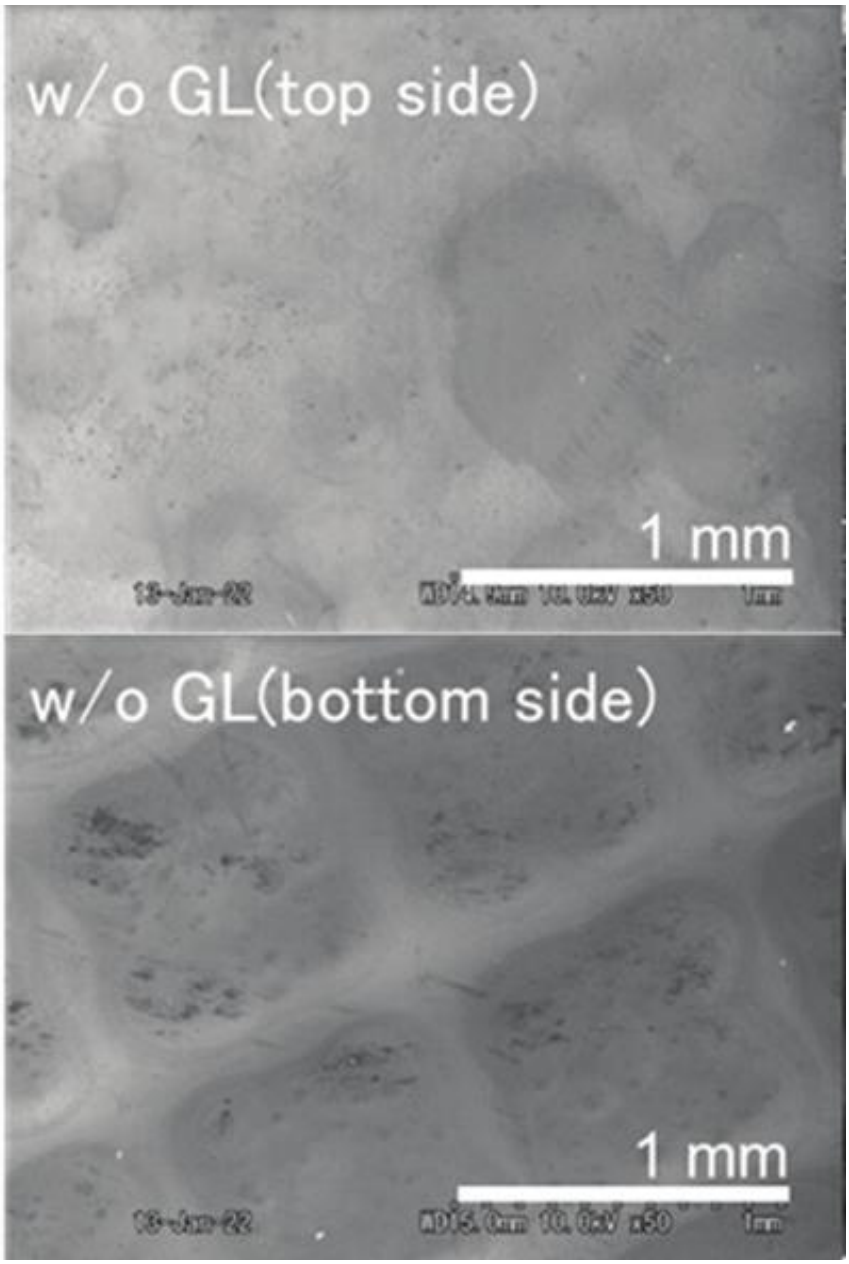

Fig.4.4 (a) SEM images of top and bottom side of cover glass without GL.

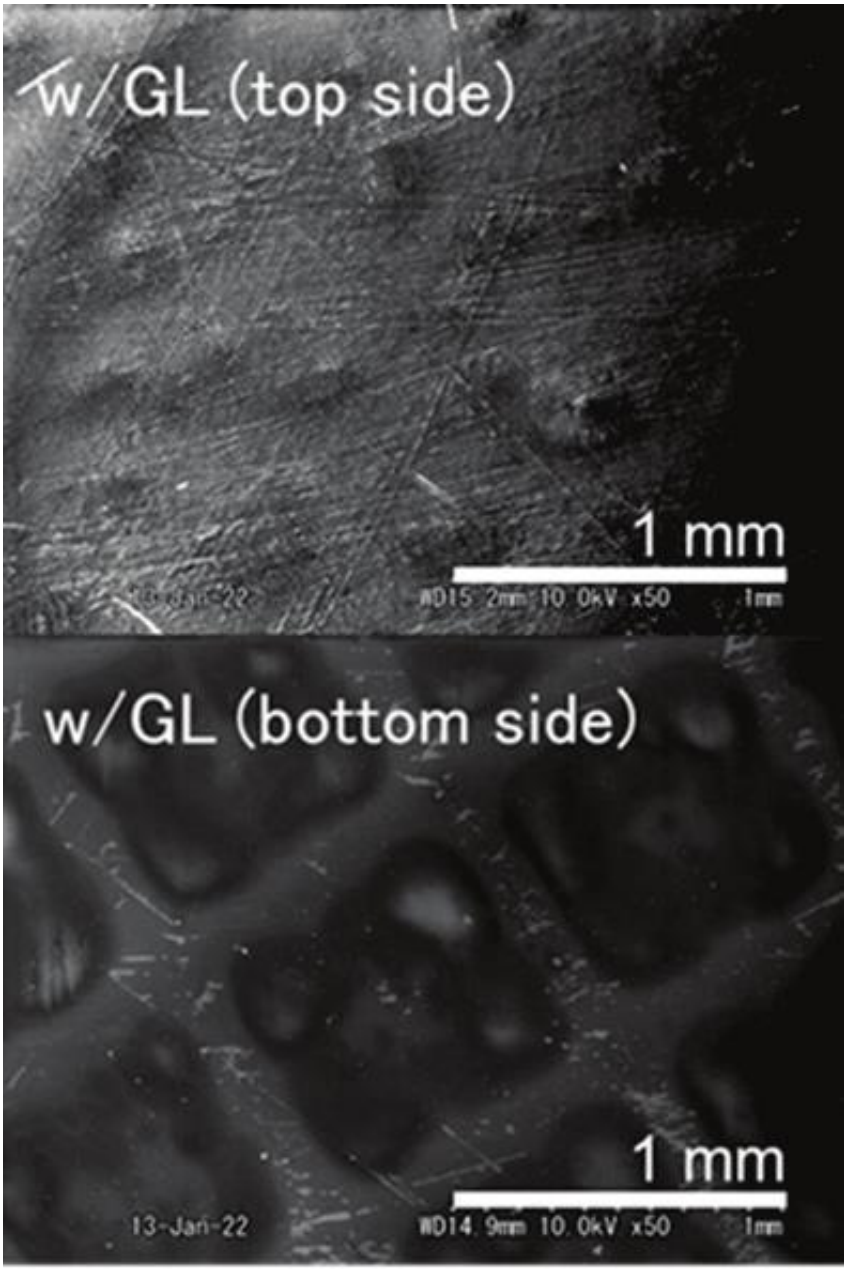

Fig .4.4 (b) SEM images of top and bottom side of cover glass with GL.

The surface morphologies of GL were quite different between the top and bottom sides of the cover glass even after the GL was formed. In the case of GL formed on the top side, many scratch-like hair lines were observed all over the surface. These lines were probably formed during spreading the liquid glass by using tissues. On the other hand, in the case of bottom side, the GL had the hair lines only around the ridge of the grid. This means that there are bumps and dips on the GL surface. The tissue probably contacts only to the ridge of the grid. Since the component of GL (the liquid glass) is accumulated in the dent of the grid during spreading the liquid glass solutions, the averaged thickness is likely to be larger than that for the top side. Additionally, during the SEM measurement, sudden darkening appeared, and no SEM images were obtained when the SEM measurements were conducted for the cover glass coated more than double GL. This is suggesting that the GL has large resistance, therefore, the surfaces of cover glass were charged up quickly by exposing electron beams during the SEM measurements which disables the emitting of secondary electrons for the imaging when the thick GL existed at the surface of cover glass.

4.1.3 Thickness of glass layer (GL)

Since the surface morphology of cover glass makes difficult to estimate the thickness of GL, the thickness of GL was measured by forming the GL on a flat slide glass (Asone, ASLAB) prepared with the same way. The thickness measurement was conducted by using a 3D Laser scanning microscope (Keyence, VK-X200K) as shown in Fig.4.5. According to the measurement the thickness of GL was estimated approximately as about 1 ~ 2 μm. Compared to the height of the grid structure shown in the previous section by SEM, the thickness of GL is much smaller. Additionally, the difference between the thickness of cover glass and GL is about three orders of magnitude.

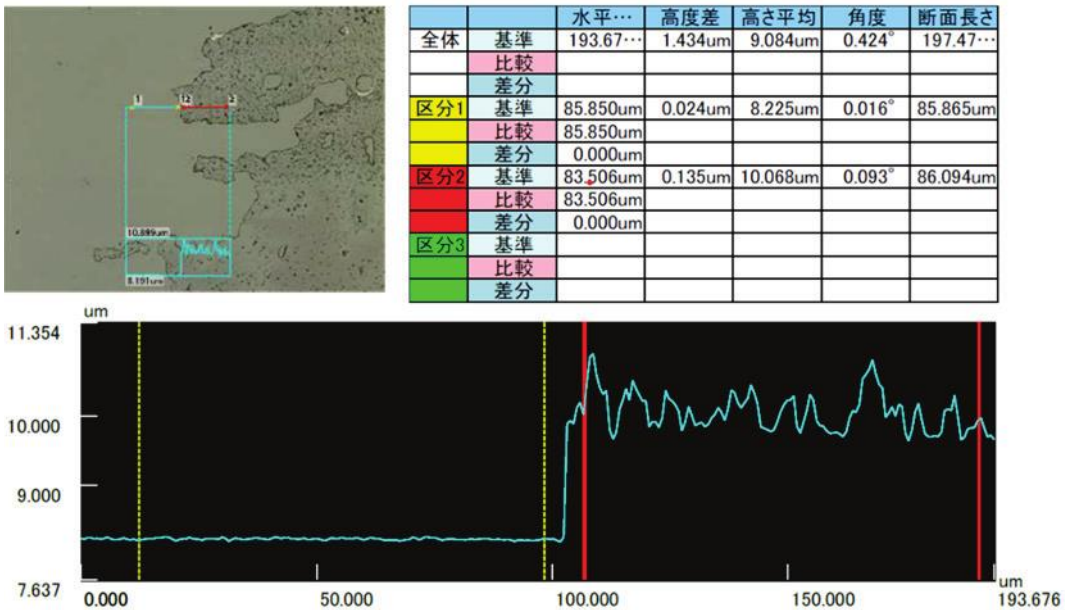

Fig.4.5 Analytical image at the boundary between the glass layer and the cover glass surface using a laser microscope.

4.1.4 Resistance measurement of cover glass with and without GL

The resistances measurements were conducted for the cover glass itself by applying -100 V up to 3 h from bottom side of cover glass at RT. Schematic diagram of resistance measurement set up was shown in Fig.2.12 in chapter 2. Note that the -100 V was used to suppress the migrations of Na ions by the voltage application during the measurement which occurs during the PID test conditions of -1000 V at 85 °C. Additionally, the resistance values were not converted to resistivity because of the difficulty to estimate the exact thickness of GLs on the cover glass because of grid structures on the bottom side of cover glass.

Fig.4.6 shows the time dependence of resistances of the cover glasses with and without GL. According to Fig.4.6, the resistances of all the samples were increased in the first 10 minutes, then no more significant changes were observed after 10 minutes to 180 hours. The increases in resistances in the first 10 minutes possibly originates from the charge accumulations and/or polarizations by applying the voltage. Thus, the intrinsic resistances of the cover glasses with and without GLs were obtained after 10 minutes. The resistance of cover glass after 10 minutes of voltage applications showed about 4×10^{10} Ω. The resistances were increased to 2×10^{11} Ω, about one order of magnitude, by forming GLs at both top and bottom side of cover glass. It is noted that no significant difference was observed in the resistances of cover glass with GL at top and bottom side, although the surface morphologies were quite different as shown in the section 4.1.2.

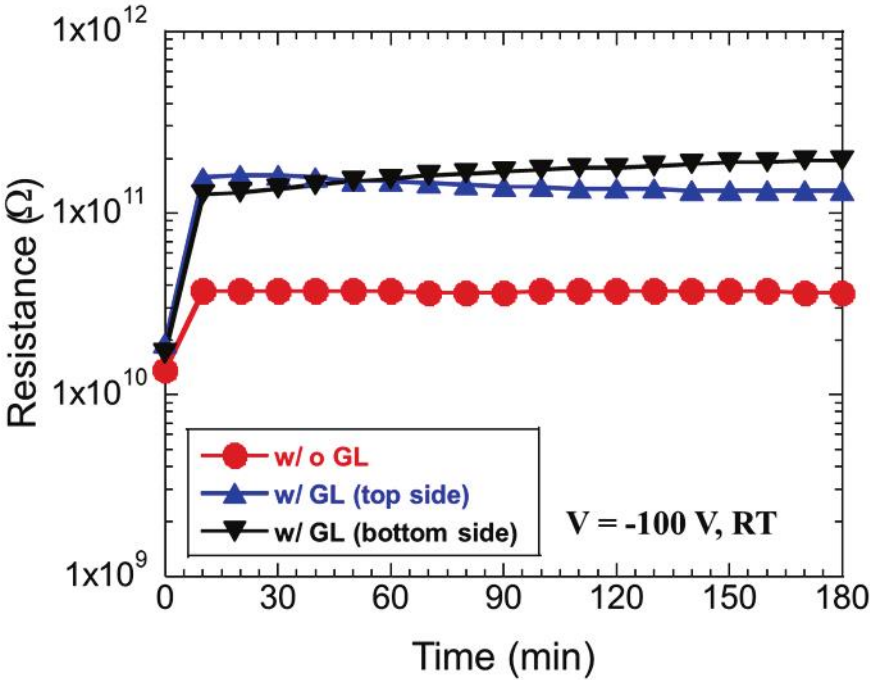

Fig.4.6 Time dependence of resistance values of cover glass with and without GLs measured at RT.

4.1.5 Transmittance spectra of quartz substrate with GL

One of the main roles of cover glass in one cell PV module as well as in commercialized PV module is to transmit sunlight as much as possible to expose the sunlight to the cell. However, the cover glass has grid structure, and the thickness is about 3.3 mm. Such structures make difficult to measure the light transmission measurement because of light scattering by the structures. Therefore, in this section, to understand the influence of GL for the light transmission, transmittance spectra of the glass layer with and without GL was analyzed using a quartz glass substrate. Fig.4.7 shows transmittance spectra of quartz substrate with and without GL. Measured wavelength range is 400 to 2500 nm. In both transmission spectra, the transmittance decreased significantly from around 500 nm to the shorter wavelength side which is originated from absorption of quartz substrates. Additionally, the transmittance of quartz without GL is slightly higher than with GL. However, the difference around the 1% and is near limit of the accuracy of measurement. Therefore, we concluded that formation of GL on the surface of cover glass is almost negligible for the transmittance of light into the solar cell. However further light transmission measurement is needed by using thick GL to understand the influence of GL to the conversion efficiency of PV modules.

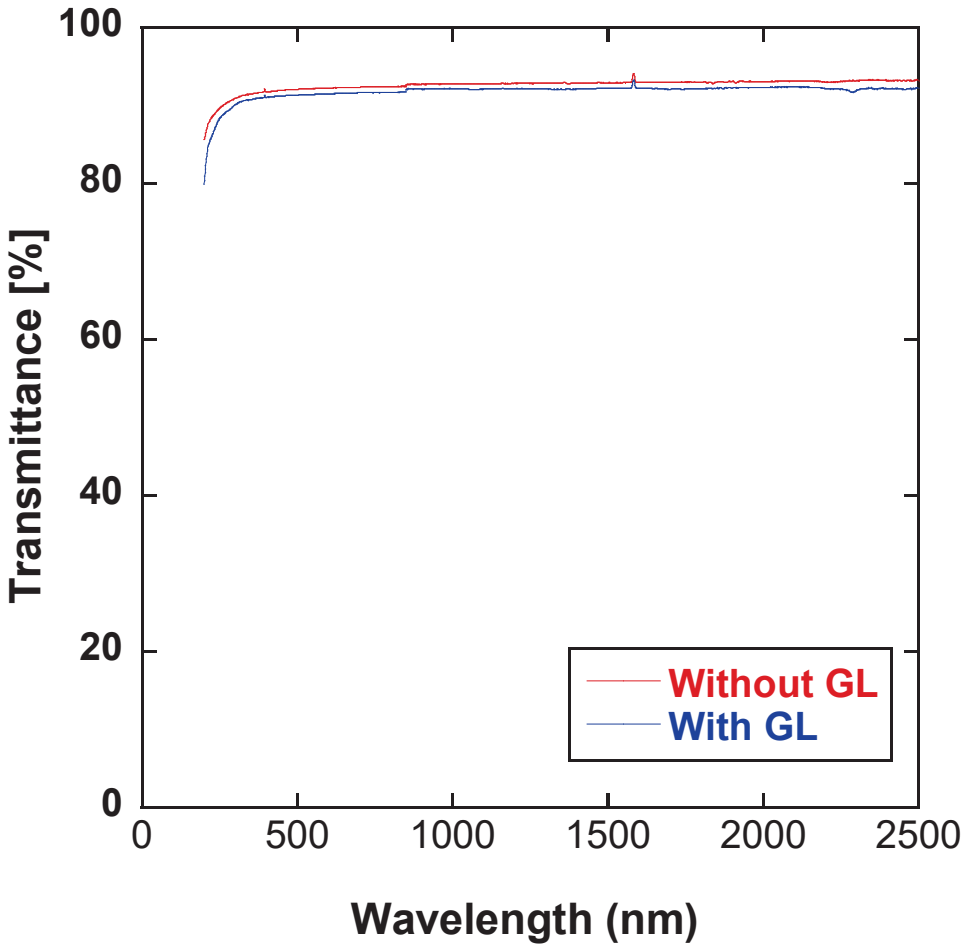

Fig.4.7. Transmittance spectra of quartz substrate with and without GL.

4.2 PID suppression effect on PV module

4.2.1 Photo *J-V* measurement with and without GL

To evaluate the PID suppression effect on PV modules by forming GLs at the top and bottom side of cover glass, PV characteristics of PV modules were analyzed before and after the PID tests. In this study, a standard PV module and PV modules coated with GL on top and bottom side of cover glass were mainly used to investigate the influence of GL insertions on PID. A voltage of -1000 V was applied up to 12 h to the terminals of PV modules while the Al plate was grounded. Figs.4.8 (a) – (c) show the *J-V* characteristics of the PV modules prepared with and without GL for before and after the PID tests conditions. Additionally, the numeric photovoltaic characteristics of the PV modules obtained from these measurements are summarized in table 4.2. Note that, in these experiments, the short circuit current (J_{sc}) of PV modules prepared with GL before the PID tests appeared about 4 to 5% smaller than those of PV modules prepared without GL before PID. According to the light transmittance measurements as shown in section 4.1.5, difference in the transmittances of the quarts substrates with and without GL was less than 1%. Therefore, we considered that the differences in the J_{SC} with and without GL were mainly originated from the individual properties of PV cells used in this research.

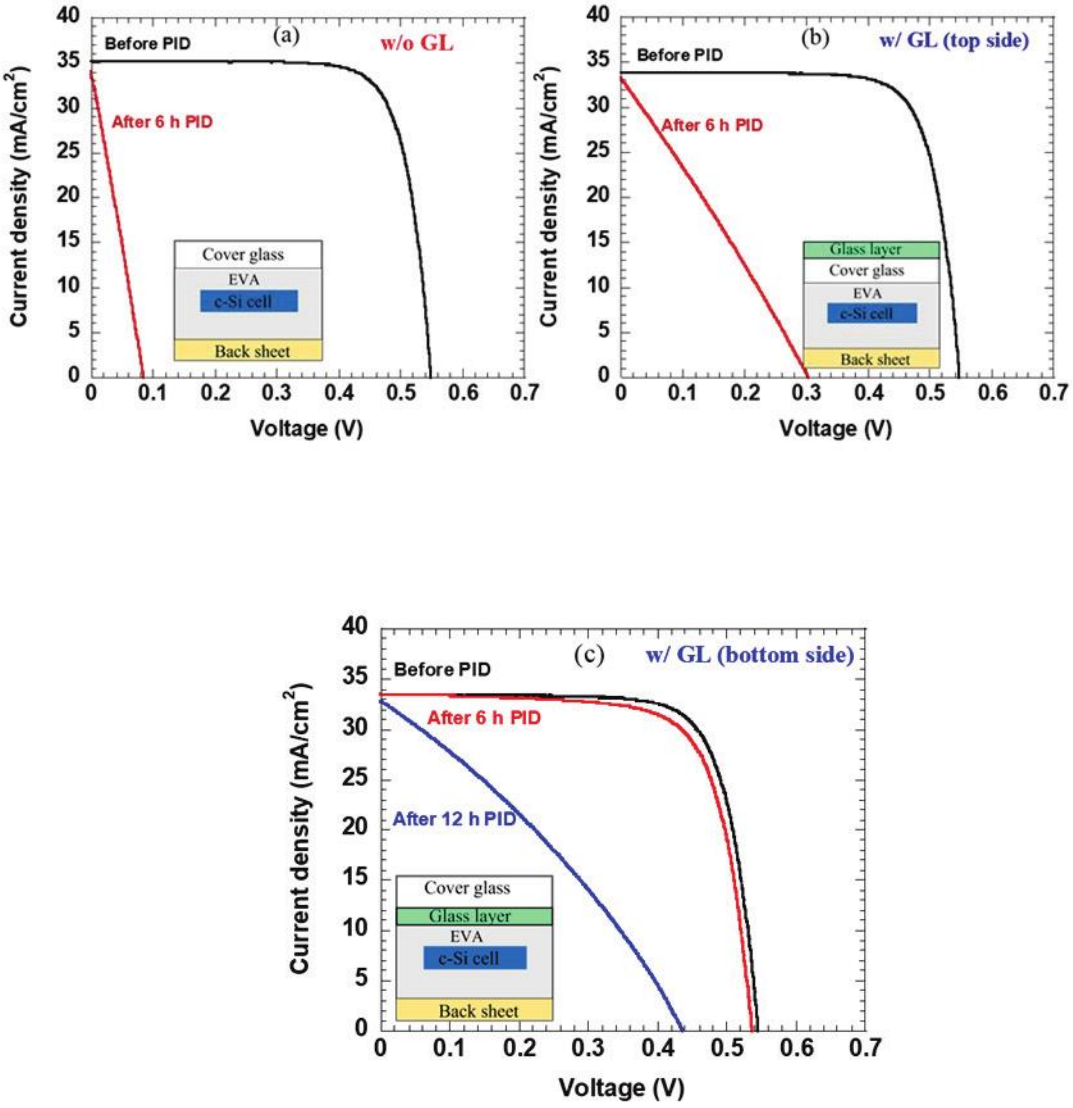

Fig.4.8 Photo *J-V* curves for PV modules before and after the PID test by applying -1000V at 85 ℃for 6 h: (a) PV module without GL, (b) PV module with GL at top side of cover glass and (c) PV module with GL at bottom side of cover glass.

Table 4.2 Power generation characteristics of PV modules prepared with and without GL before and after the PID tests obtained from the *J-V* curves shown in Fig.4.8.

PV module structure	PID test time (h)	J_{SC} (mA/cm^2)	V_{OC} (V)	FF	η (%)
w/o GL	0	35.1	0.55	0.77	14.8
	6	33.8	0.08	0.26	0.8
w/ GL at top	0	33.9	0.54	0.76	14.0
	6	33.1	0.30	0.27	2.7
w/ GL at bottom	0	33.4	0.55	0.76	13.8
	6	33.5	0.54	0.72	13.0
	12	32.9	0.44	0.32	4.5

For PV module without the GL (Fig.4.1(a)), the open circuit voltage (V_{OC}), the current density (J_{SC}), the fill factor (FF), and the conversion efficiency (η) was decreased to about 18%, 89%, 36%, 6% of initial values after the 6 h PID test, respectively. The drastic degradation of η was induced mainly by decreases in V_{OC} and FF. This is the typical phenomenon reported previously as PID [39]. On the other hand, for PV modules with GL (Figs.4.1 (b) and 4.1 (c)), less degradations were observed after the PID tests. For the PV module with GL at the top side of cover glass (Fig.4.1 (b)), the V_{OC}, J_{SC}, FF and η were decreased to about 66%, 97%, 37% and 24% of initial values, respectively. For the PV module with GL at the bottom side of cover glass (Fig. 4.1(c)), the V_{OC}, J_{SC}, FF and η were decreased to 98%, 100%, 96% and 94%, respectively, after the 6 h PID test, and to 80%, 98%, 42% and 33% after the 12 h PID test, respectively. It was observed that the insertions

of GL maintained better PV characteristics after the 6 h PID tests. In particular, the GL insertion at bottom side of cover glass is found to be much effective to suppress the PID.

4.2.2 Time dependence of PV characteristics of PV modules with and without GL

Figs.4.9 (a) and 4.2(b) show the solar-cell parameters (V_{OC}, J_{SC}, FF and η) of PV modules without and with GL as a function of PID test durations. All parameters were normalized by those of initial values. Note that each PID test was conducted for 1 h, and the photo *J-V* characteristics were measured at RT after each PID test. In the case of PV modules without GL (Fig. 4.2 (a)), the η was decreased to about 80% of the initial values after 1 h PID test, and further degradation occurred by following the decreases of the V_{OC} and FF. On the other hand, for PV module with GL at the bottom side of cover glass, the η was still maintained over 80% even after the 4 h PID test (the bottom of blue parts in the figures depicts the 80%). These results demonstrate that the formation of the GL at the bottom side of cover glass of PV modules delays the occurrence of PID about 4 times.

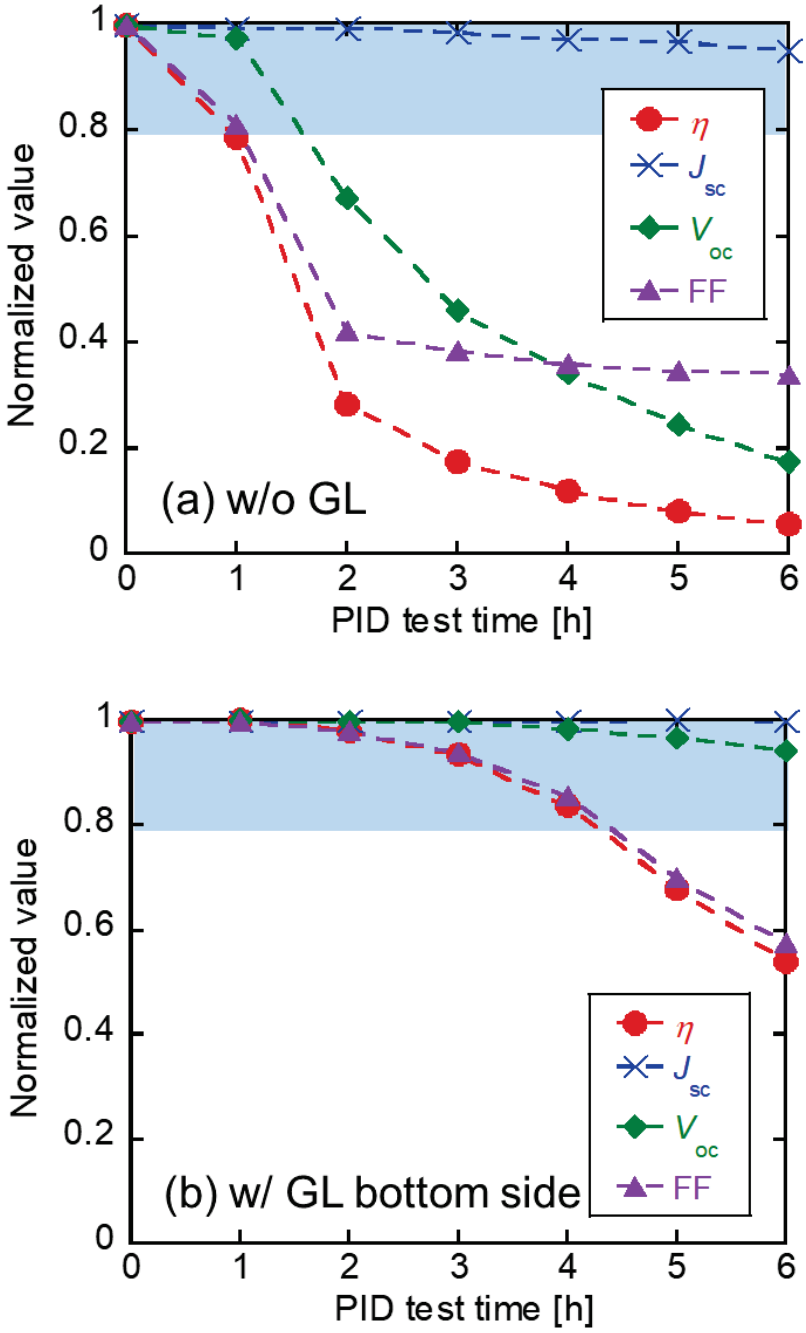

Fig.4.9 Normalized PV properties as a function of PID test duration for (a) without GL and (b)with GL at bottom side of cover glass. Each PV parameter before PID test was normalized by using the values obtained before PID tests.

4.2.3 Leakage current through cover glass of PV modules during PID tests

To analyze the influence of GL on anti-PID, leakage currents flowing from the Al plate to the solar cells through the cover glass and EVA was measured under the conditions of -1000 V at 85 ℃ as shown in Fig.2.14. The resistances were estimated from the leakage current. Fig.4.10 shows the time dependence of the resistances in the case of the cover glasses without and with formation of GL at the bottom side. According to the measurements, the resistance value of PV module without GL showed about 3×10^8 Ω and the value was gradually decreased with the PID test time. On the other hand, in the case of PV module with GL formed at the bottom side, the resistance value was about 4×10^9 Ω when the PID test was started. Then the value was increased in the first 1 h PID test and decreased later. The difference in the resistance values of the PV module prepared with GL were almost one order of magnitude larger than those without GL which is well consistent with the resistance measurements on the cover glass at RT as shown in the section 4.1.4. In addition, measured resistance values at RT were much higher than those measured during PID. The reason why the resistance value is quite different between RT and 85℃ originates from the temperature dependence of electrical conductivity of glasses (SiO_2). Usually, the electrical conductivities of glasses vary one or two magnitudes in this temperature range [100]. Thus, the large difference in the resistance originates from the formation of GL on the cover glass. The increase of the resistance in first 1h PID test using PV modules with GL appeared possibly by the decrease of Na ions in the cover glass while subsequent gradual decrease appeared possibly by the migrations of Na ions into the SiN_x films at the surface of the cells in the

modules. The migrations of Na ions into SiN_x films results in the decreased of resistivity of SiN_x films and increase of effective area where the leakage current flow as reported by F. Ohashi *et al*. [39]

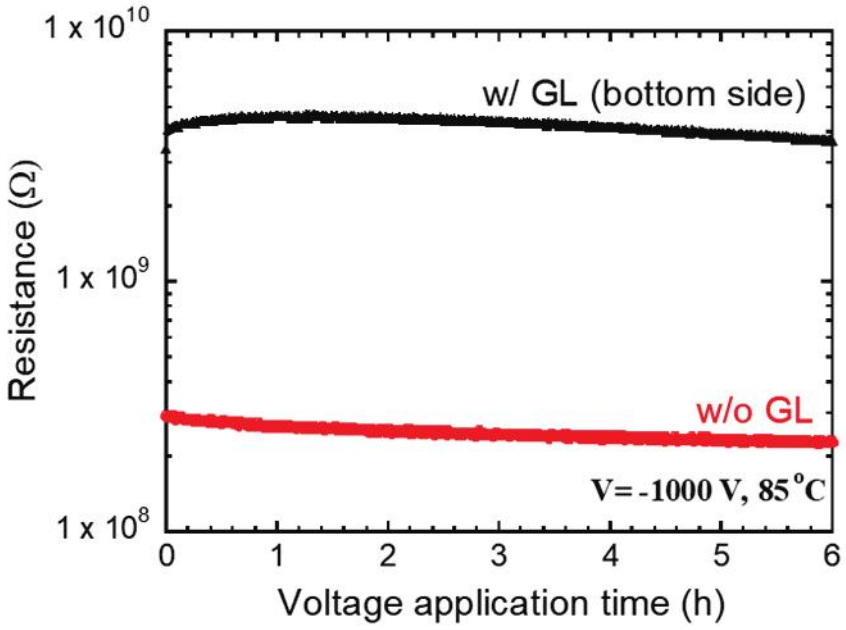

Fig.4.10 Time dependence of resistance values measured between Al plate and electrodes of PV module with and without GL.

4.3 Discussions of PID suppression effects by using GL on PV modules

4.3.1 Position of GL in PV modules

The PID suppression effect appeared not only at the bottoms side but also the top side, while the formation of GL at the bottom side of cover glass showed higher suppression effects. By the formation of GL on top or bottom the cover glass, the resistance values of the cover glass was increased about one order of magnitude. Additionally, the leakage currents through the cover glass and EVA during the PID tests were decreased by the formations of GLs on the cover glass. However, the thicknesses of GLs were estimated about a few μm while the thickness of cover glass is about 3.3 mm. This is indicating that the volume resistivity of GLs is about 4 orders of magnitude higher than that of cover glass (2.4×10^{11} Ω.cm,). Inserting of such the high-resistivity GL is able to decrease the voltage distributed to the cover glass, giving rise to decrease in the electric field in it. This suppresses the drift of metal ions, leading to anti-PID. Additionally, according to the XPS measurements, the GL is almost free from metal ions and includes large amount of carbon. Therefore, the GL formed at the bottom of cover glass possibly acted as a barrier to avoid the migration of metal ions from the cover glass.

4.3.2 For the practical use as the PID suppression technique

In this study, a new technique to delay the PID occurrence was developed by formations of a GL on a cover glass of PV module. The GL is almost the same material with the car coating. The formation of GL at the bottom side of cover glass leads to the better performance for the anti-PID compared to that formed at the top side of cover glass. However, the GL at the bottom side of cover glass should be prepared before fabrication of PV modules. That means only the PV module manufacturers or cover glass manufacturers can prepare GL and can apply the technique to the PV modules. These situation limits wider use of the technique to the PV modules. On the other hand, in the case of GL formation at the top side of cover glass, anti-PID effects were observed and the GL at the top side can be formed even for the PV modules which are already installed as a part of PV system. In the viewpoint of the technique with wider use, this technique is more easily to be introduced. To obtain better anti-PID effects by the formation of GL at the top side of cover glass, further optimization work is necessary such as the change in the thickness, atomic compositions or use of multiple layers to obtain higher resistance values.

4.4 Conclusions

The followings can be concluded from this study.

1. A new PID suppression method was developed by the formation of a glass layer (GL) on the surface of cover glass using liquid glass.
2. According to XPS measurements, atomic composition of metals was below the detection limit while the caron was included with more than 36 at. % .
3. Thickness of GL was estimated as approximately 1 ~ 2 μm.
4. According to the UV-vis measurement, the formation of GL resulted in the no significant difference in the transmittance spectrum.
5. Resistance value of cover glass were increased from 4×10^{10} Ω to 2×10^{11} Ω by the formation of GLs at top or bottom side of cover glass.
6. Leakage current flowing through the cover glass and EVA during the PID tests were decreased about one order of magnitude.
7. Both the GLs formed at top or bottom side of cover glass suppressed the occurrence of PID.
8. Results of time dependence of PV characteristics of PV modules demonstrate that the formation of the GL at the bottom side of cover glass of PV modules showed better suppression effect
9. PV module with the GL formed at the bottom side of cover glass delayed the occurrence of PID about 4 times compared with that without the GL.

10. Inserting of high resistivity GL is able to decrease the voltage distributed to the cover glass, giving rise to decrease in the electric field in it. This suppresses the drift of metal ions, leading to anti-PID.
11. GL formed at the bottom of cover glass possibly acted as the Na barrier.

Chapter 5
Conclusions

5.1 PID recovery technique

Potential-induced degradation (PID) of photovoltaic (PV) modules based on p-type crystalline Si occurs in large-scale PV systems. In this work, we studied a simple PID recovery method for PID-affected one cell PV module based on p-type mc-Si. PID recovery was conducted by applications of a reverse DC-bias voltage to the p-n junction of solar cells in PV modules without temperature control devices. The conversion efficiency of a one cell PV module reduced prior to approximately 20 % of their initial value by the PID test was recovered up to 92 % by using a reverse DC-bias voltage. Additionally, nonuniform temperature increases at the surface of PV modules were observed during the voltage application. Clear recovery was observed with a 10 min application, which is faster than the conventional recovery process in which high voltage is applied between the surface of cover glass and terminals of PV modules. However, when a reverse DC-bias voltage of − 17 V was applied for 360 min, the PV module temperature was elevated to the temperature higher than that for vacuum lamination and a slight decrease in the J_{SC} appeared. These phenomena suggests that the components of the PV modules were damaged by the high temperature at these settings. To the best of our knowledge, in our experiments, the optimum recovery conditions by using a reverse DC-bias voltage is the voltage of − 17 V for about 10 minutes.

From the viewpoint of the application of this technique to commercialized PV modules, further optimization works are crucial. To maximize the recovery and to minimize damage to the PV module components. Furthermore, in our experiment, we used one cell PV modules while the commercialized PV modules include bypass diodes which are connected in parallel with series-connected solar cells. The bypass diodes possibly cancel the effects of the reverse DC-bias voltage applications, and series connections of solar cells results in the partial applications of the voltages. To avoid the effect of bypass diode, a system for the application of a reverse DC bias voltage has to be attached in the junction box of PV modules. Additionally, the optimization of recovery process for the series connected solar cells are still necessary.

5.2 Anti-PID technique

In this paper, a new suppression technique of the PID was developed by a formation of glass layer (GL) on the top or bottom surface of cover glass using a chemical solution known as liquid glass. PID tests were conducted using PV modules prepared with and without GL. A clear suppression effects of the PID were observed by forming the GLs, and the occurrence of the PID was delayed about 4 times by the formation of GL at the bottom side of cover glass in PV modules. We considered the GL are worked to reduce the voltage applied to the cover glass by the high resistance of GL. Additionally, Na barrier effects possibly

appeared when the GL was formed at the bottom side of cover glass which resulted in the better anti-PID effect.

Although the GL formation at the bottom side of cover glass leads to the best performance for the anti-PID, the GL should be prepared before the fabrications of PV modules. As mentioned above, the anti-PID effects were observed even when the GL was formed at the top side of cover glass. Since the GL can be formed at top side of cover glass even for the PV modules which are installed already as the PV system, anti-PID technique by the formations of GL at the top side of cover glass is more likely to be commercialized. To obtain better anti-PID effects by the formation of GL at top side of cover glass, optimization work for the conditions of GL formations is necessary such as formations of thicker GL to obtain the higher resistance. Anyway, these anti-PID technique are considered to be one of the powerful tools to suppress the occurrence of PID with low cost in the various PV modules.

References

[1] https://en.wikipedia.org/wiki/Edmond_Becquerel.

[2] W.G. Adams, R.E. Day, The action of light on selenium. Proc R Soc A25, 113 (1877).

[3] W. Shockley, Bell System Tech. J., 28(1494)435.

[4] J. Bardeen and W.H. Brattain, Phys. Rev.,74(1948) 230.

[5] D.M. Chapin, C.S. Fuller, and G.L. Pearson, J.Appl.Phys.,25(1954)676.

[6] Carlson, D.E., Wronski, C.R., Appl. Phys.Lett.,28(1976)671.

[7] Mitchell K.W., Eberspaecher C. et al., Trans Elec. Dev., 37 (1990)469.

[8] Research Cell Efficiency Records. Available online: https://www.nrel.gov/pv/assets/pdfs/best-research-cell-efficiencies.

[9] Choubey, P.C., Oudhia, A. and Dewangan, R. (2012) A Review: Solar Cell Current Scenario and Future Trends. Recent Research in Science and Technology, **4**, 99-101.

[10] McEvoy, A., Castaner, L. and Markvart, T. (2012) Solar Cells: Materials, Manufacture and Operation. 2nd Edition, Elsevier Ltd., Oxford, 3-25.

[11] Fahrenbruch, A.L. and Bube, R.H. (1983) Fundamentals of Solar Cells. Academic Press Inc., New York.

[12] Bagher, A.M., Vahid, M.M.A. and Mohsen, M. (2015) Types of Solar Cells and Application. American Journal of Optics and Photonics, 3, 94-113.

[13] Srinivas, B., Balaji, S., Nagendra Babu, M. and Reddy, Y.S. (2015) Review on Present and Advance Materials for Solar Cells. International Journal of Engineering Research-Online, **3**, 178-182.

[14] Chopra, K.L., Paulson, P.D. and Dutt, V. (2004) Thin-Film Solar Cells: An Overview. Progress in Photovoltaics, **12**, 69-92.

[15] Klaus-Dieter Jäger, Olindo Isabella, Arno H.M. Smets, René A.C.M.M. van Swaaij, Miro Zeman (2014). *Solar energy: fundamentals, technology, and systems.* UIT Cambridge, Cambridge, 2016.

[16] https://www.renovainc.com/en/business/power_plant/yokkaichi_solar/.

[17] Assadeg, Jalal, Kamaruzzaman Sopian, and Ahmad Fudholi. "Performance of grid-connected solar photovoltaic power plants in the Middle East and North Africa." *International Journal of Electrical and Computer Engineering* 9.5 (2019): 3375.

[18] S. Goel and R. Sharma, "Performance evaluation of stand-alone, grid connected and hybrid renewable energy systems for rural application: A comparative review," Renewable and Sustainable Energy Reviews, vol. 78, p. 1378-1389, 2017.

[19] I. A. Ibrahim, et al., "Optimal modeling and sizing of a practical standalone PV/battery generation system using numerical algorithm," 2015 IEEE Student Conference on Research and Development (SCOReD), p. 43-48, 2015.

[20] L. Bartolucci, et al., "Hybrid renewable energy systems for household ancillary services," International Journal of Electrical Power & Energy Systems, vol. 107, pp. 282-297, 2019.

[21] Z. M. Omara, et al., "Improving the productivity of solar still by using water fan and wind turbine," Solar Energy, vol. 147, pp. 181-188, 2017.

[22] J. A. Razak, et al., "Optimization of PV-wind-hydro-diesel hybrid system by minimizing excess capacity," vol/issue: 25(4), pp. 663-671, 2009.

[23] R. Hasan, et al., "Grid-connected isolated PV microinverters: A review," Renewable and Sustainable Energy Reviews, vol. 67, pp. 1065-1080, 2017.

[24] A. M. Humada, et al., "Modeling and characterization of a grid-connected photovoltaic system under tropical climate conditions," Renewable and Sustainable Energy Reviews, vol. 82, pp. 2094-2105, 2018.

[25] Sayigh, A. A. M. (Ed.). (2012). Solar energy engineering. Elsevier.

[26] Rehman, S., Bader, M. A. & Al-Moallem, S. A. (2007). Cost of solar energy generated using PV panels. Renewable and sustainable energy reviews, 11, 1843–1857.

[27] Abu-Rumman, Ala'K., Iyad Muslih, and Mahmoud Barghash. "Life cycle costing of PV generation system." *Journal of applied research on industrial engineering* 4.4 (2017): 252-258.

[28] https://www.nrel.gov/pv/lifetime.html.

[29] M. A. Quintana, D. L. King, T. J. McMahon, and C. R. Osterwald, "Commonly observed degradation in field-aged photovoltaic modules," in Conference Record of the Twenty-Ninth IEEE Photovoltaics Specialists Conference (2002), pp.1436-1439.

[30] Quintana, M. a., King, D. L., McMahon, T. J., & Osterwald, C. R. (2002). Commonly observed degradation in field-aged photovoltaic modules. *Conference Record of the Twenty-Ninth IEEE Photovoltaic Specialists Conference, 2002.*, 1436–1439.

[31] Sharma, V., & Chandel, S. S. (2013). Performance and degradation analysis for long term reliability of solar photovoltaic systems: A review. *Renewable and Sustainable Energy Reviews*, *27*, 753–767.

[32] W. Luo et al., Energy Environ. Sci. 10, 43 (2017).

[33] M. Kambe, K. Hara, K. Mitarai, S. Takeda, M. Fukawa, N. Ishimaru, M. Kondo, PID-free c-Si PV module using aluminosilicate chemically strengthened glass, in: Proceedings of the 28th EU PVSEC, Paris, France, 2013, pp. 2861–2864.

[34] K. Mishina, A. Ogishi, K. Ueno, T. Doi, K. Hara, N. Ikeno, D. Imai, T. Saruwatari, M.Shinohara, T. Yamazaki, A. Ogura, Y. Ohshita, A. Masuda, Investigation on antireflection coating for high resistance to potential-induced degradation, Jpn. J. Appl.Phys. 53 (2014) (03CE01-1–03CE01-4).

[35] K. Mishina, A. Ogishi, K. Ueno, S. Jonai, N. Ikeno, T. Saruwatari, K. Hara, A. Ogura, T. Yamazaki, T. Doi, M. Shinohara, A. Masuda, Plasma-enhanced chemical-vapor deposition of silicon nitride film for high resistance to potential-induced degradation, Jpn. J. Appl. Phys. 54 (2015) (08KD12-1–08KD12-6).

[36] K. Hara, H. Ichinose, T.N. Murakami, A. Masuda, Crystalline Si photovoltaic modules based on TiO2-coated cover glass against potential-induced degradation, RSC Adv. 4 (2014) 44291–44295.

[37] K. Hara, S. Jonai, A. Masuda, Crystalline Si photovoltaic modules functionalized by a thin polyethylene film against potential and damp-heat-induced degradation, RSC Adv. 5 (2015) 15017–15023.

[38] S. Jonai, K. Hara, Y. Tsutsui, H. Nakahama, A. Masuda, Relationship between cross linking conditions of ethylene vinyl acetate and potential-induced degradation for crystalline silicon photovoltaic modules, Jpn. J. Appl. Phys. 54 (2015) (08KG01-1-08KG01-5).

[39] F. Ohashi, Y. Mizuno, H. Yoshida, H. Kosuga, T. Furuya, R. Fuseya, R. J. Freitas, Y. Hara, A. Masuda, and S. Nonomura, Jpn. J. Appl. Phys. 57, 08RG05 (2018).

[40] V. Naumann, D. Lausch, A. Graff, M. Werner, S. Swatek, J. Bauer, A. Hähnel, O. Breitenstein, S. Großer, J. Bagdahn, Phys. Status Solidi: Rapid Res. Lett. 2013, 7, 315.

[41] V. Naumann, D. Lausch, A. Hähnel, J. Bauer, O. Breitenstein, A. Graff, M. Werner, S. Swatek, S. Großer, J. Bagdahn, C. Hagendorf, Sol. Energy Mater. Sol. Cells 2014, 120, 383.

[42] V. Naumann, C. Hagendorf, S. Grosser, M. Werner, J. Bagdahn, Energy Procedia 2012, 27, 1.

[43] J. Bauer, V. Naumann, S. Großer, C. Hagendorf, M. Schütze, O. Breitenstein, Phys. Status Solidi: Rapid Res. Lett. 2012, 6, 331.

[44] V. Naumann, D. Lausch, S. Großer, M. Werner, S. Swatek, C. Hagendorf, J. Bagdahn, S. Großer, Energy Procedia 2013, 33, 76.

[45] V. Naumann, C. Brzuska, M. Werner, S. Großer, C. Hagendorf, Energy Procedia 2016, 92, 569.

[46] A. Masuda, M. Akitomi, M. Inoue, K. Okuwaki, A. Okugawa, K. Ueno, T. Yamazaki, and K. Hara, Curr. Appl. Phys. 16, 1659 (2016).

[47] A. Masuda, Y. Hara, and S. Jonai, Jpn. J. Appl. Phys. 55, 02BF10 (2016).

[48] J. Oh, S. Bowden, and G. Tamizhmani, Proc. 40th IEEE Photovoltaic Specialists Conf., 2014, p. 0925.

[49] J. Oh, S. Bowden, and G. TamizhMani, IEEE J. Photovolt. 5, 1540 (2015).

[50] D. Lausch, V. Naumann, A. Graff, A. Hähnel, O. Breitenstein, C. Hagendorf, J. Bagdahn, Energy Procedia 2014, 55, 486.

[51] D. Lausch, V. Naumann, A. Graff, A. Hähnel, O. Breitenstein, C. Hagendorf, and J. Bagdahn, Energy Procedia 55, 486 (2014).

[52] C. Taubitz, M. Schütze, and M. B. Köntopp, Proc. 27th European Photovoltaic Solar Energy Conf. Exhib., 2012, p. 3172.

[53] J. Hattendorf, W.-M. Gnehr, R. Löw, T. Roth, D. Koshnicharov, and M. Zentgraf, Proc. 28th European Photovoltaic Solar Energy Conf. Exhib., 2013, p. 3303.

[54] A. Raykov, H. Nagel, D.-J. Amankwah, and W. Bergholz, Proc. 27th European Photovoltaic Solar Energy Conf. Exhib., 2012, p. 3399.

[55] C. Taubitz, M. Schütze, M. Kröber, and M. B. Köntopp, Proc. 29th European Photovoltaic Solar Energy Conf. Exhib., 2014, p. 2490.

[56] C. Taubitz, M. Kröber, M. Schütze, and M. B. Köntopp, Proc. 28th European Photovoltaic Solar Energy Conf. Exhib., 2013, p. 3321.

[57] S. Jonai, T. Tanahashi, H. Shibita, and A. Masuda, Jpn. J. Appl. Phys. 57, 08RG01 (2018).

[58] M. Kambe, K. Hara, K. Mitarai, S. Takeda, M. Fukawa, N. Ishimaru and M. Kondo: Proc. the 28th EU PVSEC, Paris, (2013) p. 2861.

[59] T. Kajisa, H. Miyauchi, K. Mizuhara, K. Hayashi, T. Tokimitsu, M. Inoue, K. Hara and A. Masuda: Jpn. J. Appl. Phys. 53 (2014) 092302.

[60] K. Hara, H. Ichinose, T.N. Murakami and A. Masuda: RSC Adv. 4 (2014) 4429144295.

[61] E. Jang, K. Oh and S. Ryu: Processes 10 (2022) 334.

[62] S.-H. Schulze, A. Apel, R. Meitzner, M. Schak, C. Ehrich and J. Schneider: Proc. 28th European Photovoltaic Solar Energy Conf. Exhib., (2013) pp. 503507.

[63] J. Kapur, A. Bennett, J. Norwood, B. Hamzavytehrany and I. Kueppenbender: Proc. 28th European Photovoltaic Solar Energy Conf. Exhib., (2013) pp. 476479.

[64] S. Jonai, K. Hara, Y. Tsutsui, H. Nakahama and A. Masuda: Jpn. J. Appl. Phys. 54 (2015) 08KG01.

[65] P. Lechner, D. Sanchez, D. Geyer and H.-D. Mohring: Proc. 27th European Photovoltaic Solar Energy Conf. Exhib., (2012) p. 3152.

[66] S.-H. Schulze, A. Apel, R. Meitzner, M. Schak, C. Ehrich and J. Schneider: Proc. 28th EU PVSEC, Paris, (2013) pp. 503507.

[67] C.G. Reid, S.A. Ferrigan, J.I.F. Martinez and J.T. Woods: Proc. 28th EU PVSEC, Paris, (2013) pp. 33403346.

[68] J. Oh, S. Bowden and G. TamizhMani: IEEE J. Photovolt. 5 (2015) 15401548.

[69] P. Hacke, M. Kempe, K. Terwilliger, S. Glick, N. Call, S. Johnston, S. Kurtz, I. Bennett and M. Kloos: Proc. 25th European Photovoltaic Solar Energy Conf. Exhib./5th World Conf. Photovoltaic Energy Conversion, (2010) pp. 37603765.

[70] P. Hacke, K. Terwilliger, R. Smith, S. Glick, J. Pankow, M. Kempe, S.K.I. Bennett and M. Kloos: Proc. 37th IEEE Photovoltaic Specialists Conf., (2011) pp. 814820.

[71] M. Schütze, M. Junghänel, M. Koentopp, S. Cwikla, S. Friedrich, J.W. Muller and P. Wawer: Proc. 37th IEEE Photovoltaic Specialists Conf., IEEE, Piscataway, NJ, (2011) pp. 821826.

[72] M. Kambe, K. Hara, K. Mitarai, S. Takeda, M. Fukawa, N. Ishimaru and M. Kondo: Proc. 42nd IEEE Photovoltaic Specialists Conf., IEEE, Piscataway, NJ, (2013) pp. 35003503.

[73] S. Pingel, O. Frank, M. Winkler, S. Daryan, T. Geipel, H. Hoehne and J. Berghold: Proc. 35th IEEE Photovoltaic Specialists Conf., (2010) pp. 28172822.

[74] J. Berghold, O. Frank, H. Hoehne, S. Pingel, B. Richardson and M. Winkler: Proc. 25th European Photovoltaic Solar Energy Conf. Exhib./ 5th World Conf. Photovoltaic Energy Conversion, (2010) pp. 3753 3759.

[75] X. Gou, X. Li, S. Zhou, S. Wang, W. Fan and Q. Huang: Int. J. Photoenergy 2015 (2015) 863248.

[76] K. Mishina, A. Ogishi and K. Ueno: Proc. the 28th European Photovoltaic Solar Energy Conference and Exhibition, Paris, France, (2013) pp. 11391143.

[77] V. Naumann, K. IIse and C. Hagendorf: Proc. 28th European Photovoltaic Solar Energy Conference and Exhibition, Paris, France, (2013) pp. 29942997. 32) S. Pingel, S. Janke and O. Frank: Proc. 27th European Photovoltaic Solar Energy Conference and Exhibition, Frankfurt, Germany, (2012) pp. 33793383.

[78] S. Koch, D. Nieschalk, J. Berghold, S. Wendlandt, S. Krauter and P. Grunow: Proc. 27th EU PVSEC, Frankfurt, (2012) pp. 19851990.

[79] S. Koch, J. Berghold, O. Okoroafor, S. Krauter and P. Grunow: Proc. 27th EU PVSEC, Frankfurt, (2012) pp. 19911995.

[80] K. Mishina, A. Ogishi, K. Ueno, T. Doi, K. Hara, N. Ikeno, D. Imai, T. Saruwatari, M. Shinohara, T. Yamazaki, A. Ogura, Y. Ohshita and A. Masuda: Jpn. J. Appl. Phys. 53 (2014) 03CE01.

[81] Yamaguchi, S., Van Aken, B. B., Masuda, A., & Ohdaira, K. (2021). Potential-induced degradation in High-Efficiency n-Type Crystalline-Silicon Photovoltaic Modules: A Literature Review. *Solar RRL*, *5*(12), 2100708.

[82] N. G. Dhere, V. V. Hadagali and S. M. Bet, Proceedings of the 19th European Photovoltaic Solar Energy Conference and Exhibition, Paris, France, 2004.

[83] S. Voswinckel, V. Wesselak, E. Fokuhl, C. Schmidt and K. Watzlawik, Proceedings of the 31st European Photovoltaic Solar Energy Conference and Exhibition, Hamburg, Germany, 2015, pp. 2508–2512.

[84] S. Yamaguchi, S. Jonai, K. Hara, H. Komaki, Y. ShimizuKamikawa, H. Shibata, S. Niki, Y. Kawakami and A. Masuda, Jpn. J. Appl. Phys., 2015, 54, 08KC13.

[85] S. Voswinckel, P. Manz, C. Schmidt and V. Wesselak, Energy Procedia, 2014, 57, 56.

[86] https://www.cleanenergyreviews.info/blog/solar-panel-components-construction.

[87] AGC_Solite-LR.

[88] A. Kitiyanan, A. Ogane, A. Tani, T. Hatayama, H. Yano, Y. Uraoka, and T. Fuyuki, J. Appl. Phys., 106, 043717, (2009).

[89] T. Fuyuki, and A. Kitiyanan, Appl. Phys. A, DOI:10.1007/s00339-008-4986-0, (2008).

[90] T. Fuyuki, H. Kondoh, Y. Kazi, A. Ogane and Y. Takahashi, J. Appl. Phys., 101, 023711, (2007).

[91] T. Fuyuki, H. Kondo, T. Yamazaki, Y. Takahashi and Y. Uraoka, Appl. Phys. Lett., 86, 262108, (2005).

[92] M. Kasemann, D. Grote, B. Walter, W. Kwapil, T. Trupke, Y. Augarten, R. A. Bardos, E. Pink, M. D. Abbott, and W.Warta, "Luminescence imaging for the detection of shunts on silicon solar cells," Prog. Photovoltaics 16(4), 297–305(2008).

[93] O. Breitenstein, J. Bauer, T. Trupke, and R. A. Bardos, "On the detection of shunts in silicon solar cells by photo-and electroluminescence imaging," Prog. Photovoltaics 16(4), 325–330 (2008).

[94] O. Breitenstein *et al.*, "LOCK-IN THERMOGRAPHY -A UNIVERSAL TOOL FOR LOCAL ANALYSIS OF SOLAR CELLS," in *20th European Photovoltaic Solar Energy Conference*, 2005.

[95] R. Ebner, B. Kubicek, G. Újvári, S. Novalin, M. Rennhofer, and M. Halwachs, "Optical Characterization of Different Thin Film Module Technologies," *Int. J. Photoenergy*, vol. 2015, pp. 1–12, 2015.

[96] /ehps/rem/laboratory/equipment safety/Research Equipment/sem.html

[97] I. W. Drummond, "XPS: Instrumentation and performance," in Surface Analysis by Auger and X-ray Photoelectron Spectroscopy, edited by D. Briggs and J. T. Grant (Surface Spectra, Chichester, 2003), pp. 117–144.

[98] B. D. Ratner and D. G. Castner, "Electron spectroscopy for chemical analysis," in Surface Analysis: The Principal Techniques, edited by J. C. Vickerman (Wiley, Chichester, 2009), pp. 80–88.

[99] https://www.agilent.com/cs/library/primers/public/primer-uv-vis-basics-5980-1397en-agilent.pdf.

[100] M. Tatsumisago, New Glass, 23, pp. 89 (2008).

List of figures

Chapter 1

Chapter 2

Chapter 3

Chapter 4

List of tables

Chapter 3

Chapter 4

List of publications

1. Go Sian Huai, Kiyoshiro Takada, Kota Ono, Shingo Hashimoto, Naing Lin Htun, Fumitaka Ohashi, Norimitsu Yoshida, Yasushi Sobajima, and Shuichi Nonomura.

   "Recovery of potential-induced degraded p-type multicrystalline Si PV modules by application of a reverse DC bias", Go Sian Huai *et al 2022 Jpn. J. Appl. Phys. 61 041002.*

2. Go Sian Huai, Takhiko Haga, Fumitaka Ohashi, Hiroki Yoshida, Tetsuji Kume, Shuichi Nonomura.

   "Development of a suppression technique of potential-induced degradation by a formation of glass layer in Si PV modules", Huai, Go Sian, *et al. MATERIALS TRANSACTIONS* 64.1 (2023): 165-170.

Acknowledgements

I would like to express my gratitude and appreciation to all those who gave me the opportunity to complete this study.

I would like to offer my special thanks to Professor Shuichi NONOMURA for his greatest support, and giving the opportunity to do this study.

I should not forget to thank senior Professor Kazuma NAKAZAWA for his interesting to my mother land, Myanmar and opening the gate for me to study at Gifu University, Japan.

The next person whom I would like to extend my sincere thanks to Professor Tetsuji KUME for his insightful comments, suggestions in laboratory seminar and support throughout the entire years of my studentship.

I would like to acknowledge Associate Professor Norimitsu YOSHIDA and Associate Professor Yasushi SOBAJIMA for their insightful discussions and valuable assistances.

The completion of this study could not have been possible without the guidance of thesis adviser, Associate Professor Fumitaka OHASHI, for his greatest support, patience, motivation, enthusiasm, immense knowledge, invaluable guidance, understanding me during my study for Ph.D degree in Gifu University, Japan.

In addition, my thanks go to Assistant Professor Himanshu Shekhar Jha and Dr. Raul Kumar for their suggestions and continuous supporting to handle the experimental apparatus.

I owe a deep sense of gratitude to my senior Yoshiki MIZUNO (Mitsubishi Electric) for his incredible teaching and helping me for everything during my time in Japan. I would like to thank to co-workers Hirokazu TAKAHASHI, Takahiko HAGA, Ryo FUSEYA, Naing Lin HTUN, Takashi SUZUKI and all the laboratory members for their helping and nice working atmosphere during my study period.

I would also like to thank to thesis examiners committee members for letting my defense be an enjoyable moment, and for their brilliant comments and suggestions on this work.

I would like to express my appreciates to the AGP program from the Graduate School of Engineering, Gifu University for giving a chance to study and providing endless support for my study life in Japan. I would also like to acknowledge to the Japan Student Service Organization (JASSO), the Iwatani Naoji International Scholarship Foundation, the Kubota International Scholarship Foundation, and the International Club for their awarding scholarships.

My thanks go to New Energy and Industrial Technology Development Organization (NEDO) and Bureau of Waterworks Tokyo Metropolitan Government for their supporting for this work.

I am extremely grateful to my friends, Zaw Min Han, Phyo Myat Lin, Muhammad Ulung Sutop, Chirahu TSUNOGAE and Haruki YASUDA for many helps, kind friendship and great moments that we shared together.

I am very sorry that I am not able to mention all people who have given a contribution to this study. I am sure that some people will be missing to be mentioned. I would like to thank all of you.

At last, but not the least, I would like to express special gratitude to my dad, mom, and lovely younger brother for their praying and endless supporting to achieve my dream.

I say to the LORD, “You are my LORD; apart from you I have no good thing.”

Every single day in Japan was passed by God’s amazing grace.

GO SIAN HUAI

March,2023.

VITA

The author, Go Sian Huai was born in Northern Shan State, Myanmar on November 10th, 1993. Only one daughter of U Mang Khen Kam and Daw Dau Naw. Only one sister of her younger brother Kap Sian Khai. She went to Basic Education High School, Bant Bwe from elementary to senior high school. She graduated from Yadanabon University, Mandalay, Myanmar with B.Sc (Hons) Nuclear Physics in February 2013. She entered the Graduate School of Engineering, Gifu University on April 1st, 2015, and received her Master of Engineering on March 25th , 2017. On April 1st of 2017, she joined the doctoral course in the same university majoring in Electrical and Electronic Engineering under the guidance of Associate Professor Fumitaka OHASHI. Her research field is focusing on p type based multi-crystalline silicon PV modules and developing in recovery and suppression techniques for potential-induced degradation (PID) affected PV modules. Her hobbies are eating, sleeping, and watching Korean Dramas and Japanese animation. Chibimaruko chan is one of her favorite Japanese animations. The author lived in Japan for almost a decade, and she loved to eat Japanese foods and she travelled around Japan to study the history and culture of Japan in her free time.